NANYANG TECHNOLOGICAL UNIVERSITY
SINGAPORE

INVESTIGATION OF TRANSFORMATION PROCESS OF 1,3-DIPHENYLGUANIDINE IN DISINFECTION WATER TREATMENT

Ying Lebing
SCHOOL OF CIVIL AND ENVIRONMENTAL ENGINEERING

2023

INVESTIGATION OF TRANSFORMATION PROCESS OF 1,3-DIPHENYLGUANIDINE IN DISINFECTION WATER TREATMENT

YING LEBING

School of Civil and Environmental Engineering

A thesis submitted to the Nanyang Technological University
in partial fulfilment of the requirement for the degree of
Master of Engineering

2023

1 Statement of Originality

I hereby certify that the work embodied in this thesis is the result of original research, is free of plagiarised materials, and has not been submitted for a higher degree to any other University or Institution.

July 29, 2023

Date

Ying Lebing

2 Supervisor Declaration Statement

I have reviewed the content and presentation style of this thesis and declare it is free of plagiarism and of sufficient grammatical clarity to be examined. To the best of my knowledge, the research and writing are those of the candidate except as acknowledged in the Author Attribution Statement. I confirm that the investigations were conducted in accord with the ethics policies and integrity standards of Nanyang Technological University and that the research data are presented honestly and without prejudice.

02 August, 2023

. . . . . .

Date

. . . . . .

Shane Allen Snyder

3 Authorship Attribution Statement

*(B) This thesis contains material from one paper published in the following peer-reviewed journal in which I am listed as an author.

Chaper 4, Chapter 5, and Chapter 6 have been published as Ying, L., Dos Santos, M. M., Jia, S., Li, C., Lee, T. H., Mensah, A. T., & Snyder, S. A. (2024). Comparison of monochloramination and chlorination of 1, 3-diphenylguandine (DPG): Kinetics, transformation products, and cell-based in-vitro testing. Science of The Total Environment, 906, 167743. DOI: 10.1016/j.scitotenv.2023.167743

The contributions of the co-authors are as follows:

- Prof S.A Snyder provided the resources, initial project direction, and edited the manuscript drafts.
- I prepared the manuscript's original drafts, designed the experiments, and conducted the laboratory work, and data analysis.
- The manuscript was revised by Dr. Shenglan Jia, Mauricius Marques dos Santos, Dr. Caixia Li, Theodora Lee and Dr. Mensah Tele Anette.
- Dr. S.L Jia guided the design of the cell experiments and Dr. C. Li assisted in the collection and provided guidance in the interpretation of the genotoxic part data.

Jan 29, 2024

. . . . . .

Date

Ying Lebing

. . . . . .

Ying Lebing

ACKNOWLEDGEMENTS

The research work presented in this report was primarily conducted at Nanyang Research Institute, Nanyang Technological University (NTU), Singapore. I would like to express my heartfelt appreciation to everyone who has consistently encouraged and supported me throughout my MENG study journey.

First and foremost, I extend my deepest gratitude to my supervisor, Professor Shane Snyder from the School of Civil and Environmental Engineering (CEE), for his unwavering support, invaluable guidance, and abundant resources that have played a crucial role in my learning, growth, and pursuit of my goals. I am also immensely grateful to Dr. Shenglan, Dr. Anette, Dr. Caixia, and Mauricius for their dedicated mentorship. Their guidance has not only encompassed the intricacies of specific experiments but has also provided a broader direction for my overall research. I would like to express my sincere appreciation to Theodora, who not only served as my senior but also became my first friend in Singapore. I would also like to extend my gratitude to my friends I met in NEWRI and CEE, Genevieve, Arvin, Dexter, Bingjie, and Zhouyao, who have always offered their enthusiastic encouragement and warm support during times of confusion or despair. The laboratory work at SMTC and AEBC would not have been possible without the assistance of Dr. Mabel, Hui Ying, Jia Wei, Mei Shan, Ka Keng, and Emily. Their guidance and advice have been immensely valuable. I would also like to thank my beloved partner Li Xing, and all the good friends I met in NTU including Yanyu, Yuting, Fang Zhou, Chenlu, Cao Zhen, Daiqi, Zhenyu. At last, I wanna say thank you to GSA EXCO members, especially Arun, regarding the help and warmness they gave me.

Lastly, I want to acknowledge the valuable experiences gained during my time at Tuas Desalination Plant while operating MIMS. The memories and lessons from my time at Tuas Plant will remain cherished and unforgettable, serving as a stepping stone in my journey to become a proficient researcher and resilient engineer.

TABLE OF CONTENTS

SUMMARY

Tire wear products (TWPs) potentially pose risks to human health and the environment when introduced into surface water cycle. Among all TWPs, 1,3-diphenylguanidine (DPG), a widely used vulcanization accelerator in the rubber industry, has gained increasing attention recently with high concentrations identified in the environment. To compare and comprehend the disinfection process of DPG, this work investigates (1) the effects of multiple disinfection methods towards DPG; (2) the reaction kinetics of DPG during monochloramination; (3) toxicity and bioenergetics of DPG disinfection products based on *in vitro* experiments; (4) transformation products (TPs) of DPG during chlorination and monochloramination. It has been revealed that DPG is insensitive in regards of UV alone, and that UV has neglecting effect on promoting the effect of chlorine and monochloramine effectively when degrading DPG. Additionally, the reactivity of monochloramine is significantly slower compared to chlorination of DPG, with the maximum efficiency observed at pH 7 to pH 8. While chlorination effectively degrades DPG, this process leads to the formation of transformation products (TPs) like nitrosamines, notably nitroso-dimethylamine (NDMA). NDMA, a significant byproduct closely linked with vulcanization agents used in tire manufacturing, is known for its potential toxicity. In contrast, monochloramination can generally resulted in lower concentrations of trihalomethanes (THMs), haloacetic acids (HAAs), and total organic halogen (TOX) compared to chlorination. Following this, bioassays were conducted on the DPG TPs generated treated by chlorine and NH_2Cl. An interesting outcome was found in cytotoxicity testing that that cytotoxicity hierarchy is as follows: chlorine TPs > monochloramine TPs > DPG. Moreover, oxidant-to-DPG molar ratios 10 and 20 lead to maximum cytotoxicity in both chlorination and monochloramination. Additionally, bioenergetics experiments demonstrate that chlorine and monochloramine disinfection by-products induce mitochondrial dysfunction and enhance glycolytic function in HepG2 cells. The genotoxic response from p53 cells further indicated the genotoxic effects of certain disinfection products. The variation of bioassay experiments has led to the the, analysis of TPs using high-resolution mass spectrometry (HRMS) which

identifies ten TPs, with chlorination yielding more TPs than monochloramination. Generally, a chlorine or monochloramine molar ratio to DPG of 10-20 results in an increased formation of TPs and heightened cytotoxicity. Notably, higher oxidant molar ratios increased the formation of monoguanidine TPs and DPG hydroxylation during chlorination, whereas monochloramination lead to DPG substitution predominantly generating chlorinated DPG due to weaker oxidation effects. It has been assumed that some identified TPs like DPG-119, might contribute most toxicity in chlorine 100 μM and chlorine 500 μM groups.

These findings provide valuable information for the appropriate treatment of DPG and disinfection processes in water facilities to mitigate potential risks to human health and the ecosystem.

LIST OF TABLES

LIST OF FIGURES

LIST OF ACRONYMS

AA	Ascorbic Acid
AOPs	Advanced Oxidation Processes
APCI	Atmospheric Pressure Chemical Ionisation
APPI	Atmospheric Pressure Photoionisation
ATCC	American Type Culture Collection
BA	Benzoic Acid
BDCM	Bromine Dichloromethane
Br-DBPs	Brominated Disinfection By-Products
CA	Cinnamic Acid
Cl2	Chlorine
ClO_2	Chlorine Dioxide
DBPs	Disinfection By-Products
DF	Divergence Factor
DMA	Dimethylamine
DMEM	Dulbecco'S Modified Eagle Medium
DMOB	1,4-Dimethoxybgenzene
DMRM	Dynamic Multiple Reaction Monitoring
DMSO	Dimethyl Sulfoxide
DPD	Dipropyl-P-Phenylenediamine
DPG	1,3-Diphenylguanidine
ECAR	Extracellular Acidification Rate
ER+	Estrogen Receptor-Positive
EREs	Estrogen Response Elements
ERα	Estrogen Receptor Alpha
ERβ	Estrogen Receptor Beta
ESI	Electrospray Ionisation
ETC	Electron Transport Chain
FBS	Foetal Bovine Serum
glycoPER	Glycolytic Proton Efflux Rate
GRT	Glycolysis Rate Test
GST	Glycolysis Stress Test
HAAs	Halaacetic Acids
HANs	Haloacetonitriles
HClO	Hypochlorous Acid
HK	Haloketones
HPLC	High Performance Liquid Chromatography

HRMS	High-Resolution Mass Spectrometry
m/z	Mass To Charge
MeOH	Methanol
MIMS	Membrane Introduction Mass Spectrometry
MST	Mitochondrial Stress Test
MTBE	Methyl Tert-Butyl Ether
$Na_2S_2O_3$	Sodium Thiosulfate
NB	Nitrobenzene
NCl_3	Trichloramine
NDMA	Nitroso-Dimethylamine
NH2Cl	Monochloramine
NH_3Cl^+	Protonated Chloramine Ion
$NHCl_2$	Dichloramine
NOM	Natural Organic Matter
NPIP	N-Nitrosopiperidine
NTA	Non-Targeted Analysis
O3	Ozone
OCR	Oxygen Consumption Rate
PAHs	Polycyclic Aromatic Hydrocarbons
PDH	Pyruvate Dehydrogenase
PF	Petri Factor
PMA	Phorbol-12-Myristate-13-Acetate
RF	Refelection Factor
rMFE	Recursive Molecular Feature Extraction
RR	Response Ratio
SERDs	Selective Estrogen Receptor Degraders
SERMs	Selective Estrogen Receptor Modulators
SPE	Solid Phase Extraction
TCA	Tricarboxylic Acid
THMs	Trihalomethanes
TOF	Time-Of-Flight
TOrCs	Trace Organic Compounds
TOX	Total Organic Halogen
TPs	Transformation Products
TPWPs	Tire And Road Wear Particles
TWPs	Tire Wear Particles
UV	Ultraviolet
WF	Water Factor

WTPs	Water Treatment Plants
WWTPs	Wastewater Treatment Plants
LC/QQQ	Liquid Chromatography/Triple Quadrupole

1. INTRODUCTION

1.1 Background

More than 200 organic substances have been identified as tire and road wearwear contaminants, with 145 classified as leachables, yet their toxicity and transformation byproducts remain poorly understood (Baensch-Baltruschat et al., 2020; Kole et al., 2017; Müller et al., 2022). These contaminants yield tire and road wear particles (TRWPs) when the vehicles' tired are torn by road surfaces (Z. Zhang et al., 2021). TRWPs are anticipated to initially reside on the road or the roadside and primarily disperse through stormwater effluents, road runoff and wastewater treatment plan effluents, thereby reaching various environmental compartments, including aquatic and terrestrial ecosystems (An et al., 2020; Magnusson et al., 2016.; Xu et al., 2020). Among these TRWPs, 1,3-diphenylguanidine (DPG) has emerged as one of the highly leachable compounds (Jin et al., 2021; Müller et al., 2022; Seiwert et al., 2020; Unice et al., 2015; Wagner et al., 2018). As a secondary vulcanization accelerator commonly employed in the rubber industry, the presence of DPG has been widely observed in water samples worldwide, with concentrations ranging from ng/L to mg/L (Marques Dos Santos et al., 2022; Müller et al., 2022; Schulze et al., 2019; Zahn et al., 2019). Furthermore, DPG has garnered increased attention due to its detection in human samples. A recent study revealed the DPG detection in human urine, with concentrations up to 0.79 ng mL^{-1} (Li & Kannan, 2023). Additionally, median concentrations of 1.79 ng mL^{-1} and 0.35 ng mL^{-1} of DPG was detected in human maternal serum and infant cord serum, respectively (Tang et al., 2022).

In recent years, several studies have already highlighted the potential health impacts of DPG exposure (Ghanadi et al., 2023; Kole et al., 2017; Schulze et al., 2019). Through in vivo experiments, DPG exposure has found to yield severe deformities, a lack of eye and body pigmentation in fathead minnow embryos (Chibwe et al., 2022; Kolomijeca et al., 2020). In vitro experiments have suggested that DPG exposure can lead to the decrease of cells viability and

damage cell mitochondrial proton leak (Marques Dos Santos et al., 2022). Furthermore, the introduction of DPG into water treatment facilities can lead to further questions as there is disinfection by products formed in the disinfection process, raising concerns regarding the toxicity of DPG Transformation Products (TPs).

Chlorine is commonly used as an oxidant in water treatment plants (WTPs) for drinking water treatment in Europe and the US, and to a lesser extent in some wastewater treatment plants (WWTPs) (Benitez et al., 2011; Quintana et al., 2014; Seidel et al., 2005). While chlorine is effective in degrading DPG, chlorination of DPG results in by-products such as chloroform and, haloacetonitriles (HANs) and chlorinated TPs. Additionally, the formation of nitrosamines during chlorination, with nitroso-dimethylamine (NDMA) being a prominent example, has been found to be closely associated with vulcanization agents. TWPs have been identified as potent NDMA precursors (Beita-Sandí et al., 2019; Ghanadi et al., 2023). The formation of dimethylamine (DMA), another important compound, has been observed in both the presence and absence of chloramine. Furthermore, studies have demonstrated an increase in the formation of NDMA and N-nitrosopiperidine (NPIP) from rubber gaskets over a 14-day exposure to chlorinated water. These findings highlight the need for further investigation into the implications of DPG in water treatment facilities and the potential risks associated with its transformation products. A subsequent study has indicated that some chlorinated transformation products, such as 1,3-bis-(4-chlorophenyl) guanidine showed higher cytotoxicity than DPG itself using in vitro bioassays (Marques Dos Santos et al., 2022). However, data is still sparse in regards to DPG transformation and toxicity under different chlorine and chloramine dosages. This information is vital for the sustainable management practices of disinfection and water treatment processes.

Another frequently used disinfectant for maintaining a disinfectant residual in municipal drinking water is monochloramine. Monochloramine (NH_2Cl), produced by the reaction between ammonia and chlorine, has emerged a viable alternative to chlorine for the disinfection process in recent years

(Allard et al., 2018; Duirk et al., 2005; Vikesland et al., 1998). Monochloramine has been verified to be more stable than chlorine in natural organic matter (NOM) (W. Hu et al., 2021), and thus generally resulted in lower concentrations of trihalomethanes (THMs), haloacetic acids (HAAs), and total organic halogen (TOX) (Bougeard et al., 2010; Hua & Reckhow, 2007). While the chlorination of DPG has been studied previously (Marques Dos Santos et al., 2022; Sieira et al., 2020), the number of studies evaluating monochloramine reactivity with DPG are still limited. As two of the most frequently used disinfectants in WTPs, the comparation between chlorine and NH_2Cl on DPG has not been assessed.

Thus, the aim of this work was to compare the effects of disinfection treatment methods of DPG based on chorination and chlomination of DPG. This includes DPG degradation by chlorination and, identification of TPs by LC-QtoF, and cytotoxicity assessment by cell based in-vitro assays. To compare reactivity of DPG with chlorine and monochloramine, this study investigated the reaction kinetics of monochloramination of DPG at different pH levels, building upon previous research (Sieira et al., 2020). The author also evaluates the toxicity and bioenergetics of disinfection products generated by chlorine and monochloramine at different dosages. The author selected a liver cancer cell line (HepG2) and a human leukemia monocytic cell line (THP-1) as in vitro cell models to enhance understanding of DPG disinfection product toxicity. As a widely used cell line, HepG2 represents the primary function of the human liver in first-pass detoxification, while THP-1 cell line, a human leukemia monocytic cell line, has been extensively used to study monocyte/macrophage functions. Additionally, the author investigate the disruption of energy metabolism induced by DPG disinfection products using the HepG2 cell line. Furthermore, genotoxic potential of disinfection products under different treatment oxidant doses were indicated by p53 cells. By identifying the chlorination and chloramination by-products at different stages, this work gained new insight into the varying cytotoxicity levels associated with these products.

1.2 Purpose and Scope

In light of the increasing demand for fresh water, the issues of the residual disinfection, DPG treatment efficiency and DPG related TPs in drinking water have become crucial. Thus, the necessity and the significance of this research will be accomplished by the following objective:

1) To investigate and compare the effects of UV, chlorine, monochloramine on the degradation and decomposition of DPG and to explore the disinfection by-products of DPG under different conditions.
2) To investigate TPs on different treatment conditions and assess the cytotoxicity effect of disinfection by-products of DPG and provide more thoughts for water treatment of roadwear and tirewear compounds.

1.3 Structure

The overall thesis structure is summarized in Figure 1.1. In Chapter 1, the research background, problem statement, objectives, and thesis structure are briefly introduced. Chapter 2 reviews the existing literature concerning halamine measurement in water, as well as the occurrence and treatment of tire wear particles in the aquatic environment. Moving on to Chapter 3, a comparison of various disinfection methods in terms of DPG degradation and kinetics study of monochloramination of DPG is presented. Shifting the focus to Chapter 4, the toxicity of transformation products is investigated through *in vitro* experiments. In Chapter 5, which extends the scope of Chapter 3, the identification of transformation products of DPG is primarily addressed, and the differences in toxicity found in Chapter 4 are explained.. Finally, Chapter 6 offers a summary of the major research findings and scientific contributions, while also providing recommendations for future research directions.

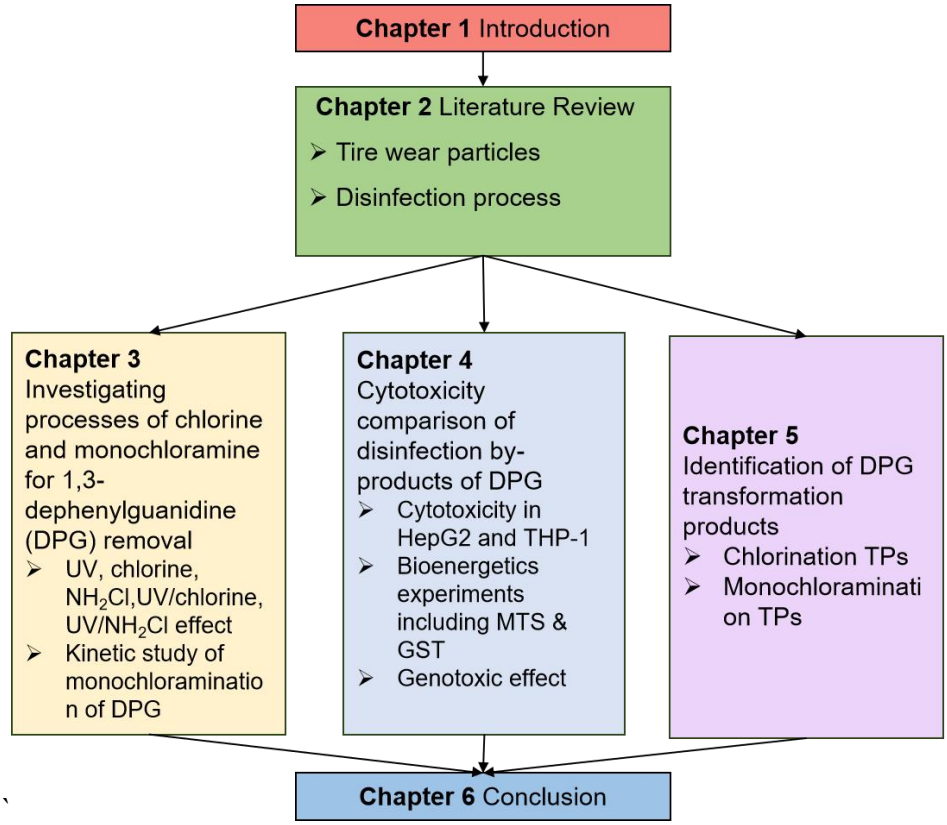

Figure 1.1 Structure of this study

2. LITERATURE REVIEW

2.1 Disinfectants

The disinfection process in a water treatment plant is a crucial step that aims to remove or inactivate harmful microorganisms, such as bacteria, viruses, and parasites, from the water supply. It helps ensure that the treated water is safe for consumption and minimizes the risk of waterborne diseases.

2.1.1 Chlorination

As most widely used disinfectant, chlorine can be added to water in the form of chlorine gas, sodium hypochlorite (liquid bleach), or calcium hypochlorite (solid form). Hypochlorous acid (HOCl) are produced when all forms of chlorine react with water. The formation of hypochlorite by the dissociation of HOCl is shown in the following Eq. (2-1):

$$HOCl \leftrightarrow H^+ + OCl^- \qquad (2\text{-}1)$$

Chlorine plays a very effective role in pathogenic microorganism removal and the dosing can be controlled easily. Chlorine reacts with organic matter and microorganisms in the water, destroying their cellular structures and preventing their growth. It provides residual disinfection to maintain water quality throughout the distribution system. However, the byproducts and incompletely oxidized compounds present in chlorinated water increasing the toxicity have become a important issue in recent years (Ishaq et al., 2018).

2.1.2 Chloramine

Chloramines are formed by combining chlorine (Cl_2) with ammonia (NH_3), as showin in the Eq. (2-2):

$$NH_3 + HOCl \leftrightarrow NH_2Cl + H_2O \qquad (2\text{-}2)$$

Chloramines are a milder and longer-lasting disinfectant compared to free chlorine. Compared to chlorine, monochloramine is 200 times weaker in oxidation (Guay et al., 2005). On the other hand, chloramines provide a more stable residual disinfection effect and reduce the formation of disinfection

byproducts (DBPs) compared to chlorine alone by generating less amount of trihalomethanes (THM) and haloacetic acids (HAA). However, the formation of N-nitrosodimethylamine (NDMA) by chloramination should also be paid attention to.

2.1.3 Chlorine dioxide

Chlorine dioxide (ClO_2), serves as both a disinfectant and an oxidant, offers unique chemical benefits that complement the conventional use of chlorine. With its remarkable efficacy in managing waterborne pathogens, chlorine dioxide stands out for its ability to minimize the formation of halogenated disinfection byproducts (DBPs). This versatile compound demonstrates broad-spectrum microbiocidal activity, proving as effective as chlorine against viruses, bacteria, and fungi, while surpassing chlorine in the inactivation of encysted parasites such as *Giardia* and *Cryptosporidium*.

2.1.4 Ozone

Ozone (O_3), known for its powerful oxidizing and disinfecting properties, is generated through the passage of oxygen via electrical discharge or ultraviolet light. Upon contact with organic matter and microorganisms, ozone rapidly reacts and disrupts their cellular structure, rendering them inactive. This versatile disinfectant effectively targets a wide range of pathogens, including bacteria, viruses, and protozoa. Additionally, ozonation contributes to the reduction of taste and odor compounds in water. The disinfection process relies on the generation of free radicals as potent oxidizers, surpassing the effectiveness of chlorination against bacteria and viruses. However, the limited solubility of ozone in water significantly hampers its disinfection capacity, while its reactive nature causes any ozone residual to dissipate rapidly. The absence of a long-lasting residual can be considered a drawback, potentially allowing for microbial regrowth and posing challenges in assessing the disinfection process's efficacy.

2.1.5 Ultraviolet (UV)

Ultraviolet (UV) light is used as a physical disinfection method. Water is exposed to UV light, which damages the DNA of microorganisms, rendering them unable to reproduce. UV light is effective against a broad range of pathogens, including bacteria, viruses, and protozoa and does not introduce chemical byproducts.

2.1.6 UV based disinfection

UV based disinfection involves the combination of UV light and other disinfection methods such as UV/chlorine, UV/NH_2Cl and UV/ClO_2. Radicals including $HO^{\bullet}$, $Cl^{\bullet}$, and $ClO^{\bullet}$ were generated in the UV based disinfection (Zhao et al., 2022) which were very effective in destroying any remaining microorganisms. The process typically includes the following steps (Bulman et al., 2019; Guo et al., 2017) (take UV/chlorine as an example):

$$HOCl \xrightarrow{hv} HO^{\bullet} + Cl^{\bullet} \quad (2\text{-}3)$$

$$OCl^{-} \xrightarrow{hv} O^{\bullet -} + Cl^{\bullet} \quad (2\text{-}4)$$

$$OCl^{-} \xrightarrow{hv} Cl^{-} + O(3P) \quad (2\text{-}5)$$

$$OCl^{-} \xrightarrow{hv} Cl^{-} + O(1D) \quad (2\text{-}6)$$

$$O(3P) + O_2 \rightarrow O_3 \quad (2\text{-}7)$$

$$HOCl + HO^{\bullet} \rightarrow ClO^{\bullet} + H_2O \quad (2\text{-}8)$$

$$OCl^{-} + HO^{\bullet} \rightarrow ClO^{\bullet} + OH^{-} \quad (2\text{-}9)$$

$$Cl^{\bullet} + OCl^{-} \rightarrow ClO^{\bullet} + Cl^{-} \quad (2\text{-}10)$$

$$Cl^{\bullet} + HOCl \rightarrow ClO^{\bullet} + Cl^{-} + H^{+} \quad (2\text{-}11)$$

$$O(3P) + OCl^{-} \rightarrow ClO_2^{-} \quad (2\text{-}12)$$

$$O_3 + OCl^{-} \rightarrow O_2 + ClO_2^{-} \quad (2\text{-}13)$$

$$HO^{\bullet} + ClO^{\bullet} \rightarrow H^{+} + ClO_2^{-} \quad (2\text{-}14)$$

$$2ClO^{\bullet} + OH^{-} \rightarrow OCl^{-} + H^{+} + ClO_2^{-} \quad (2\text{-}15)$$

2.1.7 Other Disinfection Methods

Other Disinfection Methods: In addition to the above methods, water treatment plants may employ alternative disinfection techniques such as chloramination, chlorine dioxide, hydrogen peroxide, or advanced oxidation processes (AOPs) depending on specific requirements and regulations.

2.2 Disinfection By-products

DBPs arise from the reaction of disinfectants used in water treatment plants with bromide and/or natural organic matter (NOM) in the source water. The formation of DBPs is affected by multiple factors, including: (1) the type of disinfectant, (2) the dose of disinfectant, (3) the residual disinfectant, (4) the conditions of disinfection (reaction time, temperature, and pH), (5) the constituents of water, and (6) the concentration and properties of NOM. Increased DBP formation is observed with higher disinfectant doses and residuals. Shorter reaction times can elevate trihalomethanes (THMs) and haloacetic acids (HAAs) concentrations, while longer reaction times may convert certain DBPs into end products like tribromine acetic acid and bromoform. Haloacetonitriles (HAN) and haloketones (HK) undergo decomposition. Higher temperatures accelerate reactions, necessitating higher chlorine concentrations for effective disinfection, which leads to increased formation of halogenated DBPs. Elevated temperatures also enhance the breakdown of tribromine acetic acids, HAN, and HK. At higher pH levels, more hypochlorite ions form, reducing the efficiency of chlorine disinfection. High pH values favor THM formation, whereas low pH values promote HAA formation. Hydrolysis, driven by increased pH values, facilitates the decomposition of HAN and HK. Trihalomethanes, including trichloromethane (chloroform), bromine dichloromethane (BDCM), chlorine dibromomethane, and tribromomethane, were the first DBPs discovered in chlorinated water. Bromine presence leads to the formation of brominated trihalomethanes. Trihalogenic DBPs, along with transition products like trihaloacetonitriles, contribute to the formation of trihalomethanes.

2.3 Tire Wear Particles

Tire wear particles (TWP), also known as tire-derived particles or tire debris, refer to small fragments or particles that are generated from the wearing down of vehicle tires during usage. They are released into the environment as fine particulate matter composed of various rubber compounds, fillers, additives, and trace metals, as shown in Figure 2.1. As vehicles travel on roads, the friction between the tires and the road surface causes gradual abrasion and erosion of the tire tread. This wear process leads to the release of tiny rubber particles into the environment, which are collectively referred to as tire wear particles.

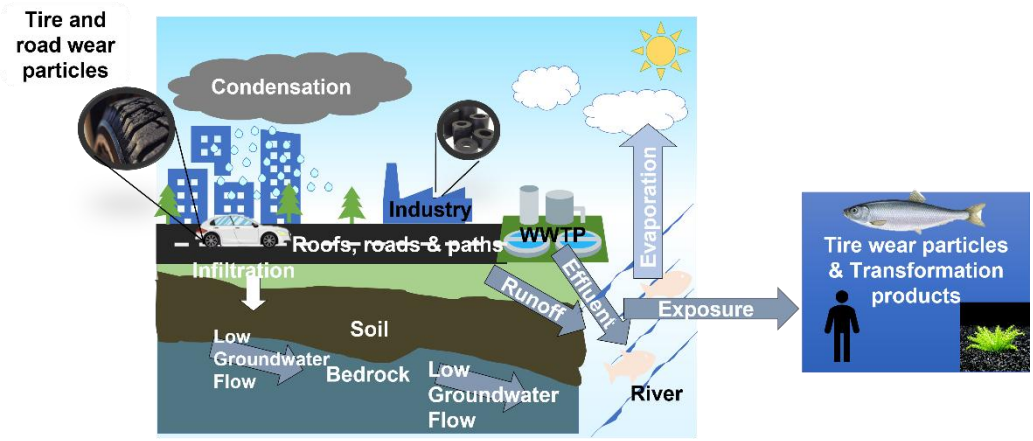

Figure 2.1 Introduction of TWP including the generation, introduction into aquatic environment

Tire wear particles are typically composed of rubber compounds that make up the tire tread. These rubber particles can vary in size, ranging from large visible chunks to microscopic particles. They can also contain various additives, such as fillers, reinforcing agents, plasticizers, and chemicals used in tire manufacturing. Due to their small size and ubiquity, tire wear particles can become widely dispersed in the environment. They can be found on road surfaces, in the air, and in various water bodies, including rivers and oceans. These particles can be transported by wind, rainwater runoff, and other natural processes, potentially reaching ecosystems far from their original source. According to the reference, ten tire leachables have been identified by the researchers as showin in Table 2.1. Among them, it has been indicated that DPG is the most leachable particles.

Table 2.1 Detail of ten identified tire leachables.

Name	Structure	Class	Chemiacal Structrure	Reference
N,N'-Diphenylguanidine	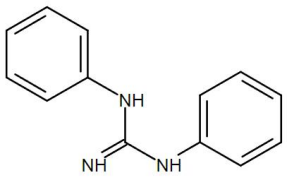	Accelerator of vulcanisation	$C_{13}H_{13}N_3$	(Baumann & Ismeier, 1998; Peter et al., 2018; Seiwert et al., 2020; Unice et al., 2015)
ε-Caprolactam	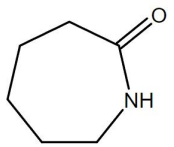	Product of decomposition	$C_6H_{11}NO$	(Seiwert et al., 2020)
Benzothiazole	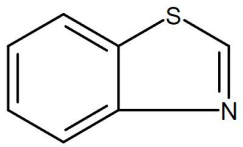	Product of decomposition	C_7H_5NS	(Seiwert et al., 2020; Unice et al., 2015)

2-Mercaptobenzothiazole	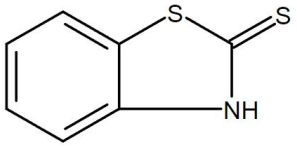	Accelerator vulcanisation	$C_7H_5NS_2$	(Kloepfer et al., 2004; Seiwert et al., 2020)
4-Hydroxydiphenylamine	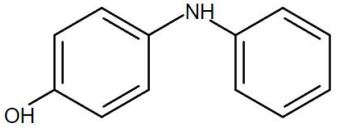	Decomposition product	$C_{12}H_{11}NO$	(Unice et al., 2015)
Tributylamine	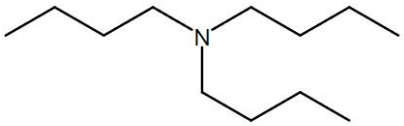	Impurity of vulcanisation accelerator	$C_{12}H_{27}N$	(Seiwert et al., 2020)
Dibenzylamine	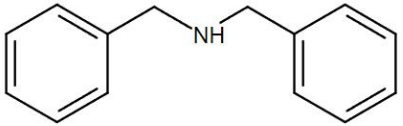	Activator of vulcanisation	$C_{14}H_{15}N$	(Baumann & Ismeier, 1998)

N,N'-Diphenylurea	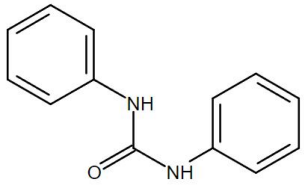	Retarder of vulcanisation	$C_{13}H_{12}N_2O$	(Baumann & Ismeier, 1998; Unice et al., 2015)
N,N'-Dicyclohexylurea	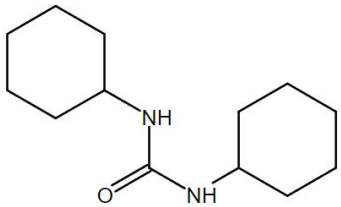	Other	$C_{13}H_{24}N_2O$	(Peter et al., 2018; Seiwert et al., 2020)
N-(1,3-Dimethylbutyl)-N'-phenyl-p-phenylenediamine	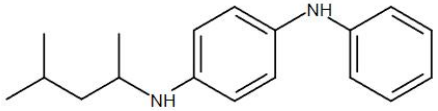	Antioxidant	$C_{18}H_{24}N_2$	(Baumann & Ismeier, 1998; Unice et al., 2015; Wagner et al., 2018)

2.3.1 Occurrence in the aquatic environment

TWPs can be introduced into the aquatic environment through the process of runoff. When it rains or snows, water flows over surfaces such as roads and parking lots, picking up and carrying TWPs along with it. This runoff water eventually makes its way into rivers, lakes, streams, and other water bodies, introducing TWPs into aquatic environments. The process of TWP introduction into aquatic three primary pathways: on-road wear, off-road wear, and artificial abrasion (Müller et al., 2022; Seiwert et al., 2020):

On-road wear: On-road wear occurs when vehicles, particularly automobiles, travel on paved surfaces. As tires roll on roads, friction and mechanical forces cause the gradual erosion of tire tread, leading to the generation of TWPs. Factors such as vehicle weight, tire design, road conditions, and driving patterns can influence the rate of on-road wear and TWP release.

Off-road wear: Off-road wear involves the generation of TWPs from vehicles operating on non-paved surfaces such as construction sites, industrial areas, or unpaved roads. Activities like mining, agriculture, and off-road recreational use can contribute to significant TWP emissions. The rougher surfaces and abrasive materials encountered off-road can accelerate tire wear and increase TWP production.

Artificial abrasion: Artificial abrasion refers to intentional processes that generate TWPs for various purposes. Examples include tire testing facilities, simulated road wear studies, or controlled experiments aimed at investigating TWP properties, behavior, or environmental impacts. These activities involve subjecting tires to specific conditions, such as specialized machines or abrasive surfaces, to replicate or accelerate wear processes.

The concentration of TWP in soil or water hinges on transport, translocation, transformation, degradation, and export. Coarse TWP are generally deposited at roadside where they interact with traffic-related particles and atmospheric deposition, forming aggregates and making source identification challenging. Depending on their size, TWP and aggregates may be

transported off streets by surface runoff, street cleaning or resuspension. During rainfall, TWP translocation is dependent on installed infrastructure for road runoff water collection and treatment. Without proper systems, TWP can be transferred to roadside soil or nearby waterways. In urban areas, runoff is often collected with municipal wastewater and treated, albeit with varying degrees of efficiency depending on particle size and treatment process. During heavy rainfall, wastewater may be discharged into surface waters without treatment. Treatment of road runoff is usually based on filtration or sedimentation, but its efficiency depends on particle characteristics and treatment process. Studies have shown that removal efficiency increases with particle size and hydraulic retention time, but it is generally inefficient for fine particles. This results in contamination, especially during stormwater events. Specific data on TWP is scarce, and global estimation of TWP reaching aquatic environments is currently impossible. However, local studies have been conducted, with TWP concentration decreasing with increased distance from the road. In general, TWP concentration is higher in sediment than in surface water due to particle settling. Further research is required to understand the fate of TWP, including processes like aggregation, sedimentation, and aging.

2.3.2 Effect on environment and human

TWPs can contribute to air pollution by releasing particulate matter and chemical compounds into the atmosphere. Their presence in air can potentially lead to respiratory issues, cardiovascular problems, and adverse health effects when inhaled. TWPs can also contaminate soils, affecting their quality and potentially impacting soil-dwelling organisms. When washed off roads or deposited in water bodies, TWPs can enter aquatic environments, posing risks to aquatic organisms and potentially affecting ecosystem health. Additionally, TWPs contain a variety of chemicals, including polycyclic aromatic hydrocarbons (PAHs), heavy metals, and organic additives. These substances have the potential to leach into the environment, leading to soil and water contamination. The long-term effects of TWP-related chemical contamination on ecosystems and human health are subjects of ongoing research.

TWPs have been reported to post threats to environment and human beings. Research indicates that various organisms inadvertently ingest these particles, leading to both immediate and long-term toxic effects in aquatic life (Redondo-Hasselerharm et al., 2018; Wik & Dave, 2009). Studies have shown that tire leachates negatively impact the development and survival of certain fish species' embryos. Furthermore, these leachates have been observed to cause harmful reactions in both microalgae and mussels (Kolomijeca et al., 2020). It has been reported that tire leachate caused both acute and sub-lethal responses in microalgae and in mussels. Specific chemicals found in tire leachates, such as benzothiazoles and aryl-amines, are linked to these toxic effects, though other uncharacterized chemicals may also contribute (Chibwe et al., 2022). Recent findings also highlight the risk of significant quantities of certain tire-derived chemicals entering waterways, posing potential ecological threats (Johannessen et al., 2022).

2.4 High-Resolution Mass Spectrometry

Non-targeted analysis (NTA) is an approach that complements targeted analysis by identifying compounds and their transformation products that may not be detected using targeted methods. NTA allows for the screening of unknown compounds without prior knowledge of their structure, adduct formation, or fragmentation. Another type of non-targeted analysis is suspect screening, which involves the screening of known suspect compounds based on prior information such as exact mass, isotope pattern, molecular formula, or adduct formation. NTA does not require precursor ion input, enabling the detection of a wider range of contaminants and their transformation products. Moreover, while most enforcement agencies focus on known priority pollutants, which represent only a fraction of the chemicals in the environment, NTA provides a more comprehensive understanding of the contaminants present, adding value to environmental monitoring efforts.

High-resolution mass spectrometry (HRMS) instruments, such as time-of-flight (TOF) or Orbitrap instruments, are commonly used in NTA to obtain accurate mass full scan MS data. Electrospray ionisation (ESI) is the most

popular ionisation technique with functions including munition compounds, personal care products, pharmaceuticals, illicit drugs, pesticides, and endocrine-disrupting hormones (Gledhill et al., 2019; Goeury et al., 2019; Petrie et al., 2016). Other techniques such as atmospheric pressure chemical ionisation (APCI) and atmospheric pressure photoionisation (APPI) are more effective for detecting less polar compounds (Gallampois et al., 2015). HRMS enables the determination of elemental compositions for precursor ions, fragment ions, and isobaric species through accurate mass measurements and isotope peaks. Fragmentation spectra of precursor ions provide information on the presence or absence of specific functional groups, aiding in structure interpretation. HRMS also allows for the monitoring of unknown chemicals and metabolites, providing valuable information during routine monitoring. The output from HRMS can be analyzed to generate two-dimensional plots or "heat maps" of compound occurrence, serving as reference fingerprints for subsequent sample comparisons (S. A. Snyder, 2014). NTA has proven to be valuable in monitoring the effectiveness of wastewater treatment processes, particularly in identifying transformation products for which commercial standards may not be available.

Over the past decade, there have been significant advancements in compound identification capabilities using HRMS and NTA approaches (Phillips et al., 2022). These methods have also been applied to the analysis of TWPs (Du et al., 2020) and their TPs as well as DBPs (Sieira et al., 2020). One significant study extracted particles from tires in artifficial freshwater, aiming to characterize leachables. They discovered 214 organic substances, 145 of which were classified as leachables by using HRMS (Müller et al., 2022). This study demonstrates the importance use of HRMS and NTA in identifying and analyzing the complex chemical makeup of TWPs.

2.5 Bioassay

2.5.1 In vitro based cells

2.5.1.1 HepG2 cells

HepG2 is a human hepatocellular carcinoma cell line that was derived from liver tissue. It is commonly used in biomedical research and drug development studies. HepG2 cells exhibit several characteristics of liver cells, including the ability to synthesize proteins and process drugs. They are also frequently used to study liver-related diseases, such as hepatitis and liver cancer. HepG2 cells are adherent and grow as a monolayer in culture. They have a relatively stable karyotype and retain many liver-specific functions, making them a valuable model for studying liver biology.

2.5.1.2 THP cells

THP-1 is a human monocytic cell line that was derived from the peripheral blood of a patient with acute monocytic leukemia. These cells have characteristics similar to monocytes and can be differentiated into macrophage-like cells by treatment with phorbol esters. THP-1 cells are widely used as a model for studying monocyte/macrophage biology, inflammation, and immune responses. They can be cultured in suspension and are often used in experiments that require a monocyte-like cell population.

2.5.2 Bioassay experiments

2.5.2.1 Cytotoxicity

A cytotoxicity assay is a test designed to evaluate the toxic effects of substances on cells. It measures the ability of a compound or agent to cause cell death or damage. Various cytotoxicity assays are available, including dye exclusion assays, metabolic activity assays, and membrane integrity assays. These assays provide information about the toxic effects of chemicals, drugs, or environmental factors on different cell types. Cytotoxicity assays are commonly used in drug discovery, toxicology studies, and environmental monitoring to assess the potential harmful effects of substances on living cells.

2.5.2.2 Bioenergy assessment

Bioenergy assessment refers to the measurement and evaluation of the energy content or metabolic activity of biological systems or processes. It involves assessing the energy production or utilization by living organisms, typically through various biochemical and physiological measurements. This assessment can provide insights into the energy status, efficiency, and overall functioning of biological systems. Bioenergy assessment is important in fields such as biochemistry, metabolism research, and studies related to energy balance, including exercise physiology and nutrition.

In recent years, the critical roles of mitochondrial and cellular metabolic processes in cell differentiation, cell proliferation, immune cell responses, hypoxia sensing, apoptosis, substrate oxidation, and ATP production have been recognized (Dimeloe et al., 2017; Ochocki & Simon, 2013; Smith et al., 2012). Dysfunctions in mitochondrial and metabolic pathways have been implicated in various pathologies. Consequently, there has been a surge of interest in identifying mitochondrial and metabolic drug targets. Consequently, sensitive and direct measurements of metabolic pathway function are essential to elucidate the specific and potential nonspecific targets of drug candidates. The mitochondrial stress test (MST) profile of Drug X (UK5099) (A. S. Divakaruni et al., 2013) indicates that dysfunction may occur in substrate oxidation and/or the electron transport chain/oxidative phosphorylation pathway (A. Divakaruni et al., 2014). These pathways involve substrate transport and the activities of rate-controlling proteins and enzymes such as glutaminases, CPT1a, pyruvate dehydrogenase (PDH), TCA cycle enzymes, electron transport, and oxidative phosphorylation machinery. The substrate-dependent pathways for pyruvate, glutamate, and succinate are depicted in Figure 2.3.

The glycolysis stress test (GST), depicted in Figure 2.4, is based on two essential energy-producing pathways in the cell: glycolysis and mitochondrial respiration. Throughout glycolysis, glucose undergoes conversion to lactate, leading to the release of protons into the extracellular media, which can be measured as the extracellular acidification rate (ECAR) using the XF Analyzer.

Moreover, the mitochondrial tricarboxylic acid (TCA) activity generates CO_2, which then hydrates and acidifies the media. During the assay, by inhibiting respiration, represented by oxygen consumption rate (OCR) with mitochondrial inhibitors targeting complex I and complex III (Rot/AA), the proton efflux rate from respiration can be calculated and subsequently subtracted from the total proton efflux rate, resulting in the determination of the glycolytic proton efflux rate (glycoPER). To validate the pathway specificity, 2-DG, an inhibitor of glycolysis, is introduced to arrest glycolytic acidification.

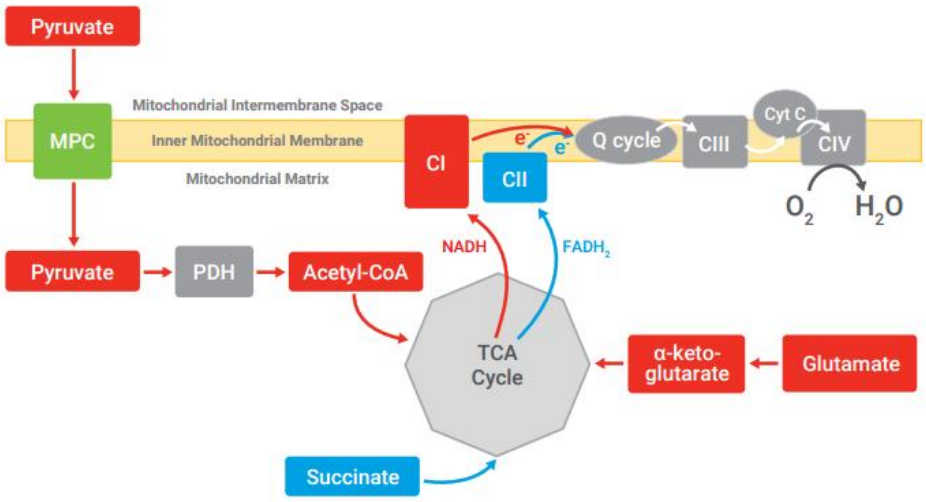

Figure 2.1 Principle of mitochondrial function, adapted form Agilent Seahorse XF protocol (Rogers, G. W. et al., 2018)

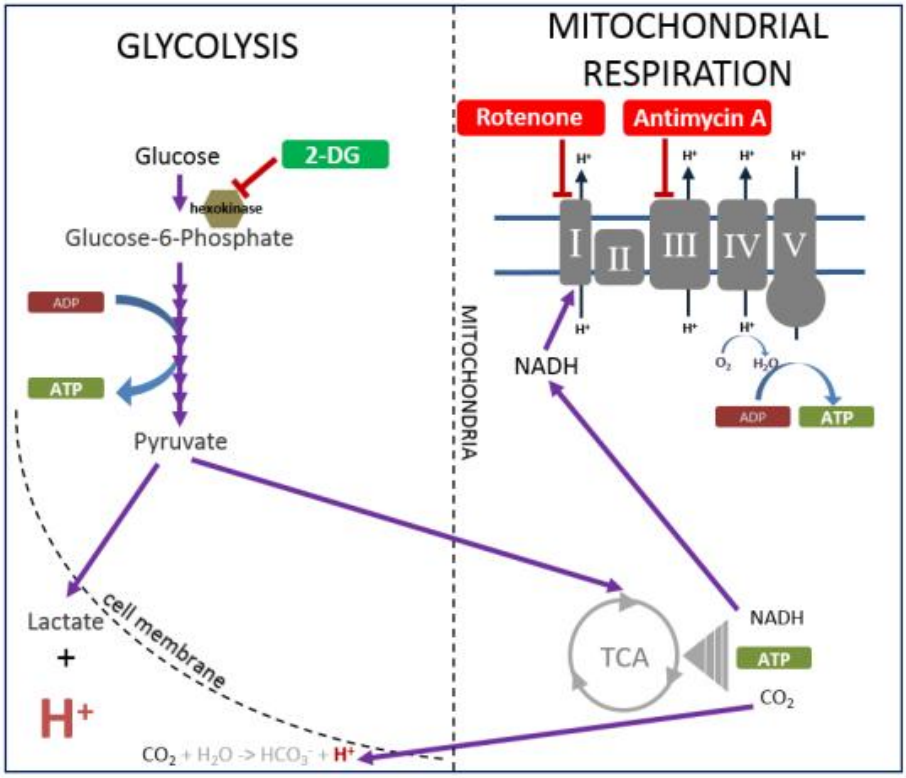

Figure 2.2 Principle of GST, adapted from Agilent Seahorse XF protocol. (Rogers, G. W. et al., 2018)

2.5.2.3 Genotoxic assessment

Genotoxicity assays are used to assess the potential of a substance to cause damage to genetic material, such as DNA, within cells. These assays evaluate the ability of a compound to induce mutations, chromosomal aberrations, or DNA damage. Genotoxicity testing is important for identifying substances that may have harmful effects on genetic material, potentially leading to the development of cancer or heritable genetic defects. Common genotoxicity assays include the Ames test (for mutagenicity), the comet assay (for DNA damage), and the micronucleus assay (for chromosomal damage). These assays are widely used in toxicology testing, drug development, and regulatory assessments to ensure the safety of chemicals and compounds.

2.5.2.4 Estrogen receptor alpha

Estrogen receptor alpha (ERα) is a protein that belongs to the nuclear receptor superfamily and is encoded by the ESR1 gene (Ali & Coombes, 2000).

It is one of the two main estrogen receptors, the other being estrogen receptor beta (ERβ). ERα is primarily expressed in various tissues, including the reproductive organs (such as the uterus and ovaries), mammary glands, bone, brain, and cardiovascular system (Ali & Coombes, 2000; Santen et al., 2009). As a transcription factor, ERα plays a critical role in mediating the effects of estrogen hormones, such as 17β-estradiol (E2). When E2 or other estrogen ligands bind to ERα, the receptor undergoes a conformational change, leading to its activation and subsequent translocation to the cell nucleus. In the nucleus, ERα binds to specific DNA sequences called estrogen response elements (EREs) located within target genes, and through protein-protein interactions, it recruits co-activators or co-repressors to modulate gene expression.

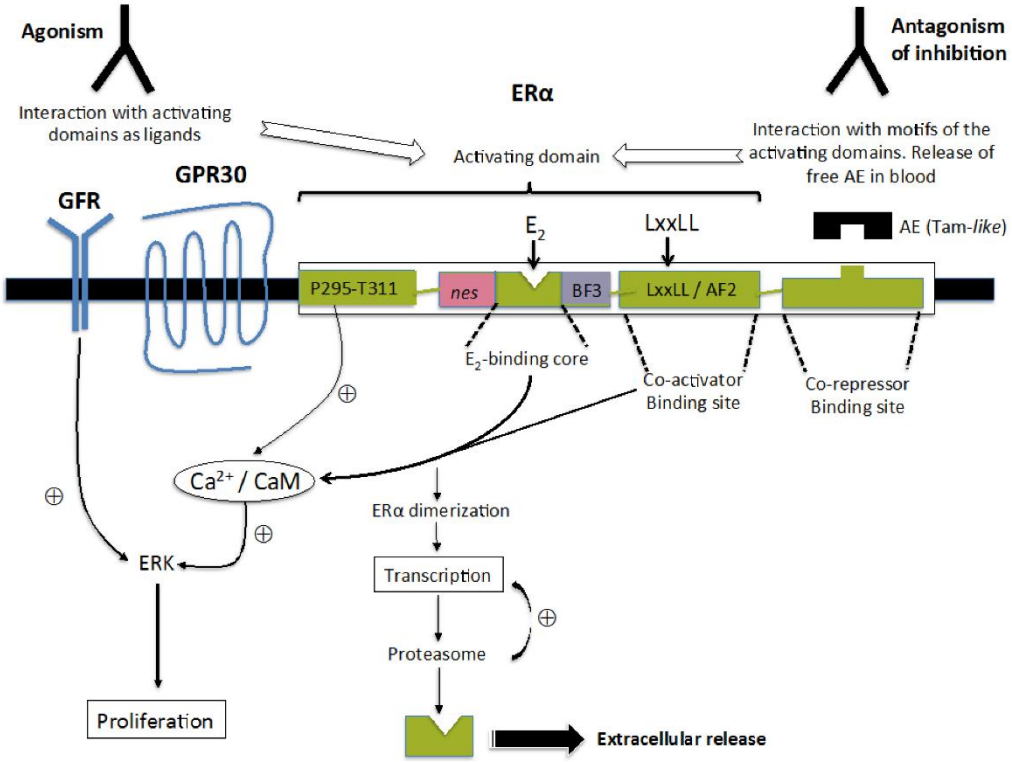

Figure 2.3 Principle of ERα antibodies able to induce extrogenic responses in breast cancer cells (Leclercq, 2018).

The activation of ERα regulates the expression of a wide range of target genes involved in various biological processes, including cell proliferation, differentiation, apoptosis, and reproductive functions. ERα signaling is particularly important in female reproductive physiology, where it controls the development and maintenance of the uterus, ovaries, and mammary glands. It

also plays a role in bone health, cardiovascular function, and cognitive processes. ERα is of significant clinical importance as well. Dysregulation of ERα signaling has been implicated in various diseases, including breast cancer. In estrogen receptor-positive (ER+) breast cancers, ERα is overexpressed, and its signaling pathway promotes tumor growth. Targeting ERα with selective estrogen receptor modulators (SERMs), such as tamoxifen and raloxifene, or selective estrogen receptor degraders (SERDs), such as fulvestrant, is a common therapeutic strategy for ER+ breast cancer.

2.5.2.5 P53

p53 is a crucial tumor suppressor protein that plays a key role in maintaining genome stability and preventing cancer development. Encoded by the TP53 gene, the p53 protein is one of the most frequently mutated genes in human cancers. Functioning as a transcription factor (Marei et al., 2021; Muller & Vousden, 2013), p53 regulates the expression of a wide range of genes involved in cell cycle control, DNA repair, apoptosis, and senescence. Its primary role is to monitor DNA integrity and initiate appropriate cellular responses upon detecting DNA damage or abnormalities. Upon exposure to DNA damage or stress signals, p53 becomes activated and accumulates in the cell nucleus. As shown in Figure 2.5, activation of p53 leads to the following cellular responses (Hafner et al., 2019; Marei et al., 2021):

(1) Cell Cycle Arrest: p53 halts cell cycle progression, allowing time for DNA repair before cell division. It upregulates the expression of genes such as p21, which inhibits cell cycle-promoting proteins.

(2) DNA Repair: p53 promotes the transcription of genes involved in DNA repair mechanisms, facilitating proper repair of damaged DNA before replication or transmission to daughter cells.

(3) Apoptosis: In cases of severe and irreparable DNA damage, p53 can initiate apoptosis, a programmed cell death process. This prevents the replication and propagation of cells with damaged DNA, reducing the risk of cancer development.

(4) Senescence: p53 can trigger cellular senescence, a state of irreversible growth arrest. Senescent cells lose their ability to divide, impeding tumor formation.

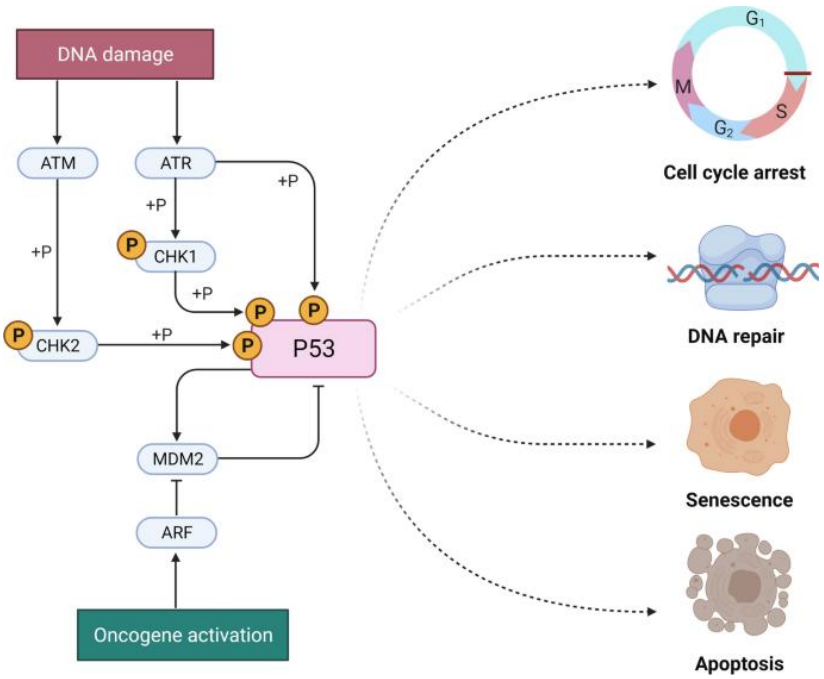

Figure 2.4 Principle of p53 gene (Marei et al., 2021).

Loss or mutation of the p53 gene function increases susceptibility to cancer development. TP53 mutations can result in the production of defective or non-functional p53 proteins, impairing their ability to properly regulate cell cycle checkpoints and DNA repair processes. Consequently, cells with damaged DNA can evade apoptosis or senescence, leading to uncontrolled proliferation and contributing to tumor formation and progression.

3. INVESTIGATING PROCESSES OF CHLORINE AND MONOCHLORAMINE FOR 1,3-DEPHENYLGUANIDINE (DPG) REMOVAL

This chapter is about the comparison of effects of UV, chlorine and monochloramine processes on the degradation of the rubber and polymer-related

chemical 1,3-Dephenylguanidine (DPG), which has emerged as a relevant water contaminant. Disinfection by-products of DPG were analyzed. The experimental process is described in Figure 3.1

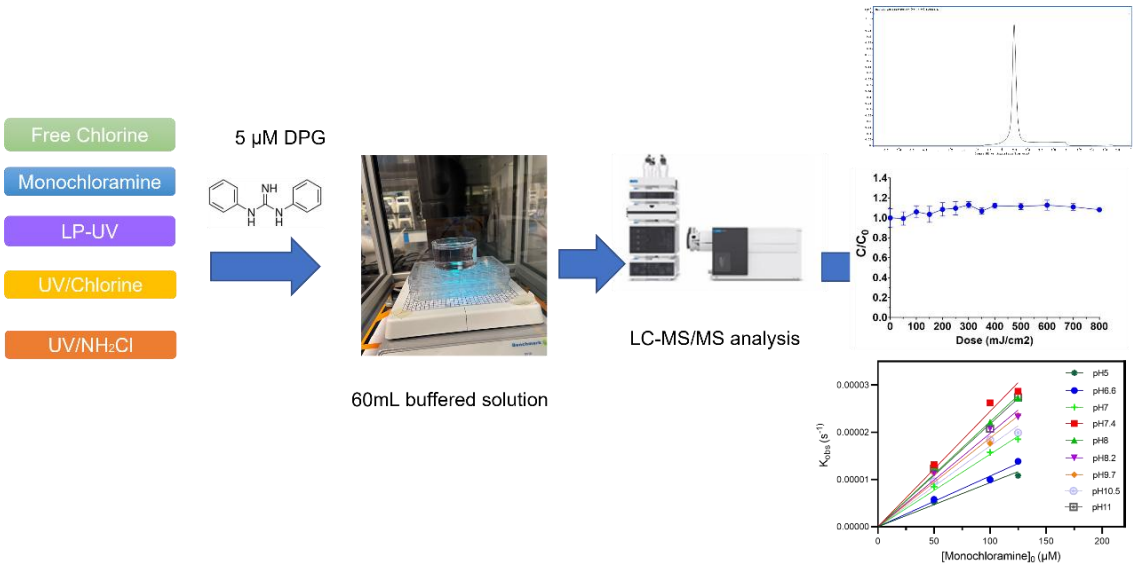

Figure 3.1 Experimental process of chapter 3

3.1 Materials and Methods

3.1.1 Reagents

Ultrapure water (MilliQ, Millipore) was used to prepare all solutions in this research. Reagent-grade chemicals, including, sodium phosphate monobasic 99%, disodium hydrogen phosphate 99%, sodium hypochlorite solution 4.0-5.0%, 1,3-dephenylguanidine 97%, ascorbic acid 99%, benzoic acid 99.5%, 1,4-dimethoxybgenzene 99%, nitrobenzene 99% and trans-cinnamic acid 99% were all purchased from Sigma-Aldrich. LC-MS grade (Optima LC/MS) solvents and reagents including methanol, acetonitrile, 2-proponol and formic acid were purchased from Fisher Scientific.

3.1.2 Oxidants

Two oxidants (chlorine and chloramine) were included in the whole experiment. Free chlorine stock solutions were prepared by diluting 4.0-5.0% NaClO solution. A High concentration of NH_2Cl stock solution was prepared

daily by dropwise adding NaClO into vigorously stirred NH_4Cl (pH adjusted to 8 with NaOH) at an NH_3-N/Cl molar ratio of 1.4 which had been equilibrated in a 4ºC refrigerator for at least 30 min. The concentrations of chlorine in-stock solutions were standardized by using the Dipropyl-P-Phenylenediamine (DPD) colorimetric methods while NH_2Cl in-stock solutions were standardized by using the indophenol methods, with a HACH DR900 instrument.

3.1.3 UV system

The UV irradiation experiments were performed with a VIQUA D4 UV lamp (254 nm, 40 W, Trojan Technologies) placed in a shuttered transparent box. A stir plate (Fisher Scientific) was placed in the center of the box, on the top of which was a KIMAX 60 × 35 mm crystallizing dish (SCHOTT company) containing a stirrer and the sample, as shown in Figure 3.2. The reactors are cylindrical glass objects with a diameter of 60 mm and a height of 17 mm.

To evaluate the effects of UV alone, a same 60 mL buffered solution with an initial 20 μM DPG concentration was directly exposed to a UV light at UV wavelengths of 254 nm and stirred at 400 RPM. The total UV fluence was appointed at 800 mJ/cm^2. The time interval was divided into 12 parts, and at each time point 100 μL sample was taken out and prepared for DPG degradation analysis. The total volume taken out from the reactor was 1.1 mL, with decrease within 2% of the original solution, therefore had minmal influence on the total UV fluence.

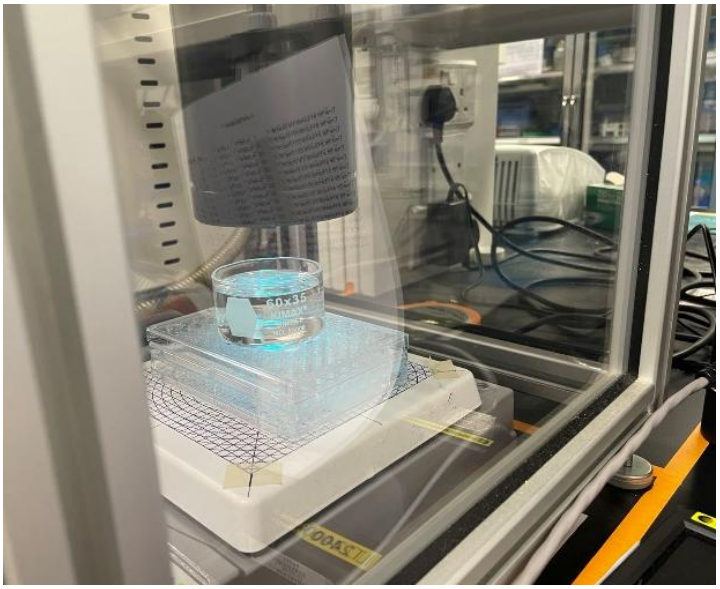

Figure 3.2 Experiment setup of UV irradiation

3.1.4 Disinfection experiment procedures

To compare the effects of oxidant, a 60 mL buffered solution (buffered 5mM phosphate buffer) with an initial 5 μM DPG concentration were prepared. For oxdidation experiments, one of the oxidant stock solutions was injected to the solutions to obtain the oxidant different concentration and initial the reactor. For UV based disinfection experiments, the experiments was intialiazed by injecting the oxidants to the sample immediately after the exposure to the UV. The mixed solution in the reactor was stirred at 400 RPM. Freshly prepared 100 mM sodium thiosulfate ($Na_2S_2O_3$) was applied as the quenching agent. After pre-calculated time intervals, samples were quenched at a $Na_2S_2O_3$: Cl_2 molar ratio of 1.25:1 and collected for analysis of DPG degradation.

The kinetic study of monochloramine was carried out similarly. Monochloramine was injected at an excess amount ([Oxidant] : [DPG] ratio of 10, 20, 100) into the solutions to initial the reactor. At different time points, 1mL of the solution was taken out and quenched by freshly prepared 100 mM ascorbic acid (AA) at an AA: Cl_2 molar ratio of 1.25:1 and collected for analysis of DPG degradation in LC-MS/MS.

3.1.5 Preparation of buffer

To control the pH of the reaction matrix, the 5mM phosphate buffer was prepared. 500mM phospate buffer (listed in Table 3.1) and 60x enriched ironic strength solution was initially prepared. To prepare 5mM phosphate buffer, 10mL high concentration buffer and 16.7mL enriched ironic strength was diluted by using MilliQ water to 1 L. The exact pH was adjusted by adding in 1M sodium hydroxide solution or 5% phosphate acid solution. The receipt for phosphate buffer is listed as below.

Table 3.1 Preparation of phosphate buffer

pH	Concentration	Monosodium phosphate	Disodium phosphate
5	500 mM	59.68 g L^{-1} (497.4 mM)	0.367 g L^{-1} (2.585 mM)
6	500 mM	55.27 g L^{-1} (460.7 mM)	5.580 g L^{-1} (39.31 mM)
7	500 mM	32.30 g L^{-1} (26.92 mM)	32.76 g L^{-1} (23.08 mM)
8	500 mM	6.251 g L^{-1} (52.10 mM)	63.58 g L^{-1} (447.9 mM)
9	500 mM	0.683 g L^{-1} (5.694 mM)	70.171 g L^{-1} (494.3 mM)
10	500 mM	0.0624 g L^{-1} (0.5203 mM)	70.909 g L^{-1} (499.5 mM)

3.2 LC/MS

Following the previous work , a 6495c liquid chromatography/triple quadrupole (LC/QQQ) (Agilent Technologies) assembled with a 1290 Infinity II high performance liquid chromatography (HPLC) was applied to analyze the concentration of DPG and study the kinetics. The detail of the method and the gradient is summarized in Appendix C. MS/MS acquisition was operated in positive-ion mode with Dynamic multiple reaction monitoring (DMRM). The capillary voltage was set at 2.5kV and the flow and temperature of the gas was 15 L min^{-1} and 150ºC. MassHunter Optimizer (Agilent Technologies) was used to select the optimum precursor and fragment ions. A 5 μL sample injection was

performed, followed by multi-wash. External calibration curves were prepared using concentrations ranging from 0.1 μg L^{-1} to 500 μg L^{-1} Data analysis was performed with MassHunter package software (Agilent Technologies). Quantification was performed in MassHunter Quantitative (QQQ Quant-My-Way) using a calibration curve of DPG and concentration in different stages obtained.

3.3 Results

3.3.1 Standard curve achived for DPG

MS chromatograph of 500 μg/L standard mixture were obtained in Figure 3.3 with higher peak representing DPG, analyzed by the Agilent MassHunter Qualitative Analysis 10.0 software. Acquisition of standard calibration curves and quantification of the concentration were obtained by the Agilent MassHunter Quantitative Analysis (for QQQ) software. As presented in Figure 3.3, the calibration curve was developed for DPG. Twelve standards were prepared and used for DPG with R^2 >0.99 achieved.

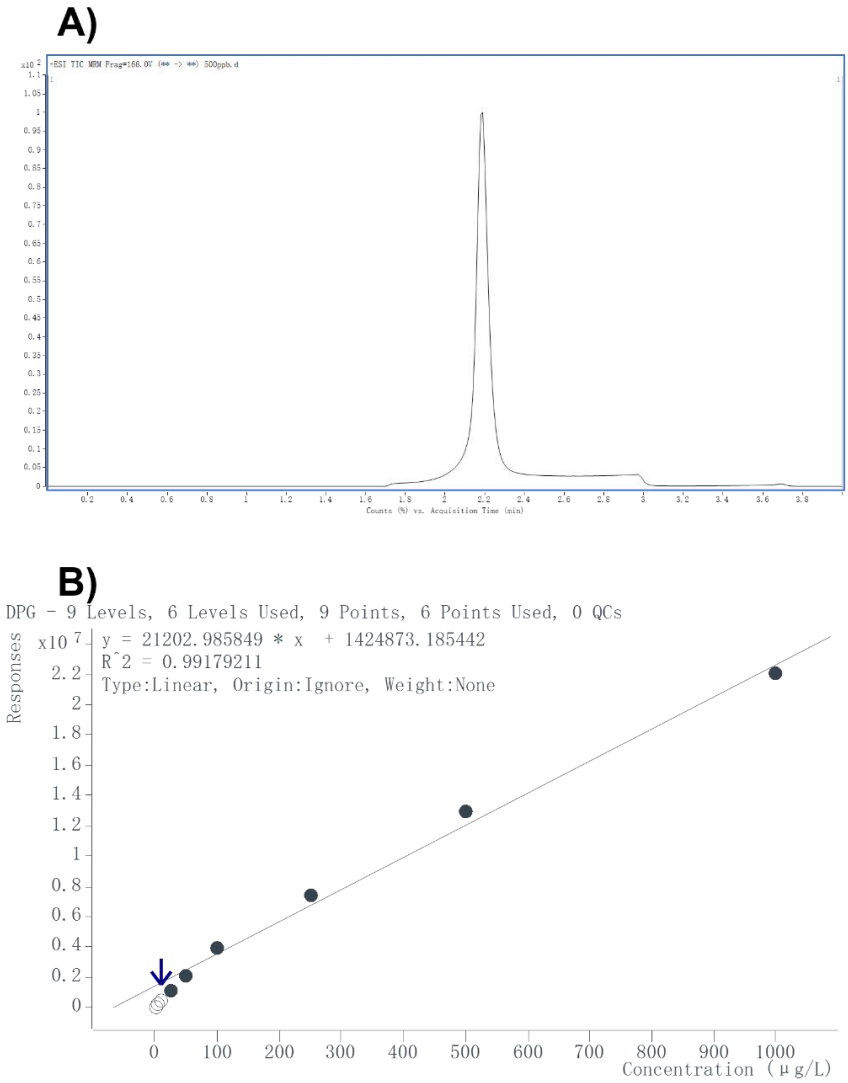

Figure 3.3 (a) LC-MS/MS chromatogram of a 500 µg/L mixture of DPG (b) Example calibration curves for LC-MS/MS method.

3.3.2 Quantification of UV fluence

Quantification of UV fluence was followed by the protocol (Bolton et al., 2015) with some minor midifications as shown in Figure 3.4. Here, reflection factor (RF) accounts for the fraction of the light that enters the water, often represented as 0.975 for air-water interfaces. The solution volume added to the Petri dish and the stirrer volume were added as the total volume in the Petri dish. Petri dish internal diameter, water path length, and the distance from UV lamp to top of water surface were obtained to calculate the divergence factor (DF), as shown in Eq.(3-1):

$$DF = \frac{L}{L+l} \qquad (3\text{-}1)$$

where L stands for the distance between the UV lamp and the water surface and l represents the vertical length of the water. As water matrices may contain species that absorb UV at the emitted wavelength, water factor (WF) accounts fot the change in irradiance in Eq. (3-2):

$$WF = \frac{1-10^{-al}}{al*ln10} \qquad (3\text{-}2)$$

where a stands for decadic absorption coefficient (cm^{-1}) and l represenst the vertical length of the water. Besides, the irradiance can vary accrose the surface areas of the sample. The Petri Factor (PF) accounts for variation by taking the ratio of the average of the incident irradiance over the area of the sample. PF was measured systematically by taking measurement at five-millimeter intervals over the area of the petri dish, dividing by the irradiance at the center, and averaging these ratios.

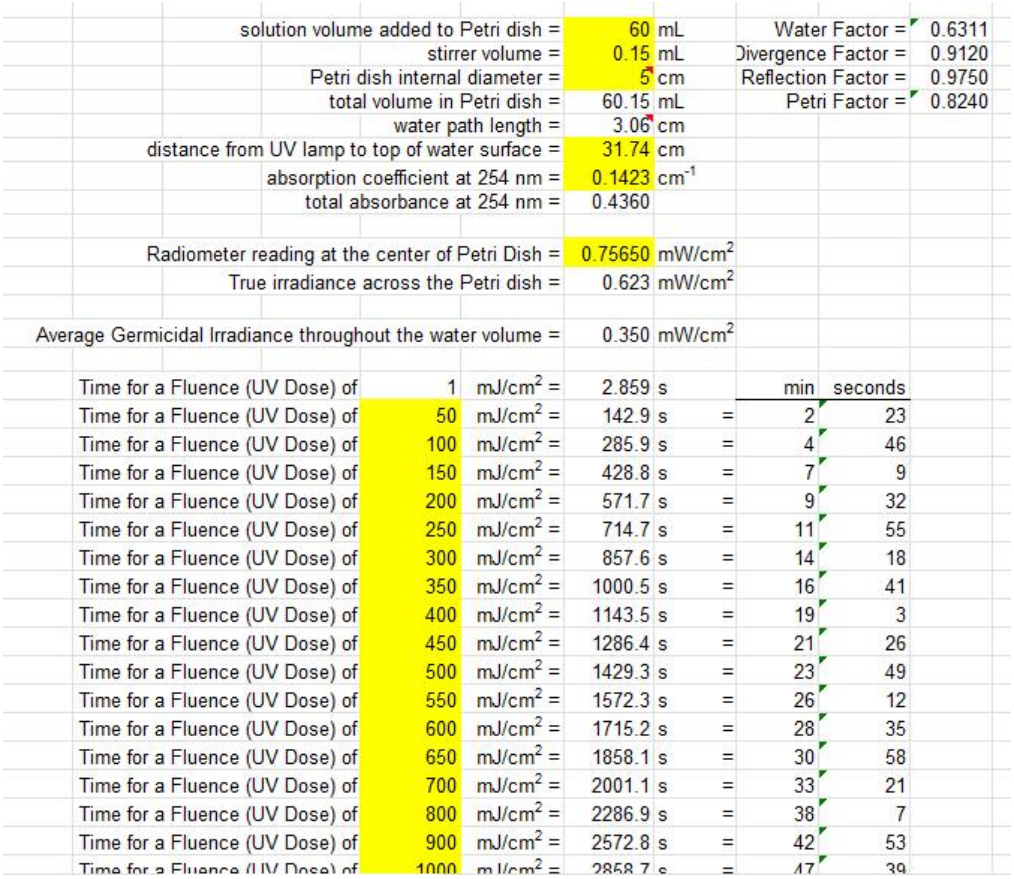

solution volume added to Petri dish =			60	mL		Water Factor =		0.6311
stirrer volume =			0.15	mL		Divergence Factor =		0.9120
Petri dish internal diameter =			5	cm		Reflection Factor =		0.9750
total volume in Petri dish =			60.15	mL		Petri Factor =		0.8240
water path length =			3.06	cm				
distance from UV lamp to top of water surface =			31.74	cm				
absorption coefficient at 254 nm =			0.1423	cm^{-1}				
total absorbance at 254 nm =			0.4360					
Radiometer reading at the center of Petri Dish =			0.75650	mW/cm^2				
True irradiance across the Petri dish =			0.623	mW/cm^2				
Average Germicidal Irradiance throughout the water volume =			0.350	mW/cm^2				
Time for a Fluence (UV Dose) of	1	mJ/cm^2 =	2.859	s		min	seconds	
Time for a Fluence (UV Dose) of	50	mJ/cm^2 =	142.9	s	=	2	23	
Time for a Fluence (UV Dose) of	100	mJ/cm^2 =	285.9	s	=	4	46	
Time for a Fluence (UV Dose) of	150	mJ/cm^2 =	428.8	s	=	7	9	
Time for a Fluence (UV Dose) of	200	mJ/cm^2 =	571.7	s	=	9	32	
Time for a Fluence (UV Dose) of	250	mJ/cm^2 =	714.7	s	=	11	55	
Time for a Fluence (UV Dose) of	300	mJ/cm^2 =	857.6	s	=	14	18	
Time for a Fluence (UV Dose) of	350	mJ/cm^2 =	1000.5	s	=	16	41	
Time for a Fluence (UV Dose) of	400	mJ/cm^2 =	1143.5	s	=	19	3	
Time for a Fluence (UV Dose) of	450	mJ/cm^2 =	1286.4	s	=	21	26	
Time for a Fluence (UV Dose) of	500	mJ/cm^2 =	1429.3	s	=	23	49	
Time for a Fluence (UV Dose) of	550	mJ/cm^2 =	1572.3	s	=	26	12	
Time for a Fluence (UV Dose) of	600	mJ/cm^2 =	1715.2	s	=	28	35	
Time for a Fluence (UV Dose) of	650	mJ/cm^2 =	1858.1	s	=	30	58	
Time for a Fluence (UV Dose) of	700	mJ/cm^2 =	2001.1	s	=	33	21	
Time for a Fluence (UV Dose) of	800	mJ/cm^2 =	2286.9	s	=	38	7	
Time for a Fluence (UV Dose) of	900	mJ/cm^2 =	2572.8	s	=	42	53	
Time for a Fluence (UV Dose) of	1000	mJ/cm^2 =	2858.7	s	=	47	39	

Figure 3.4 UV fluence quantification

Briefly, the size of the reaction platform was measured and filled into the calculation form. The absorption coefficient at 254 nm was measured to obtain total absorbance at 254 nm and calculate water factor. Reflection factor was fixed at 0.9750. Petri factor was calculated and calibrated on every experiment day by using a ILT2400 hand-held light optometer (International Light Technologies), and the process is listed below:

1) Draw a 0.5 cm × 0.5 cm grid and place the center of the grid at the center of the collimated beam

2) Measure the UV irradiance (with a radiometer) every 0.5 cm in the x and y directions and place the readings into columnsPut sensor inside system and move the sensor along x-axis and y-axis and fill in the column accordingly

3) The petri factor will be calculated through .

As a result, the UV fluence can be calculated through the below table 3.1. The time for a Fluence (UV Dose) of 1 mJ/cm^2 equals ~2.86 s.

Table 3.1 Time calculation for UV fluence

Time for a Fluence (UV Dose) of	1	mJ/cm^2 =	2.85868	s		min	seconds
	50		142.934	s	=	2	23
	100		285.868	s	=	4	46
	150		428.802	s	=	7	9
	200		571.736	s	=	9	32
	250		714.669	s	=	11	55
	300		857.603	s	=	14	18
	350		1000.54	s	=	16	41
	400		1143.47	s	=	19	3
	450		1286.4	s	=	21	26
	500		1429.34	s	=	23	49
	550		1572.27	s	=	26	12
	600		1715.21	s	=	28	35
	650		1858.14	s	=	30	58
	700		2001.07	s	=	33	21
	800		2286.94	s	=	38	7

3.3.3 Comparation of degradation effect

In Figure 3.5, the comparative effects of UV, UV-chlorine, chlorine alone, UV-NH_2Cl and NH_2Cl alone on the degradation of DPG were analyzed using $[DPG]/[DPG]_0$. Each experiment was conducted in triplicate, and the error bars are shown in the figure. The impact of UV alone on DPG degradation was found to be negligible, with less than 5% reduction in DPG concentration achieved after an 800 mJ/cm^2 UV dose (approximately 38 minutes), as depicted in Figure 3.5. When comparing the effects of chlorine and NH_2Cl, it was observed that chlorine exhibited a significantly faster degradation rate compared to NH_2Cl, consistent with previous studies (Marques Dos Santos et al., 2022). The concentration of DPG decreased to zero within 3 minutes during chlorination, while UV-chlorine exhibited a slightly enhanced degradation rate. In contrast, NH_2Cl and UV-NH_2Cl showed a more gradual decline in the C/C_0 with some fluctuations. At the end of the 32-sampling point, the C/C_0 for NH_2Cl alone was

around 0.91, while UV/NH_2Cl demonstrated an increased degradation effect, resulting in a C/C_0 of 0.84.

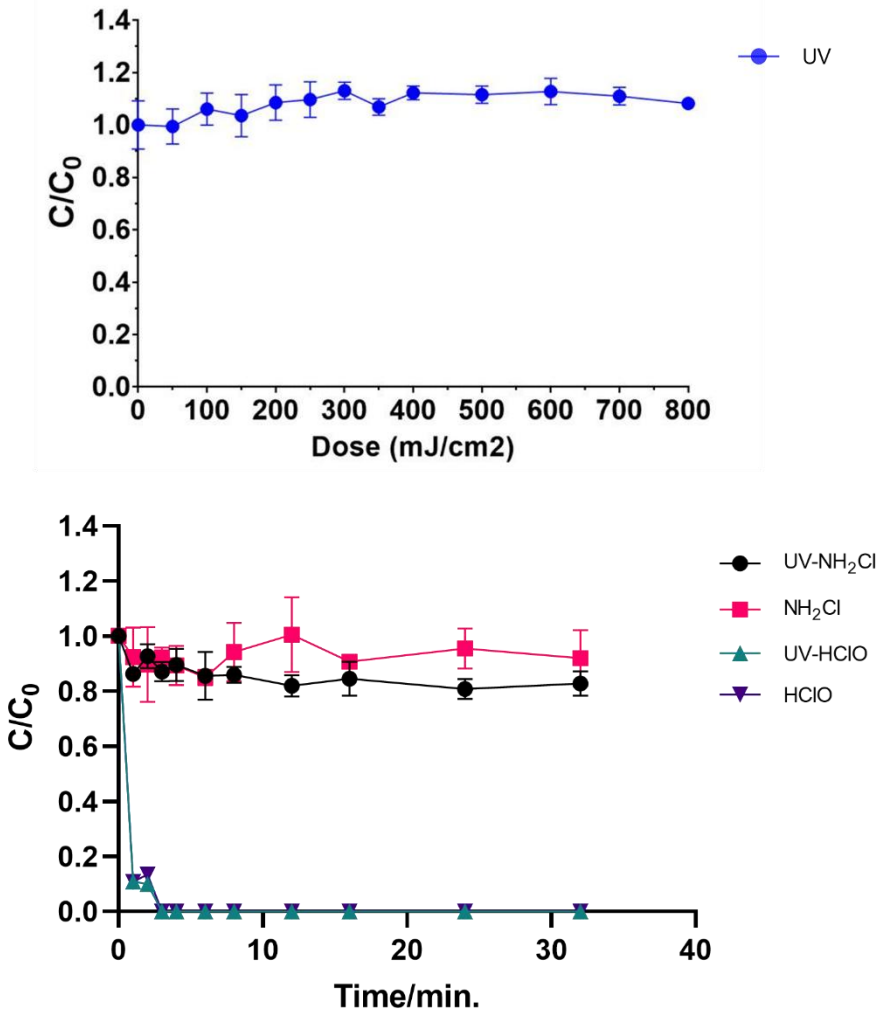

Figure 3.5 Comparation of degradation effects on DPG (a) UV alone (b) UV-NH_2Cl, NH_2Cl, UV-HClO and HClO, the dose of the oxidant was 25 μM. Results are represented mean ± SD (n = 3). $[DPG]_0$ = 5 μM, reaction was conducted in 5 mM pH 7.4 buffer. Time for a Fluence (UV Dose) of 800 mJ/cm^2 equals to 38 minutes 7 seconds

UV treatment did not exhibit a significant impact on the degradation of DPG in the presence of both chlorine and monochloramine. Therefore, the focus of this thesis will be directed towards comparing the degradation effects of chlorine and NH_2Cl, considering the pronounced contrast between the effects of these two disinfectants on DPG degradation.

3.3.4 DPG Monochloramination kinetic study

The chlorination kinetics of DPG have been comprehensively explored in previous studies. Sieira et al. established a model for the initial pseudo-first order kinetics under conditions with $[HOCl]_0 > 10\ [DPG]_0$ between pH 5 and pH 11.7 (Sieira et al., 2020). In this study, the reaction between DPG and monochloramine was analyzed kinetically across a pH range of 5-11. The investigation in the present study did not include pH values lower than 5 due to the occurrence of an acid-catalyzed disproportionation reaction of monochloramine, which result in the formation of dichloramine and ammonia(Cimetiere et al., 2009).

The plots of ln ($[DPG]_t/[DPG]_0$) versus time at pH from 5 to 11 for the experiment's reaction with NH_2Cl are presented in Figure 3.6. All plots were linear ($R^2 > 0.9$), confirming that the reaction was first order with respect to DPG. Furthermore, the linear plot for the slope of the pseudo-first-order linearization k_{obs} versus $[NH_2Cl]_0$ at pH from 5 to 11 in Figure 3.6a also confirmed that the reaction was first order with respect to NH_2Cl. The apparent rate constant k_{app} were calculated by dividing k_{obs} value by the initial concentration of NH_2Cl show in Figure 3.7. The values obtained in the pH range 5 - 11 are presented in Table 3.2. Compared to chlorine reaction with DPG (Sieira et al., 2020), the k_{app} for the reaction of NH_2Cl with DPG were 2-4 orders of magnitude lower at pH range 5 - 11 which is explain by the lower electrophilicity of the chlorine atom in NH_2Cl than in HOCl.

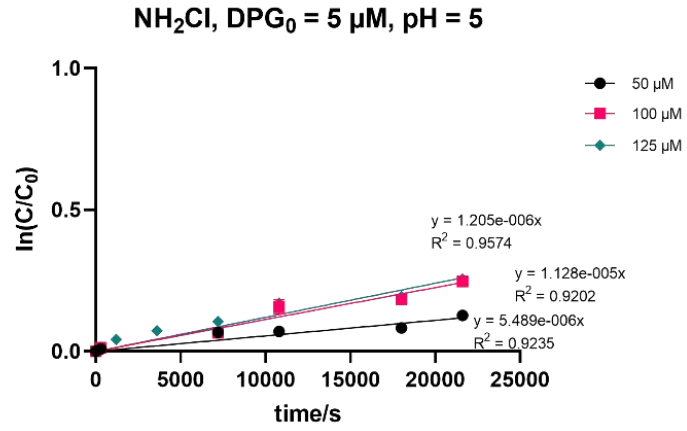
NH2Cl, DPG0 = 5 µM, pH = 5
ln(C/C0)
time/s
50 µM
100 µM
125 µM
y = 1.205e-006x
R2 = 0.9574
y = 1.128e-005x
R2 = 0.9202
y = 5.489e-006x
R2 = 0.9235

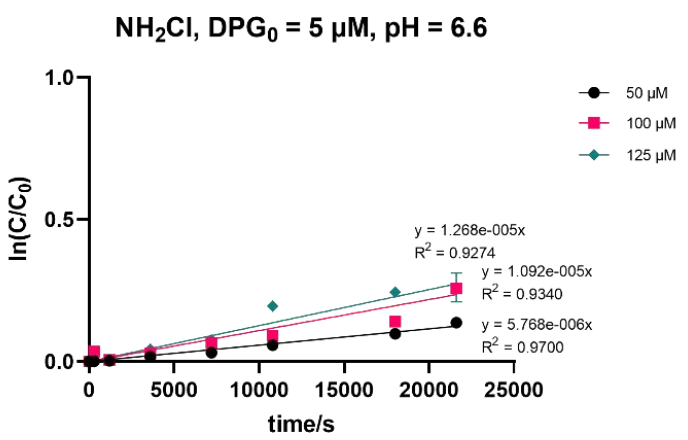
NH2Cl, DPG0 = 5 µM, pH = 6.6
ln(C/C0)
time/s
50 µM
100 µM
125 µM
y = 1.268e-005x
R2 = 0.9274
y = 1.092e-005x
R2 = 0.9340
y = 5.768e-006x
R2 = 0.9700

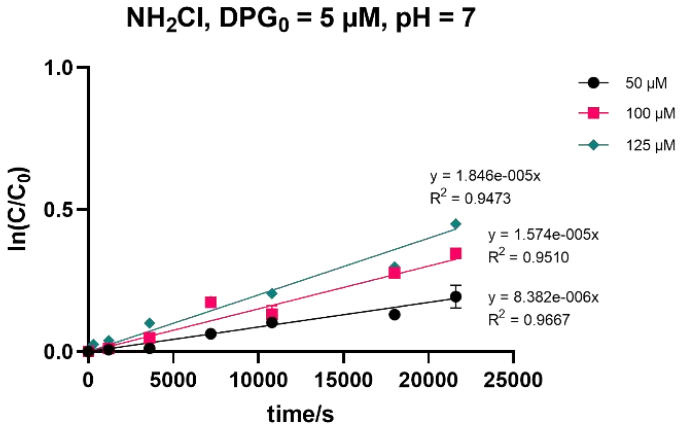
NH2Cl, DPG0 = 5 µM, pH = 7
ln(C/C0)
time/s
50 µM
100 µM
125 µM
y = 1.846e-005x
R2 = 0.9473
y = 1.574e-005x
R2 = 0.9510
y = 8.382e-006x
R2 = 0.9667

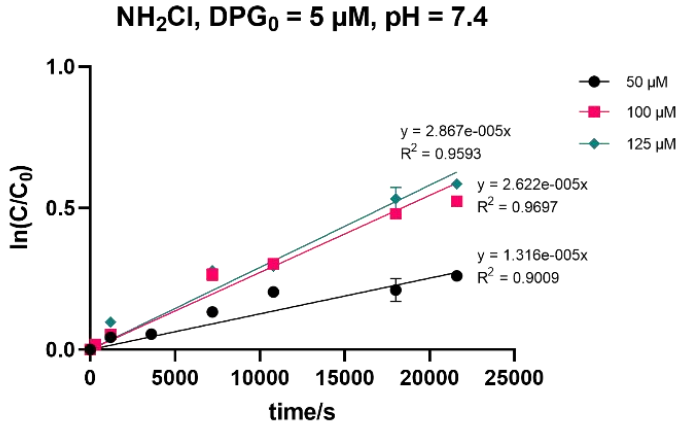
NH2Cl, DPG0 = 5 µM, pH = 7.4
ln(C/C0)
time/s
50 µM
100 µM
125 µM
y = 2.867e-005x
R2 = 0.9593
y = 2.622e-005x
R2 = 0.9697
y = 1.316e-005x
R2 = 0.9009

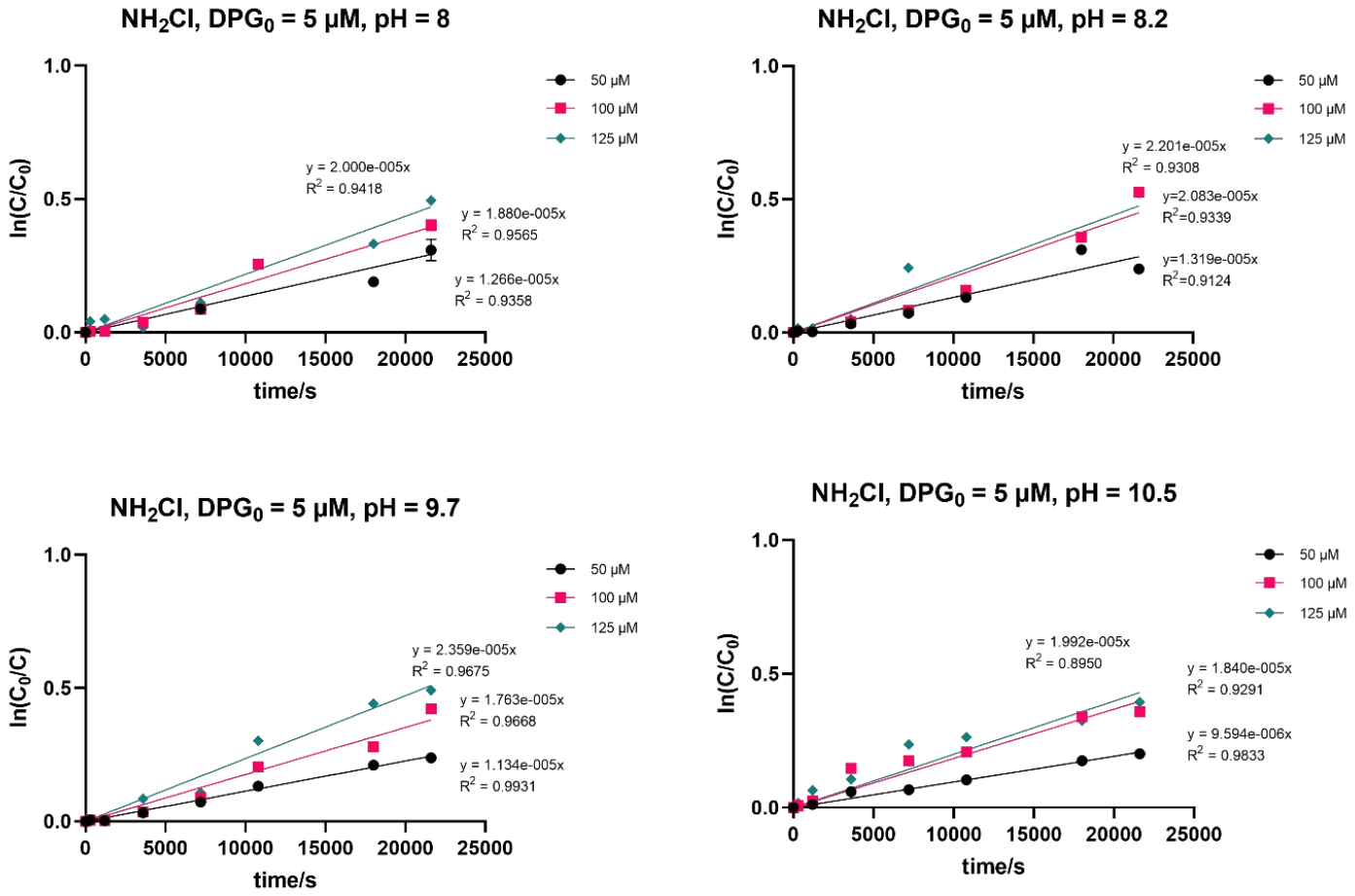

Figure 3. 6 Pseudo-first order kinetics plots obtained during monochloramination of DPG (phosphate buffer 5 mM).

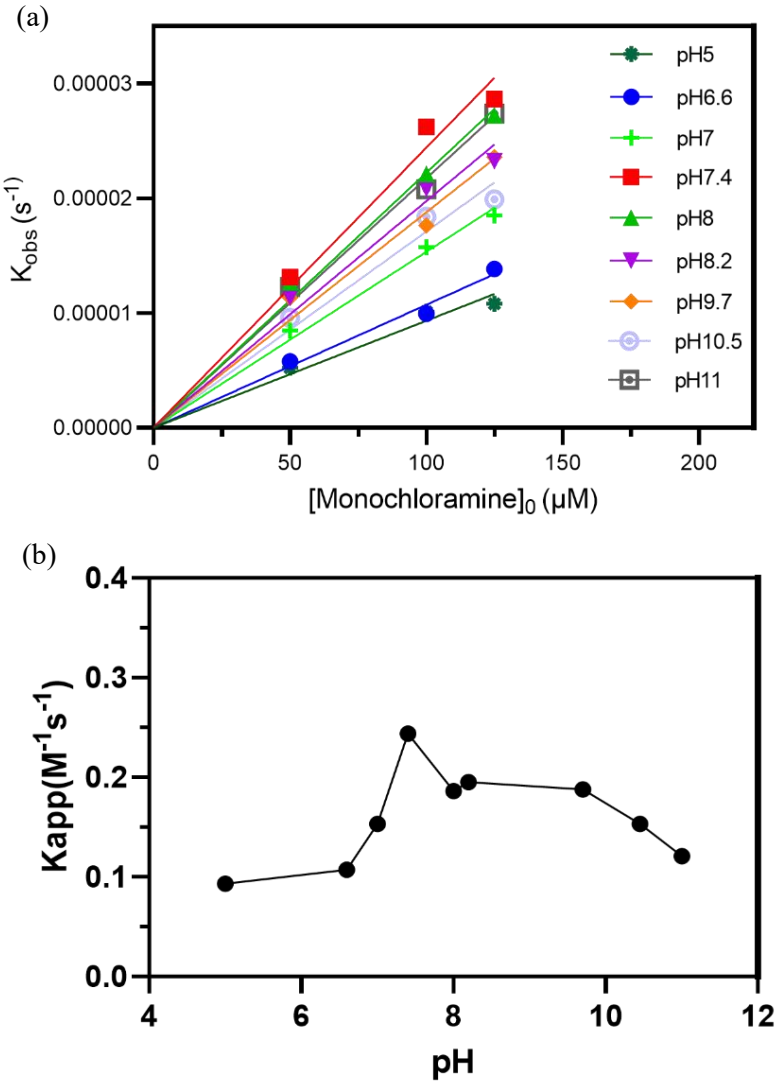

Figure 3.7 (a)Linear plot for the slope of the pseudo-first-order linearization k_{obs} versus $[NH_2Cl]_0$ at pH from 5 to 11 of monochloramination of DPG. (b) pH dependence of k_{app}.

Table 3.2 Experimentally obtained k_{obs} and $t_{1/2}$ for monochloramination of DPG at the different pH values (calculated for 50 μM NH_2Cl i.e., 3.55 mg Cl_2 L^{-1})

pH	k_{app} (M^{-1} s^{-1})	k_{obs} (s^{-1})	$t_{1/2}$ (s)
5	0.09327	5.71E-06	87535.0
6.6	0.1072	5.8E-06	86236.6
7	0.1533	8.38E-06	59651.6
7.4	0.244	1.31E-05	38051.8
8	0.1862	1.27E-05	39494.2
8.2	0.1953	1.32E-05	37907.5
9.7	0.1877	1.13E-05	44091.1
10.5	0.1533	9.59E-06	52115.9
11	0.1209	1.23E-05	40749.8

Table 3.3 Comparison of reaction rate constant of phenols, guandine, amine and amino acid during monochloramination

Compound		pKa	k_{app} ($M^{-1}s^{-1}$) at pH 7.0-7.2	Chemical Structure	Reference
Phenols	Phenol	10.0	1.60×10^{-2}	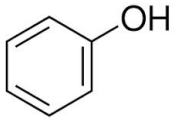	Heeb et al., 2017
	Resorcinol	9.40 11.2	1.30×10^{-1} 8.0×10^{-2}	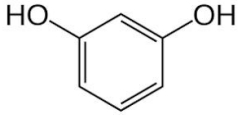	Cimetiere et al., 2009; Heeb et al., 2017
Guanidine	1,3 diphenylguanidine	10.12	1.53×10^{-1}	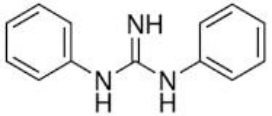	This study
Amine	Methylamine	10.80	1.89×10^{-1}	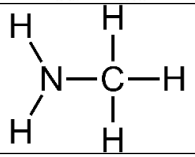	Isaac and Morris, 1985
Amino acids	Glycine	9.65	1.50 1.05	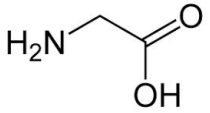	Isaac and Morris, 1985; Snyder and Margerum, 1982
	glycylglycine	8.11	5.91 5.10	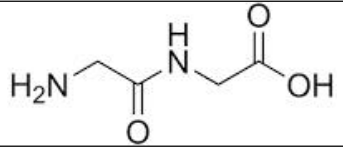	Isaac and Morris, 1985; Snyder and Margerum, 1982

The k_{app} obtained for NH_2Cl with DPG at pH ~ 7 (i.e natural water conditions) was compared to the k_{app} reported for the reaction of NH_2Cl with some nitrogen organic compounds (Cimetiere et al., 2009; Isaac & Morris, 1985; M. P. Snyder & Margerum, 1982) and phenolic compounds (Heeb et al., 2017) in Table 3.3. Results in Table 3.3 showed that the k_{app} values for the reaction of NH_2Cl increase in the order of phenol < resorcinol ≈ DPG ≈ methylamine < glycine < glycylglycine. This evolution is mainly influenced by the functional group showing amino NH_2 group (in amine, guanidine, and amino acid) as higher activating than hydroxyl OH group (in phenol, resorcinol). The similar rate constant for DPG and resorcinol is explained by the two number of OH functionals groups on the benzene ring of resorcinol, increasing the electron-rich sites of attack. The higher k_{app} observed with amino-acids (glycine and glycylglycine) compared to DPG could be explained by the high fraction of the deprotonated forms (pKa DPG < pKa glycine and glycylglycine) of the amino-acid at pH 7, which are reported to be the main species attacked by monochloramine as they are more nucleophilic than the protonated forms (Cimetiere et al., 2009; M. P. Snyder & Margerum, 1982).

The pH-dependent profile of the apparent second-order rate constant k_{app} of the reaction of NH_2Cl with DPG is presented in Figure 3.7. As shown in Figure 3.7, the k_{app} values are independent of pH for pH < 6.5, while the k_{app} increased slightly with increasing pH for pH > 6.5 and decreased for pH > 7. The shape of the pH dependence profiles was comparable to that reported for the reaction of monochloramine with amines and amino acids (Isaac & Morris, 1985; M. P. Snyder & Margerum, 1982). This pH dependence indicates that the reaction is controlled by the intrinsic reaction of the protonated chloramine ion (NH_3Cl^+) with the deprotonated N-organic compound, which is more nucleophilic than the protonated form.

A theoretical model of the pH-dependent k_{app} for the reaction between the guanidine and monochloramine was defined by considering acid-base equilibrium of NH_3Cl^+/NH_2Cl (pKa_1 NH_2Cl/NH_3Cl^+= 1.44) (Heeb et al., 2017)

and DPG^+/DPG (pKa_2 = 10.12) (Sieira et al., 2020) and the reaction of NH_3Cl^+ with the deprotonated guanidine DPG^-. The reaction is described as follows in Eq(3-3) – Eq(3-5):

$$(1)\ NH_2Cl + H^+ \leftrightarrow NH_3Cl^+ \qquad pKa_1 \qquad (3\text{-}3)$$

$$(2)\ DPG \rightarrow DPG^- + H^+ \qquad pKa_2 \qquad (3\text{-}4)$$

$$(3)\ DPG^- + NH_3Cl^+ \rightarrow TPs \qquad k \qquad (3\text{-}5)$$

The general expression for the reaction of guanidine with monochloramine is shown in Eq(3-6):

$$-\frac{d[DPG]_{tot}}{dt} = = k_{app}[NH_3Cl^+][DPG^-] \qquad (3\text{-}6)$$

The k_{app} depends on the species-specific rate constant k, the pH, and the dissociation constants Ka_1, and Ka_2. As a result, the expression of k_{app} correspond to:

$$k_{app} = \frac{kKa_2[H^+]}{(Ka_1 + [H^+])(Ka_2 + [H^+])} \qquad (3\text{-}7)$$

The species-specific rate constants k were determined by a nonlinear least-squares regression of the experimental pH profile of k_{app} above using the Excel solver tool. As shown by the solid lines in Figure 3.8, reasonable fitting was obtained between the experimental and theoretical pH profiles for pH > 7, while strong discrepancies were observed between rate constants for pH < 7 . These discrepancies could be explained by a metastable TP with oxidizing properties, reducing DPG concentration at these pHs (Sieira et al., 2020) The value of the species-specific rate constant was $k = 1.14 \times 10^8\ M^{-1}\ s^{-1}$.

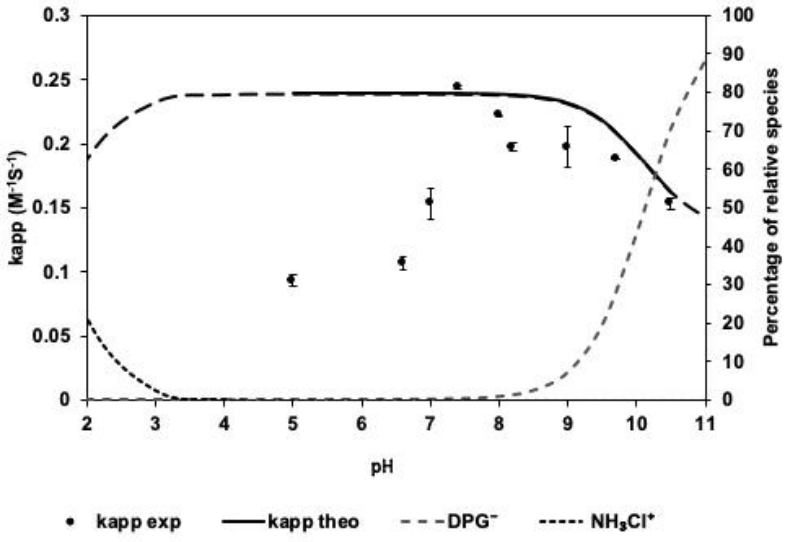

Figure 3.8 pH dependence of the apparent rate constant rate of monochloramination of DPG. Symbols indicate experimental k_{app} values, and solid lines represent theoretical k_{app} considering the reaction between NH_3Cl^+ (right axis, $pKa_1 = 1.44$) and DPG^- (right axis, $pKa_2 = 10.12$).

4. CYTOTOXICITY COMPARISON OF TRANSFORMATION PRODUCTS OF DPG

4.1 Introduction

This chapter compares the cytotoxicity of disinfection byproducts of (DPG) after chlorination and chloramination processes. The structure of this chapter is shown in Figure 4.1.

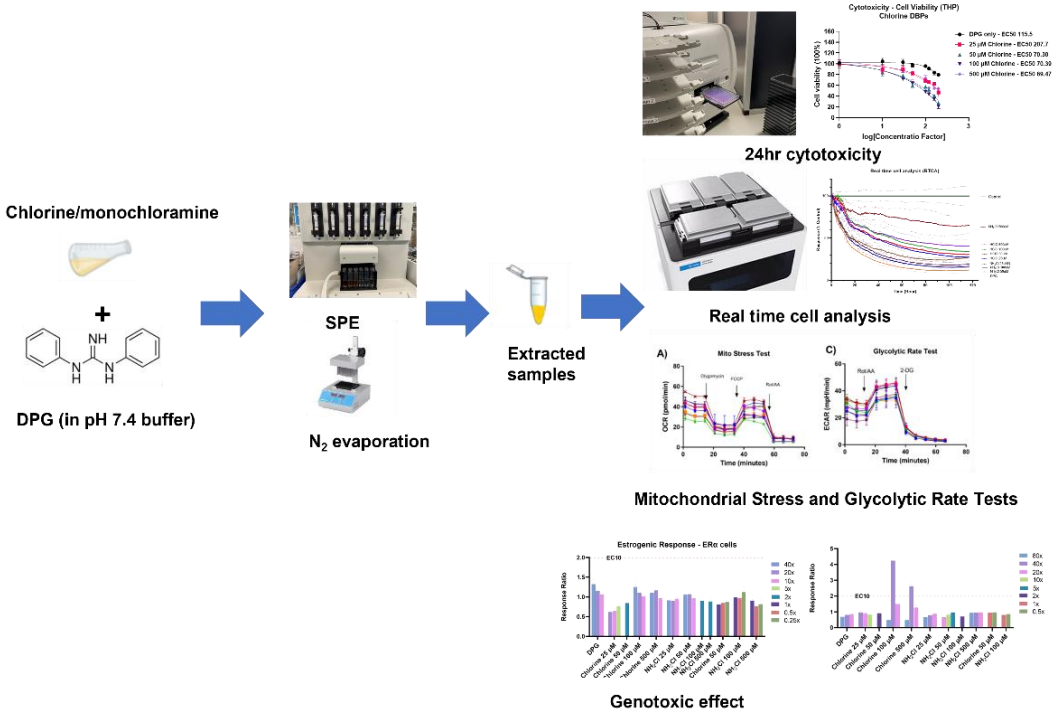

Figure 4.1 Methodology Structure of Chapter 6

4.2 Methodology

4.2.1 Materials

In this part, dimethyl sulfoxide (DMSO), and ascorbic acid (AA) was purchased from Sigma-Aldrich. HPLC grade (Optima) solvents and reagents methyl tert-butyl ether (MtBE) and methanol (MeOH) were purchased from Fisher Scientific. A milli-Q EQ 7000 water system (Millipore) was applied to generate ultrapure water. Analytical grade HepG2 (HB-8065) cells were purchased from American Type Culture Collection (ATCC). Dulbecco's Modified Eagle Medium (DMEM), Dulbecco's phosphate-buffered saline

(DPBS), certified foetal bovine serum (FBS), 0.25% trypsin EDTA solution, trypan blue solution (0.4%), and alamarBlue HS cell viability assay was purchased from Thermo Fisher Scientific.

4.2.2 Preparation of disinfection by-products of DPG after chlorination and chloramination

To prepare the byproducts of disinfection experiments of DPG, 2L buffered solutions (buffered at pH 7.4 using 5mM phosphate buffer) with an initial 5 μM DPG concentration were prepared and initiated by different oxidant doses. Each disinfection experiments were conducted in triplicate. The disinfection period lasted for 60 minutes and was quenched by freshly prepared 1M ascorbic acid (AA) at an AA: Cl_2 molar ratio of 1.25:1. The concentration of Cl_2 was quantified by using theDPD colorimetric methods with a HACH DR900 instrument. Byproduct were enriched by solid phase extraction (SPE) (see in Appendix B) procedures with Oasis HLB cartridges. Byproducts were collected in a mixture of MeOH and MtBE solvent. The elution was ultimately evaporated under a gentle flow of nitrogen at 25°C, after which the residues were redissolved in 200 μL pure DMSO for cytotoxicity analysis.

4.2.3 Cell line culture

Cytotoxicity experiments were conducted by using liver hepatocarcinoma cells (HepG2) and leukemia monocytic cell (THP-1). Mitochondrial stress test and glycolytic rate test experiments were carried out in HepG2 cells. Estrogenic response was assessed using ERα and p53 signaling was assessed via HCT-116 cell line. HepG2 cells were cultured in DMEM culture media with 10% FBS while THP-1 cells were cultured in RPMI media with 10% FBS and 2mM l-glutamine. Both cell lines were cultured at 37ºC and 5% CO_2 atmosphere, with media changed every three days and passaged before reaching 90% confluence. ERα and HCT-116 cells were grown in flasks with respective growth media (10% FBS) in 37°C and 5% CO_2 incubator until 60% (HCT-116 cells) or 90% (ERα cells) confluency for assays. HepG2 cells were

detached using 0.25% trypsin while p53 cells were detached using 0.05% trypsin.

4.2.4 Cytotoxicity, cell viability

Cells were counted by trypan blue exclusion using an automated cell counter (Countess II FL, Thermo Fisher Scientific). HepG2 cells were seeded in 96-well flat-bottomed plates (Thermo Fisher Scientific, Singapore) with a density of 5,000 cells in 50 µL DMEM phenol-red free media with 2% FBS, followed by a 16-hour long culture in a 5% CO_2 and 37ºC incubator. For THP-1 cells, which exhibit a dissociative nature and require proper attachment, PMA lines appear to be dissociative and need to attach well by adding PMA in media. THP-1 cells were transferred in RPMI media with 2% FBS and 10 ng ml^{-1} and seeded in 96-well flat-bottomed plates with a density of 10,000 cells in 50 µL. After a 48-hour long attachment process in a 5% CO_2 and 37ºC incubator, the media was changed to 50 µL per well RPMI phenol-red free media and then followed by a 16-hour long culture in a 5% CO_2 and 37ºC atmosphere.

Samples were diluted into several dilution series using media. 50 µL diluted samples were added into each well with four replicates for each diluted chemical. Negative controls were put in every plate including DMSO concentrations of 0, 0,1 and 0.5% where negligible differences were found among them in the cell viability. Positive control has been obtained by using the zero-cell control with an ultimate result of 0% cell viability. After 24 h treatment in a 5% CO_2 incubator at 37ºC, 10 µL of AlamarBlue reagent was injected to each wall and then incubated for another 2 h at 5% CO_2 and 37ºC atmosphere. The plate was ultimately measured using a microplate reader (Cytation 5, BioTec) to acquire fluorescence signal at excitation of 560 nm and emission of 590 nm and the cells viability result are presented as % of control (DMSO at 0.05% and 0.01%). The EC_{50} was calculated with GraphPad Prism 9.0 software (GraphPad Software San Diego, CA) from the best-fit curve.

4.2.5 Cell bioenergetics, mitochondrial stress test and glycolytic rate test

Extracellular flux experiments were conducted in two parts, namely the Mitochondrial Stress Test (MST) and Glycolysis Rate Test (GRT), using the Seahorse XF 96 extracellular flux analyzer (Agilent Seahorse Biosciences). The experiments were carried out with slight modifications to the Seahorse protocol with slight modifications. In accordance with previous experiments (Jia et al., 2023; Marques Dos Santos et al., 2022), HepG2 cells were plated in XF96 extracellular flux assay plates. Each well was filled with 80 µL of culture medium (pH 7.4) with 5,000 cells. After incubation in a 5% CO_2 incubator at 37ºC for 16 hours, the cells were exposed to various concentrations of test compounds (n = 4) for 24 hours. Subsequently, cell bioenergetics parameters were assayed by replacing the media with DMEM extracellular flux media. The oxygen consumption rate (OCR, pmol O_2 min^{-1}) was measured for MST, while the extracellular acidification rate (ECAR, mpH min^{-1}) was measured for GRT. The OCR and ECAR data were normalized with cell number using a standard DAPI assay (NucBlue™ Live ReadyProbes™ Reagent).

The specific concentrations mentioned in bioenergetics experiments were carefully chosen based on the absence of a significant decrease in cell viability when compared to the DMSO control ($p < 0.05$) during cytotoxicity testing. To provide a concise summary, the selected concentrations were summarized in the below Table 4.1.

These concentrations were selected as bulk parameters due to the enrichment of the reaction products through solid-phase extraction after the disinfection process, allowing for a comprehensive evaluation of the resulting compounds' effects on cell viability.

Table 4. 1 Selected concentrations for bioenergetics experiments, x represents the enrichment times. For example, 25x represents 25 times enrichment.

Chlorine Group	25 µM	25x

	50 μM	1x
	100 μM	20x
	500 μM	20x
NH_2Cl Group	25 μM	40x
	50 μM	40x
	100 μM	40x
	500 μM	40x
DPG Group	-	20x

4.2.6 Genotoxic Effects

Two reporter cell lines were used to examine pathway specific toxicities. Estrogenic response via ERα induction was assessed using ERα-UAS-*bla* GripTite™ Cells and genotoxic effect via p53 signaling was assessed using p53BE-*bla* HCT11s6 (Thermo Fisher Scientific) following manufacturer's protocols. p53 cells were seeded in 384-well clear-bottom black side plates in assay media (2% FBS) with ~30,000 per well. Cells were treated with 2x serial dilutions of samples with a final DMSO concentration of 0.5% and incubated for 16 hours. E2 and mitomycin were used as positive control for p53 assays, respectively. Standards were constructed with 9 to 10 concentration points and samples were tested with 3 to 5 points, with four replicates for each data point. At the end of treatment, LiveBLAzer™-FRET B/G loading solution containing the substrate was added into cells and incubated for another 2 hours at room temperature in dark. Fluorescence intensity was measured with excitation at 409 nm and emission at 460 and 530 nm using a BioTek Cytation 5 multi-mode reader. The β-lactamase expression ratio was calculated as the ratio of blanked signals at 460 nm and at 530 nm (the 460/530 ratio). Induction of target gene expression in a sample was further determined by dividing its 460/530 ratio by that of the DMSO control, which was named Response Ratio (RR). Samples are

considered positive when RR >= 1.5 and potentially exerting significant agonist effects when RR exceeds the threshold EC_{10} of the standard curve.

4.3 Results

4.3.1 Cell viability

To explore possible toxicity in different stages of chlorination and monochloramination of DPG, the enrichment sample of the disinfection products of DPG under different dilution factors were dosed to HepG2 cells and THP-1 cells to conduct experiments. The viability of HepG2 cells and THP-1 cells exposed to DPG disinfection by-products of chlorine and monochloramine for 24h was assessed by AlamarBlue cell viability assay.

Figure 4.2 demonstrates that, overall, the toxicity of chlorinated TPs exceeds that of chloraminated TPs. Regarding the HepG2 cell line shown in Figure 4.2A and Figure 4.2B, the cytotoxicity hierarchy is as follows: chlorine TPs > monochloramine TPs > DPG. Maximum toxicity is observed with dosing levels of 50 μM and 100 μM (at [Oxidant]: [Compounds] ratio of 10 and 20), resulting in EC_{50} values of 46.26 and 47.15 for chlorine TPs. In the case of monochloramine TPs, dosing at 100 μM and 500 μM (ratio = 20 and 100) leads to maximum toxicity, with EC_{50} values of 83.85 and 61.53, respectively. The DPG-only sample underwent the same preparation processes as the other samples, but no oxidants were added. The graph indicates that the DPG-only sample achieves an EC_{50} of 116.2 and 126.7, demonstrating lower toxicity compared to chlorine TPs and monochloramine TPs. Previous studies have demonstrated that some chlorinated products of DPG appeared to be more genotoxic than DPG, while some chlorinated products of DPG might be less toxic than DPG. For example, the study of (Marques Dos Santos et al., 2022) showed that CC 11, DPG, and CC 05 have EC_{50} of 22.6 μM, 47.7 μM, and 115.3 μM in HepG2 cells, respectively. Unlike previous studies reporting genotoxicity variations of chlorinated DPG products, findings of this work demonstrate higher toxicity in all DPG disinfection groups compared to the DPG-only group. This also suggests the generation transformation products are

more hazardous than the recently identified nitrogenous aromatic halogenated DBPs (halophenylacetamides), which appears to be less toxic than DPG (C. Hu et al., 2022).

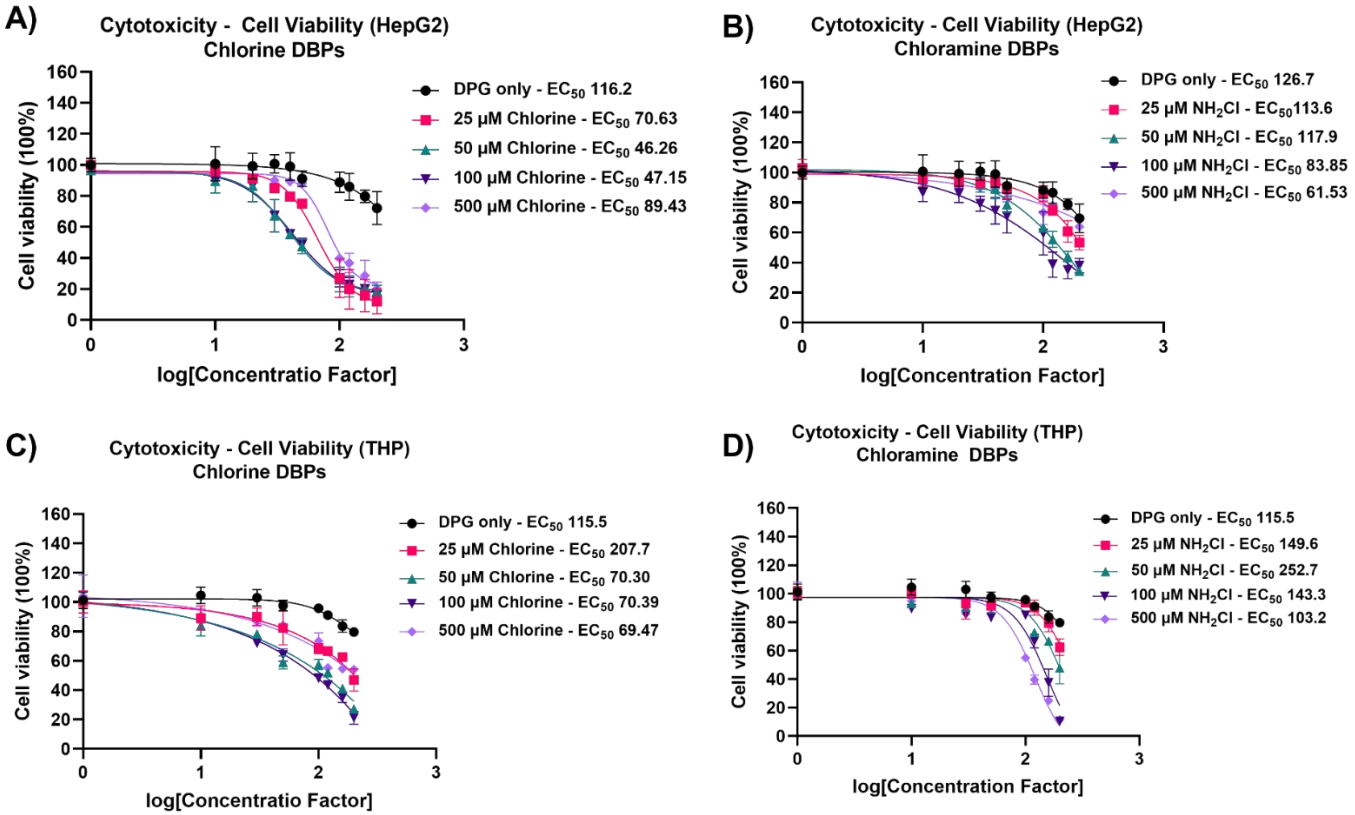

Figure 4.2 Cytotoxicity evaluation of DPG and chlorine and chloramine byproducts in HepG2 and THP cells. A) Cytotoxicity dose-response curve of chlorine byproducts for HePG2 cell line B) Cytotoxicity dose-response curve of c byproducts for HePG2 cell line C) Cytotoxicity dose-response curve of chlorine byproducts for THP-1 cell line D) Cytotoxicity dose-response curve of chloramine byproducts for THP-1 cell line fitted using log(inhibitor) vs. response – variable slope (four parameters); Data are given as mean ± SD (n = 4).

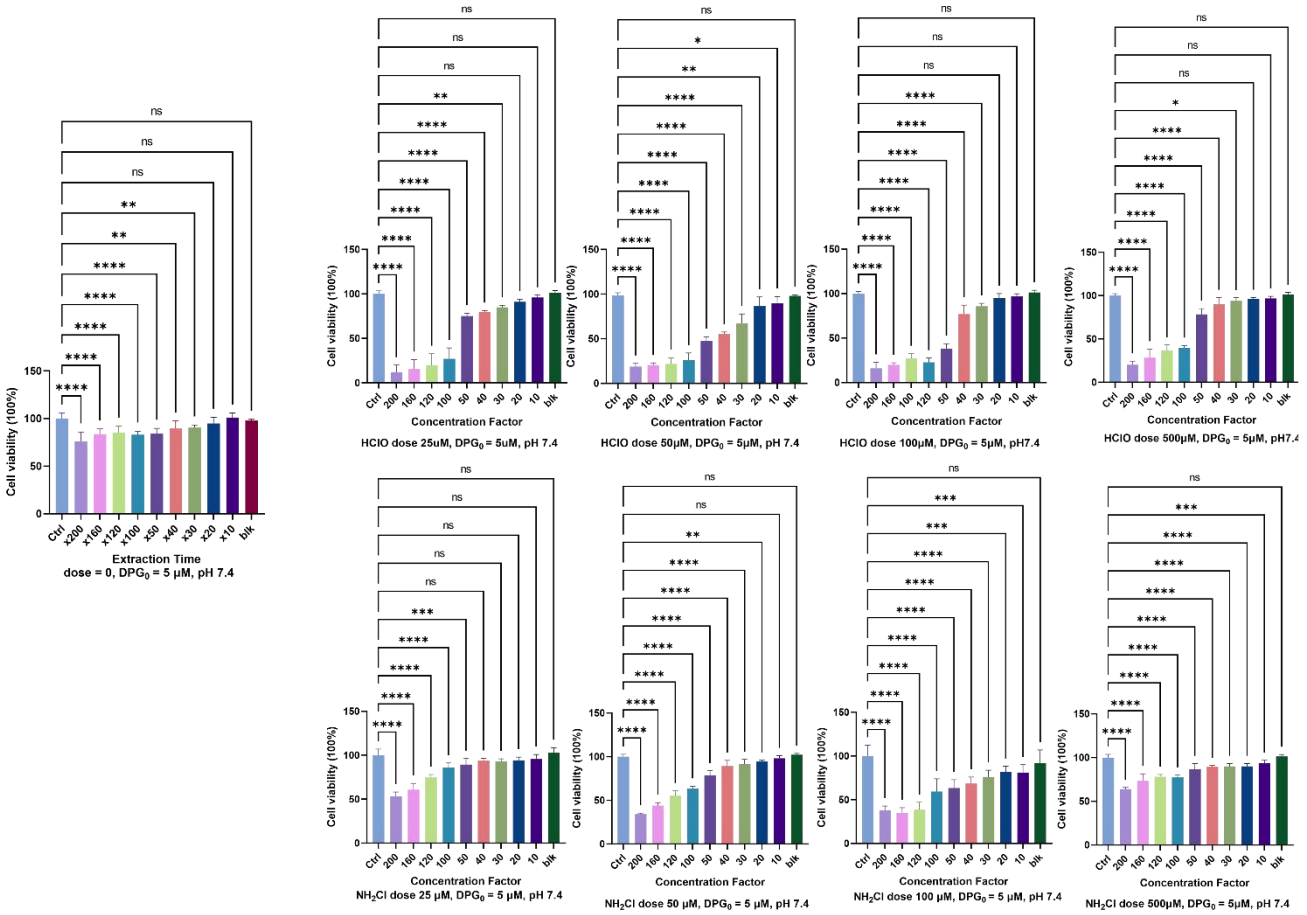

Figure 4.3 Cytotoxicity effects of byproducts in HepG2 cells after 24h. The results are the means ± SD of four cells. Compared with control, ****p < 0.0001, ***p<0.0005, **p<0.01, and *p<0.05.

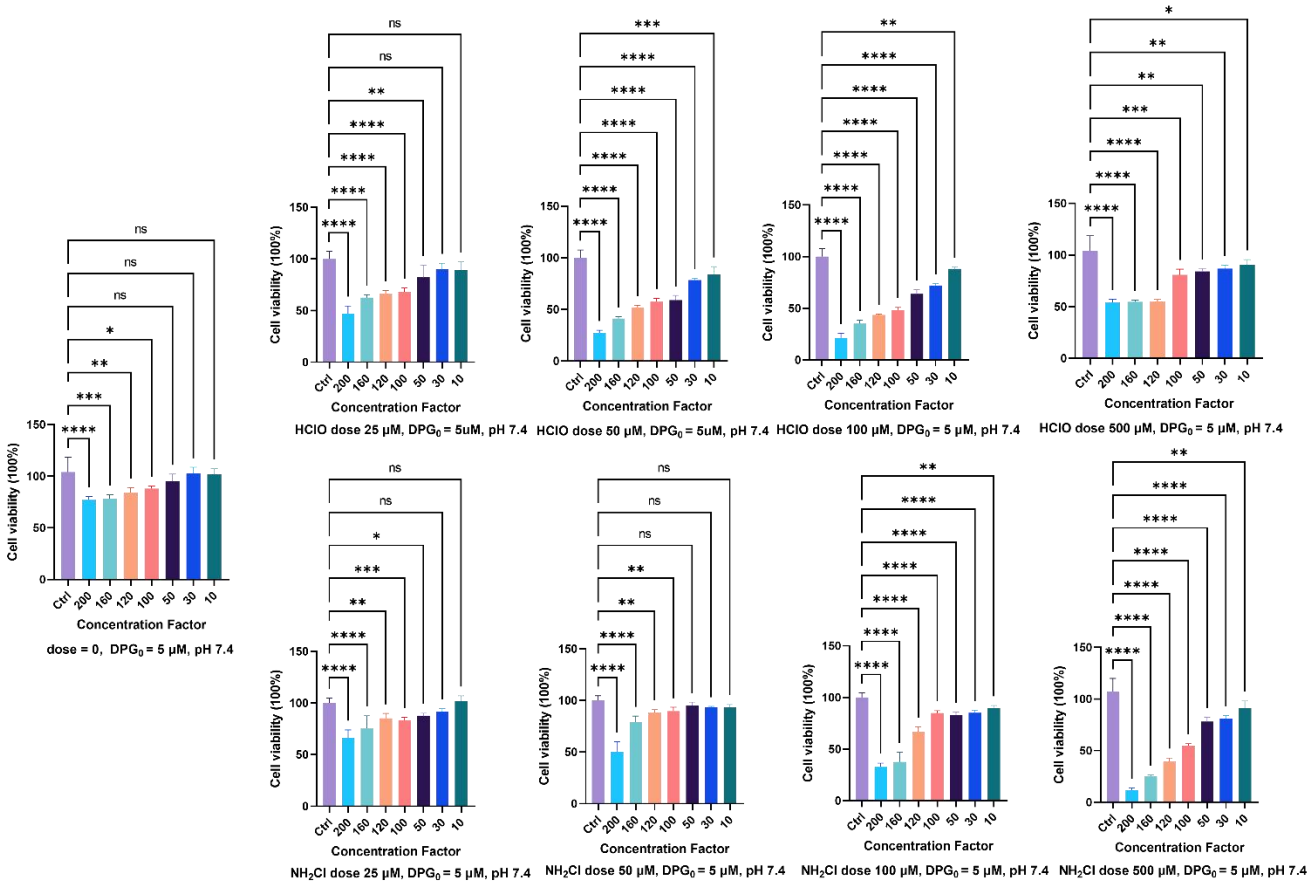

Figure 4.4 Cytotoxicity effects of byproducts in THP-1 cells after 24h. The results are the means ± SD of four cells. Compared with control, ****$p < 0.0001$, ***$p < 0.0005$, **$p < 0.01$, and *$p < 0.05$.

In Figure 4.2C and Figure 4.2D, it is evident that for THP-1 cells, chlorinated disinfection products exhibit higher toxicity than chloraminated disinfection products in general. However, the cytotoxicity hierarchy for THP-1 cells differs significantly. For chlorine TPs, maximum toxicity is observed at dosing levels of 50 μM, 100 μM, and 500 μM (at an [Oxidant]:[Compounds] ratio of 10 and 20), resulting in EC_{50} values of 70.30, 70.39, and 69.47, as shown in Figure 4.2C. Surprisingly, at a chlorine dosage of 25 μM (at an [Oxidant]:[Compounds] ratio of 5), the toxicity to THP-1 cells is weaker than that of the original DPG compound. A similar trend is observed in the chloraminated group, with 25 μM, 50 μM, and 100 μM resulting in 50% inhibition values of 149.6, 252.7, and 143.3, respectively, all higher than the DPG EC_{50} of 115.5. The maximum cytotoxicity is observed in the 500 μM NH_2Cl group with an EC_{50} of 103.2. Detailed cell viabilities of HepG2 and THP-1 is shown in Figure 4.3, and Figure 4.4, respectively.

The observed differences in toxicity between THP-1 cells and HepG2 cell line might be attributed to their distinct cellular characteristics. HepG2 cells are non-phagocytic cells, whereas THP-1 cells are professional phagocytes, known for their significant endocytotic and exocytic activities (Burgoyne & Morgan, 2003; Lankoff et al., 2012; Mohamed et al., 2011; Yen et al., 2011). Additionally, HepG2 cells are liver cancer cells, exhibiting higher metabolic activity (Gerets et al., 2012; Jia et al., 2023; Marques Dos Santos et al., 2022) compared to THP-1 cells. Consequently, it is inferred that the higher resistance of THP-1 can be explained by their ability to efficiently uptake and release these compounds, while the metabolism within HepG2 cells may be more affected, resulting in higher cytotoxicity.

4.3.2 Cell bioenergetics

In order to investigate potential mechanisms of toxicity induced by DPG disinfection products in HepG2 cells, cell bioenergetic experiments, including MST and GRT were conducted, using enriched samples of DPG disinfection products. Specific concentrations of the samples were selectedfor experimentation to exclude cell death factor. These specific concentrations were

determined based on a lack of significant decrease in cell viability compared to the DMSO control ($p < 0.05$), as assessed through cytotoxicity testing. While assessing cytotoxic effects is crucial for toxicity evaluation, it is equally important to examine more subtle toxic effects, such as alterations in cell bioenergetics, as they can provide valuable insights into the underlying mode of toxicity (Jia et al., 2023; Marques Dos Santos et al., 2022; Zuo et al., 2017). To investigate changes in cellular bioenergetics, extracellular flux analysis were employed, which involved the use of various electron transport chain (ETC) modulators. The sample names indicated the dosage and type of oxidant used, while the original concentration of DPG remained constant during sample preparation. These findings demonstrated that exposure to specific disinfection product groups resulted in mitochondrial dysfunction and dysregulation of glycolysis, indicating that the molar ratio of oxidant to DPG may play a critical role in the generation of highly toxic products.

The results from MST (Figure 4.5A) indicate that most tested disinfection products adversely affect the OCR and cell bioenergetic parameters. Significant effect on basal respiration was observed in certain groups. For instance, fold change = 0.68 ($p < 0.01$) at Chlorine 100 μM group, fold change = 0.56 ($p < 0.01$) at NH_2Cl 25 μM group, and fold change = 0.69 ($p < 0.01$) at NH_2Cl 50 μM group as shown in Figure 4.5B. Additionally, significant impact were also found in other parameters indicating the function of mitochondrial like ATP production (fold change = 0.47, $p < 0.01$ at Chlorine 100 μM group and fold change = 0.54, $p < 0.01$ at NH_2Cl 50 μM group), and maximal respiration (fold change = 0.60, $p < 0.01$ at Chlorine 25 μM group, fold change = 0.54, $p < 0.01$ at Chlorine 50 μM group, fold change = 0.56, $p < 0.01$ at Chlorine 100 μM group, fold change = 0.61, $p < 0.01$ at NH_2Cl 25 μM, and fold change = 0.70, $p < 0.01$ at NH_2Cl 50 μM group), as shown in Figure 4.5B. Meanwhile, the DPG sample showed no significant effects on maximum respiration and ATP production. The notable inhibition of proton leak (as depicted in Figure 4.5B) may signify mitochondrial damage (Gu et al., 2021; Marques Dos Santos et al., 2022), which were observed in Chlorine 100 μM and NH_2Cl 25 μM, 50 μM, suggesting these groups exhibit detrimental effects

on cell mitochondria in HepG2 cells. Specifically, the proton leakage caused by chlorine 100 μM group, NH_2Cl 25 μM group and NH_2Cl 50 μM group suggest they exhibit detrimental effects on HepG2 cell mitochondria.

Contrary to the observed decrease in MST, GST showed that HepG2 cells exposed to most DPG disinfection products had a significant increase in ECA (Figure 4.5C). In the liver, glucose is metabolized and broken down through glycolysis with cytoplasm to form pyruvate. TCA cycle will transport the pyruvate to the mitochondrial for ATP production (Bricker et al., 2012). However, in the presence of mitochondrial dysfunction, glycolysis becomes the primary source of ATP, leading to elevated acid production. A shift in extracellular lactate production rate upon the exposure of chlorine and chloramine disinfection products was indicated by the elevation in basal glycolysis and basal PER (Figure 4.5D). Furthermore, figure 4.5C demonstrates that the extracellular acidification rate (ECAR) of the experimental groups is generally higher than that of the control groups, indicating possible mitochondrial dysfunction. Compensatory glycolysis shows a significant increase in chlorine 50 μM, chlorine 500 μM, and NH_2Cl 100 μM (as shown in Figure 4.5D). Furthermore, the disorder in glycolytic rate is evident in chlorine 50 μM and NH_2Cl 100 μM groups, as observed in Figure 4.5D, where post 2-DG acidification provides insights into non-glycolytic acid production in cells. The altered extracellular lactate production rate was reflected in the increased basal glycolysis and basal proton efflux rate (PER) upon exposure to the Chlorine 50 μM group and NH_2Cl 50 μM groups. In these groups, significant increases on both basal glycolysis (fold change = 1.57, $p < 0.0001$ at Chlorine 50 μM group, fold change = 1.56, $p < 0.0001$ at NH_2Cl 50 μM group) and basal PER (fold change = 1.3, $p < 0.05$ at Chlorine 50 μM group and fold change = 1.8, $p < 0.0001$ at NH_2Cl 50 μM group) were found. These findings were in contrast to the evidential decrease observed in parameters of MRT. Compensatory glycolysis was significantly higher in Chlorine 50 μM, Chlorine 500 μM and NH_2Cl 100 μM groups, indicating that after inhibiting mitochondrial respiration, the rate of glycolysis in cells was higher than control.

In summary, chlorine and NH_2Cl disinfection products reduced mitochondrial function, and on the contrary, elevated glycolysis in HepG2 cells, while DPG itself doesn't have significant effect on mitochondrial and glycolysis functions, which complies with the previous studies (Marques Dos Santos et al., 2022). Among all the groups, mitochondrial function and glycolysis rate were affected adversely to maximum by Chlorine 50 μM group ([Chlorine] : [DPG] = 10) and NH_2Cl 50 μM group ([NH_2Cl] : [DPG] = 10) in HepG2 cells.

.

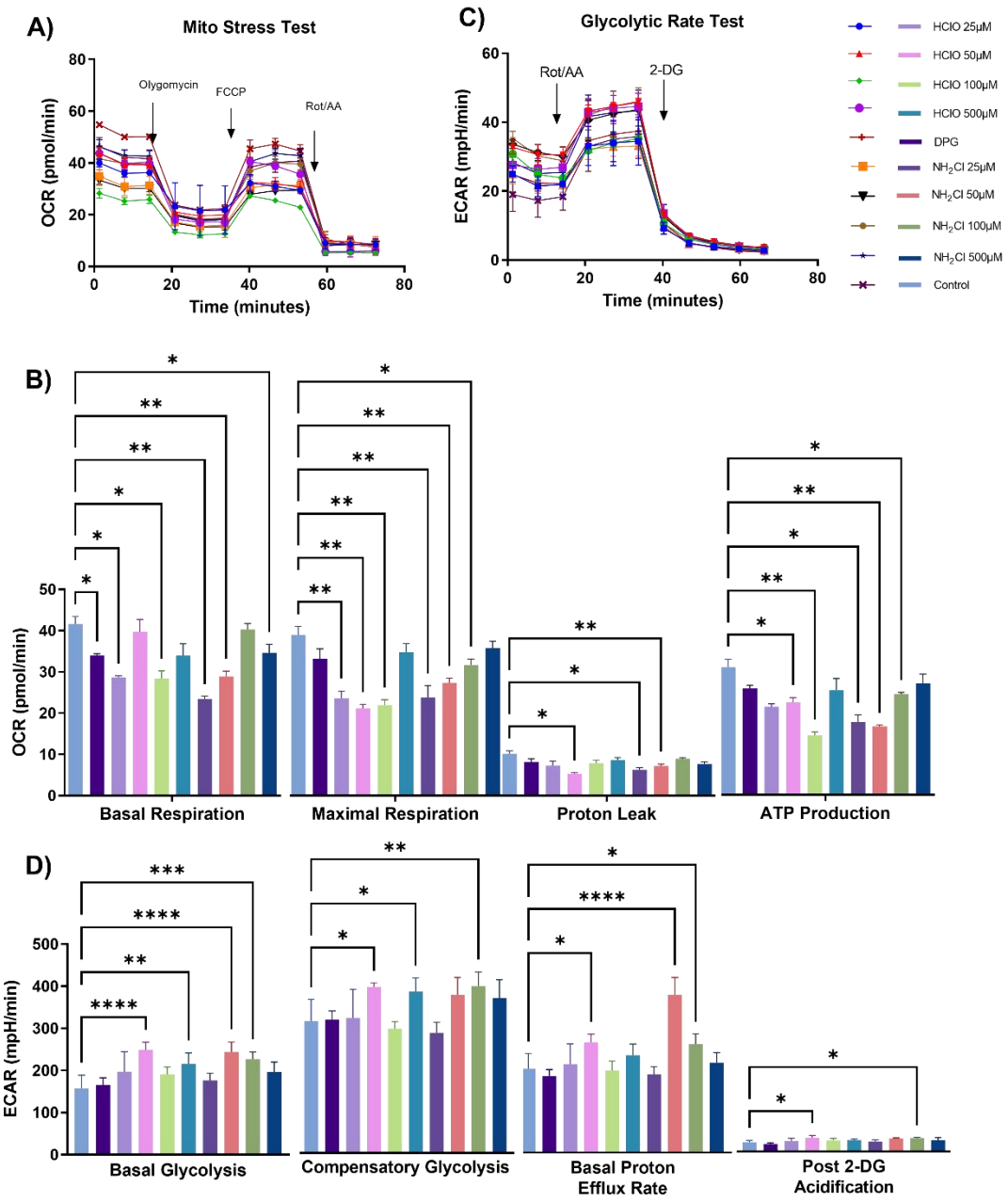

Figure 4.5 Cell bioenergetics evaluation of HepG2 cells treated with a 24-hour exposure to samples or controls A) MST profile of HepG2 cells evaluated for cellular oxygen consumption rate (OCR). Oligomycin, Carbonyl cynanide-4 (trifluoromethoxy) phenylhydrazone (FCCP) and Rotenone& antimycin A （Rot/AA） were the electron transport chain (EST) modulators in MST. B) MST parameters C) GST profile of HepG2 cells evaluated for extracellular acidification rate (ECAR). Rot/AA and glycolysis inhibitor 2-deoxy-D-glucose (2-DG) were the EST modulators in GST. D)GST parameters. Data expressed as mean ± SD (n = 5) from DMSO control using one-way ANOVA analysis. ***, **, and * denotes p-values < 0.001, < 0.01, and < 0.05.

4.3.3 Genotoxic Effects

A dose-response curve of mitomycin was constructed using Gen5 software (Version 3.11, BioTek) using 5 parameter nonlinear regression in below figure. EC_{10}, EC_{20} and EC_{50} were determined to be 98 ng mL^{-1} (RR~1.5), 226 ng mL^{-1} (RR~1.9) and 921 ng mL^{-1} (RR~3.4), respectively. To set a minimal threshold of response that might lead to biological consequences, we set RR>1.5 (50% higher signal as compared to the vehicle control) which is approximately EC_{10} of the mitomycin curve obtained. We thus denoted a dotted EC_{10} line in the plots presented in the submission.

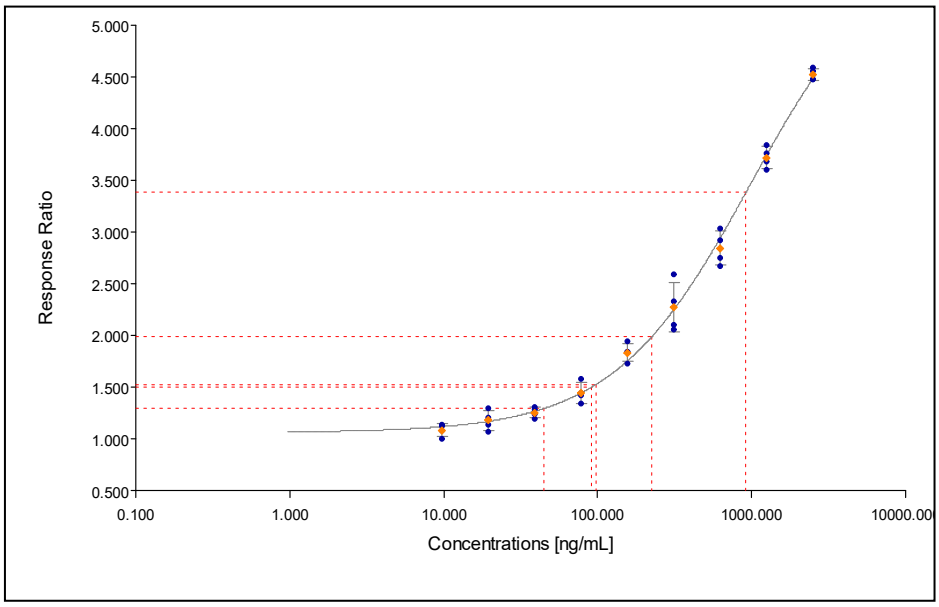

Figure 4.6 Determination of **EC10, EC20 and EC50 in genotoxic experiments**

As shown in Figure 4.7 A, no ERα induction with RR>1.5 was detected in any of the samples. The DPG without disinfection had a weak increase of RR=1.33 (1.33±0.12) as compared to the control, while the RR decreased in all samples after disinfection (Fig 4.7A). No p53 signals were detected in the DPG without disinfection or most of the samples after disinfection except chlorine 100uM and chlorine 500uM, shown in Figure 4.7B. Chlorine 100uM showed effects exceeding EC10 (RR=4.26) at 40x enrichment and the positive response remained (RR=1.50) at 20x enrichment, while chlorine 500uM showed induction (RR=2.64) only at 40x enrichment. Reporter cell assays showed that for disinfection conditions tested, no by-products with significant estrogenic

effects generated were observed; however, higher chlorine treatment of 20:1 or 100:1 ratio might generate by-products with weak genotoxicity.

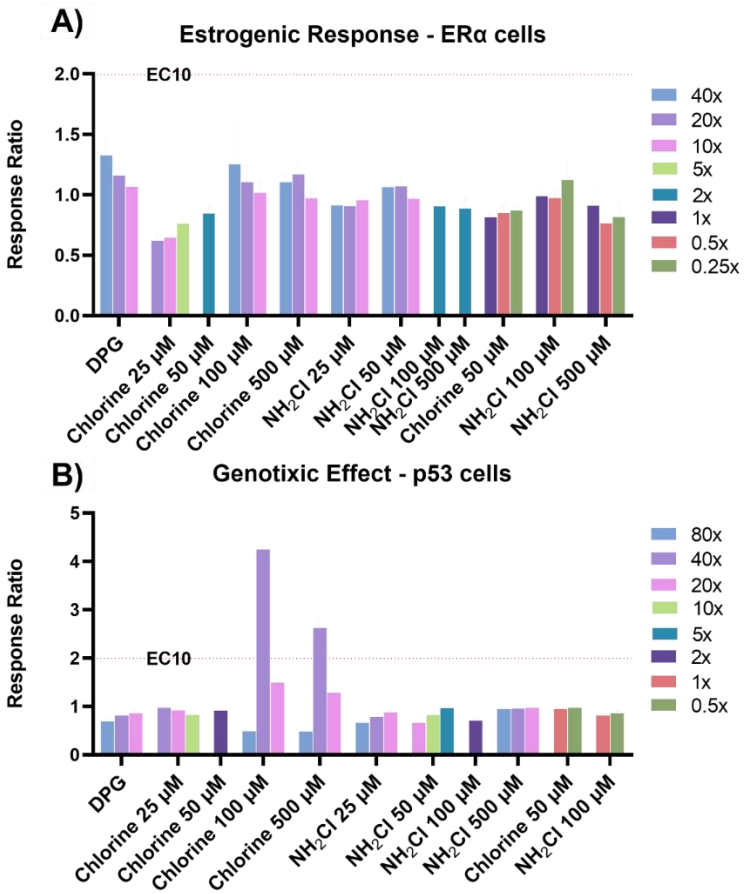

Figure 4.7 Genotoxic effects of DPG disinfection products (A) Estronic response from ERα (B) signal from p53.

5. IDENTIFICATION OF DPG TRANSFORMATION PRODUCTS

This chapter is about the identification of DPG transformation products of chlorine and monochloramine processes. The experimental process is described in Figure 5.1

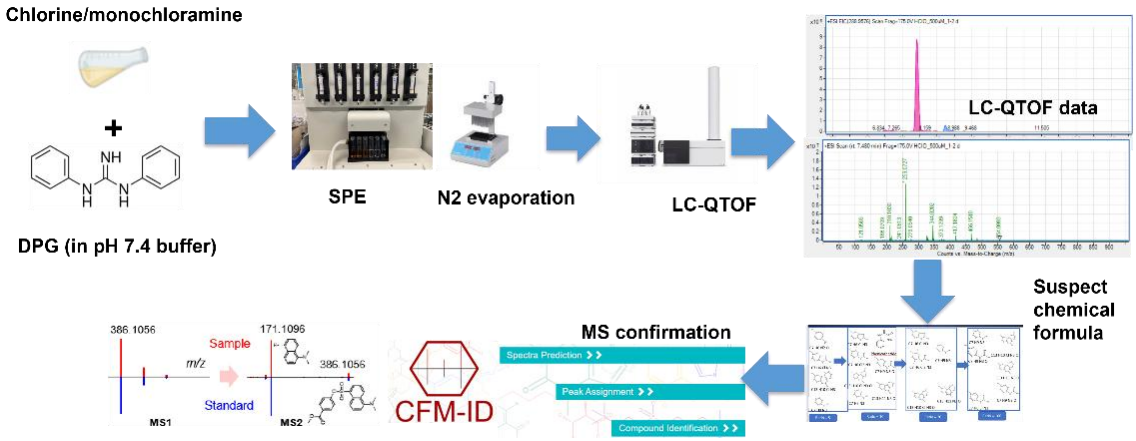

Figure 5.1 Methodology Structure of Chapter 5

5.1 Methodology

5.1.1 Reagents

Ultrapure water (MilliQ, Millipore) was used to prepare all solutions in this research. Reagent-grade chemicals, including, sodium phosphate monobasic 99%, disodium hydrogen phosphate 99%, sodium hypochlorite solution 4.0-5.0%, 1,3-dephenylguanidine (DPG) 97%, ammonium chloride 99%, ascorbic acid 99%, sodium thiosulfate 99%, ammonium acetate 97%, dimethyl sulfoxide (DMSO), phorbol-12-myristate-13-acetate (PMA) 99% was all purchased from Sigma-Aldrich. LC-MS grade (Optima LC/MS) solvents and reagents including methanol, acetonitrile, 2-proponol, methyl tert-butyl ether (MTBE) and formic acid were purchased from Fisher Scientific.

5.1.2 Experiement procedure

To determine the byproducts of disinfection experiments of DPG, 100 mL buffered solutions (buffered at pH 7.4 using 5mM phosphate buffer) with an initial 5 µM DPG concentration were prepared and initiated by different oxidant doses. Each disinfection experiment was conducted in triplicate. The disinfection period lasted for 60 minutes and was quenched by freshly prepared 1M ascorbic acid (AA) at an AA: Cl_2 molar ratio of 1.25:1. As shown in literature, AA showed less interference than sodium thiosulfate on the analysis of chloro-organic byproducts (Zhao et al., 2022). Transformation products were

enriched by using the Dionex™ Autotrace 280 Solid-Phase Extraction Instrument (Thermo Fisher Scientific) with Oasis Hydrophilic-Lipophilic Balance (HLB, 500 mg/6 cc) cartridges (Waters Corporation). The solid phase extraction (SPE) was done as previously described in Zhang et al., 2019. Briefly, the SPE process was initialized by preconditioning cartridges with 5 mL of MTBE, 5 mL methanol, and 5 mL of ultrapure water, and followed by loading sample onto cartridges. After that the cartridges were dried with nitrogen and enriched samples were collected in a mixture of 5 mL of methanol and 5 mL of 10/90 (v/v) methanol/MTBE. The elution was ultimately evaporated under a gentle flow of nitrogen at 25ºC, after which the residues were redissolved in methanol for TP determination. The detailed procedure is shown in Appendix B.

5.1.3 LC-QTOF

TPs were analyzed by an Agilent 1200 Series LC (Agilent Technologies) equipped with a degasser, an autosampler, an LC column oven, and a binary high-pressure pump. The LC system was coupled with an Agilent 6550 Series Quadrupole-Time of Flight (QTOF) MS with a Dual AJS ESI ion source. High-purity nitrogen gas was supplied to the LC-QTOF for MS/MS scans in the collision cell. The column and mobile phase being used in the LC-QTOF are the same as used in LC-QQQ. The detail of the method is summarized in Appendix D. Each sample was injected and analyzed three times.

5.2 Data Processing

The general process of data processing is shown in Figure 5.2. To control the instrument and process data, different software programs in the MassHunter package by Agilent Technologies were used. MassHunter Qualitative provided an overall view of the samples, while the "Find by Molecular Feature" function in the same software was used to generate a list of features from the MS data by combining ions with common retention time and mass relationships into a Molecular Feature Extraction (MFE) spectrum. Peaks with counts above 1000 and quality scores higher than 70.00 were filtered. To

align the time and preprocess the data, Agilent MassHunter Profinder 10.0 was used for batch processing, with a pool mix of all samples run every 10 samples. When searching for a specific list of ions, the 'Batch Recursive Feature Extraction' with 'Find by Ion' in Profinder was used to extract and filter the data files using recursive Molecular Feature Extraction (rMFE). The resulting data generated as CEF files were then imported to Mass Profiler Professional (Agilent Technologies) to indicate entities after normalization and compared to blank samples with the condition of frequency of 66% out of all sample groups and statistically significant ($p < 0.05$ & fold change >= 2.0). Possible TPs were identified as features whose intensity increased compared to blank, and formulas were generated for those features in the 'ID browser'. The software grouped the isotope pattern matching and error between the experimental m/z values and those calculated from the generated formula to provide a percentage score, where a perfect match would score 100%. The chemical structures of DPG TPs were all drawn using ChemDraw Ultra (version 14.0).

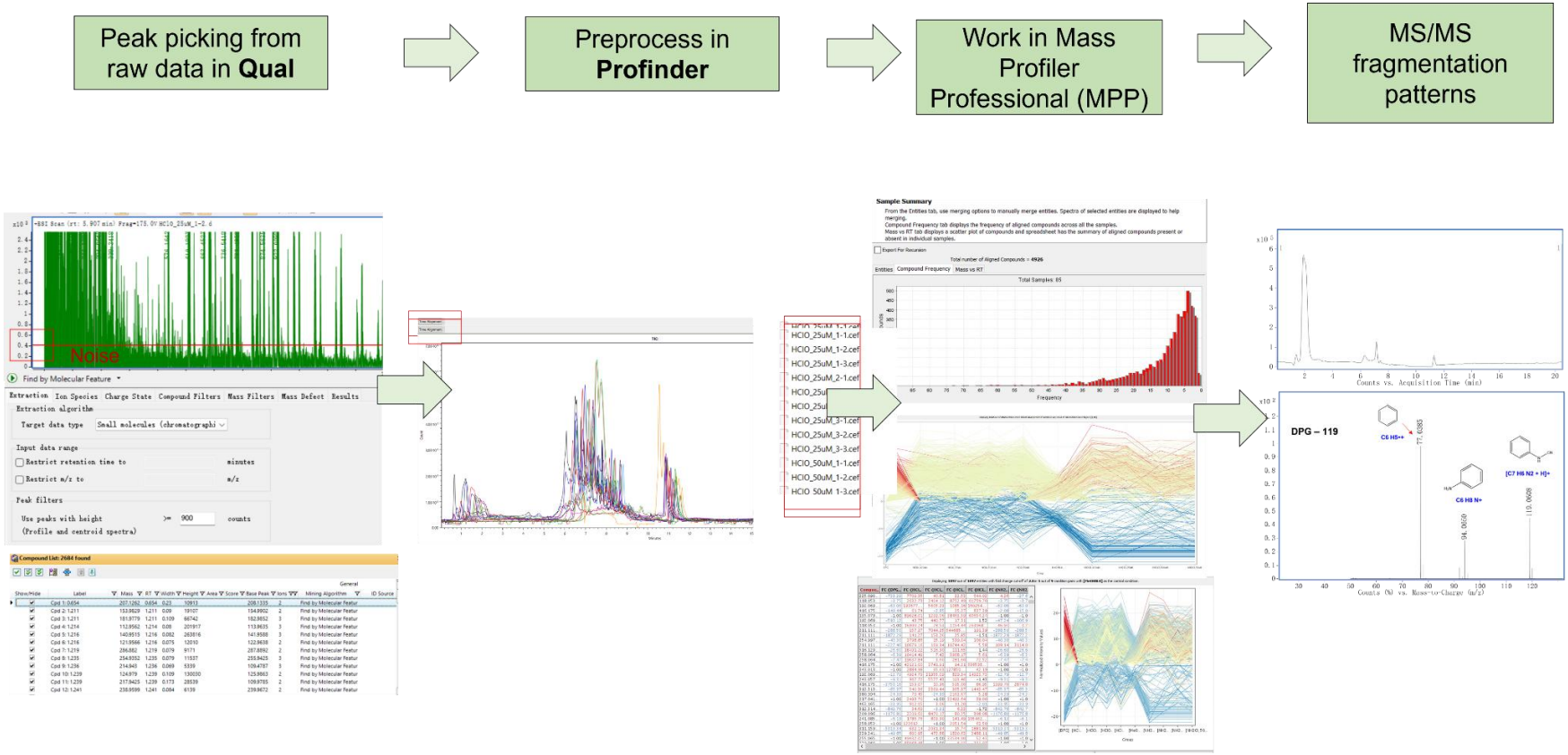

Figure 5.2 Data processing of NTA.

5.3 Results

5.3.1 Grouping of TPs in different treatment conditions

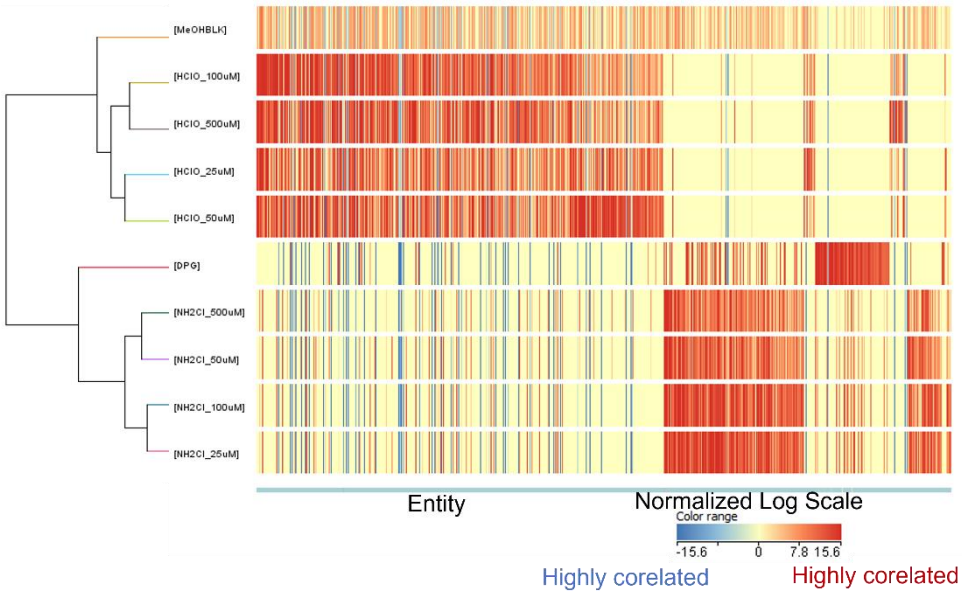

Figure 5.3 Heat map of all the detected compounds in the samples using hierarchical clustering from MPP. The results are from ESI positive. Numerical values in the legent are log_2 normalized intensity values.

A heat map using hierarchical clustering for the compounds detected is shown in Figure 5.3. The clustering indicate a significant differences between the compounds detected in chlorination group and monochloramination group despite some overlapping between two groups.

5.3.2 Transformation products of chlorination

Given the observed disparities in cytotoxicity and bioenergy experiments, it is crucial to explore the transformation products within various oxidant groups. LC-QTOF and non-target analysis have identified a total of 10 TPs among DPG chlorination and 2 TPs among DPG monochloramination in different stages as shown in Figure 5.4, with some of them being uniquely present in a few specific groups, whereas no transformation products were found in the negative mode scan. TPs were named with the precursor compound abbreviation followed by the nominal mass of its $[M + H]^+$ ion. The

chemical formula, mass measurement errors, and the elemental compositions for each compound are summarized in Table 5.1. The variations in TP types and concentrations may contribute to the differences in cytotoxicity among the different groups. To facilitate understanding, the transformation products are listed based on the Oxidant-to-compounds ratio. Differences between groups were listed in Figure 5.4. The proposed structures are based on the chemical structure of DPG itself and the interpretation of the MS/MS spectra. As reported by (Sieira et al., 2020), the chlorination of DPG results in four primary types of TPs: monoguanidine derivatives formed through ipsochlorination, introduction of chlorine atoms into an aromatic ring, hydroxylation, and intramolecular cyclization.

In Figure 5.4A, when the chlorine-to-DPG ratio was 5:1, six types of TPs were identified, and their chemical structures resembled diphenylguanidine or DPG formed a 7-membering cycle, indicating insufficient oxidant to cleave the aromatic ring. As the ratio increased to 10:1, more small molecular compounds were generated, suggesting the cleavage of the aromatic ring by the oxidant. Additionally, there was an apparent increase in chlorine atoms attached to the aromatic ring and a higher frequency of hydroxylation. With a total of 10 TPs, chlorine ratio 10 had the most TPs formed among all treatment methods, including all the TPs found, which partially explains the maximum toxicity in HepG2 cells and THP-1 cells (Chapter 4). TPs identified at ratios of 10, 20, 100 exhibited similarities with eight TPs being the same. Notably, the chlorine ratio 20 and the chlorine ratio 100 did not generate DPG-246 which has a similar chemical structure to DPG but with one hydrogen atom replaced by a chlorine atom. Furthermore, DPG-204, a monoguanidine with two chlorine atoms replacing hydrogen atoms, was absent in the chlorine ratio 100 group, implying the degradation of the aromatic ring by increased oxidants. Figure 5.4A indicated that DPG – 210 and DPG -244 had maximum intensity at the chlorine 10:1 ratio while DPG-226 and DPG-260 had maximum intensity at the chlorine 20:1 ratio. Chlorine ratio 10:1 and 20:1 had maximum cytotoxicity, supported by high intensity and the presence of multiple TPs. However, as indicated in Section 3.3, only the chlorine ratio 10:1 had damage to the

mitochondrial activity, which might be contributed to the unique presence of certain TPs compared to other groups or the generally higher intensity of the TPs in the ratio 10:1 group. As shown in Figure 5.4B, DPG-119, showed an obviously higher intensity in chlorine ratio 20:1 and chlorine ratio 100:1 than other groups. This observation may partially contribute to the genotoxic effects observed in the chlorine 100 μM (chlorine ratio 20:1) and chlorine 500 μ M (chlorine 100:1) groups discussed in Section 3.4.

5.3.3 Transformation products of NH_2Cl

Regarding the NH_2Cl group, as shown in Figure 5.4B, only two TPs were identified, implying relatively weaker disinfection effects of NH_2Cl. DPG-246 was ubiquitously found in all NH_2Cl groups (shown in Figure 5.C) but it was the only TP identified in NH_2Cl ratio 5 group. Additionally, the intensity showed an increasing trend when NH_2Cl ratio increased as shown in Figure 5.4B. Except for DPG-246, another TP found in NH_2Cl ratios of 10, 20 and 100 was DPG – 210, with an empirical formular similar to DPG itself but with 2 H atoms less. Maximum intensities of DPG-210 were found at chlorine ratios 10 and 20, which could contribute to the maximum cytotoxicity in HepG2 cells.

Table 5.1 Detailed information of DPG transformation products

Name	Molecular formula	Experimental m/z	theoretical m/z	Error (ppm)	Error (mDa)	Chemical Structure
DPG-119	C7 H6 N3	119.0608	119.0604	3.35	0.40	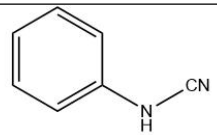
DPG-136	C7 H9 N3	136.0866	136.0869	-2.20	-0.30	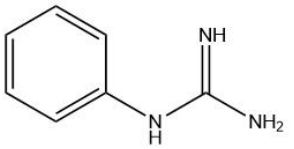
DPG-152	C7 H9 N3 O	152.0816	152.0818	-1.31	-0.20	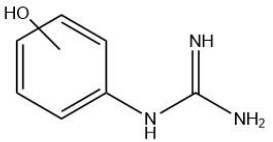
DPG-204	C7 H7 N3 Cl2	204.0086	204.009	-1.85	-0.38	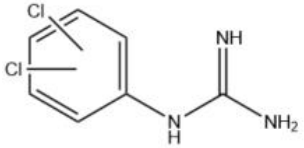
DPG-210	C13 H11 N3	210.1025	210.1026	-0.47	-0.10	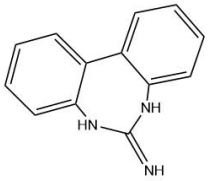

DPG-226	C13 H11 N3 O	226.0977	226.0975	-0.44	-0.10	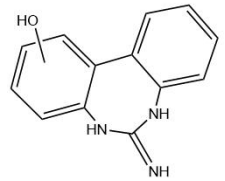
DPG-242	C13 H11 N3 O2	242.0924	242.0924	0	0.00	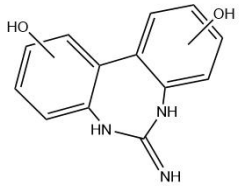
DPG-244	C13H10N3Cl	244.064	244.063	4.09	1.00	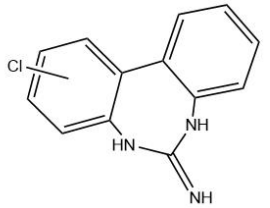
DPG-246	C13 H12 N3 Cl	246.0608	246.0793	-1.85	-0.46	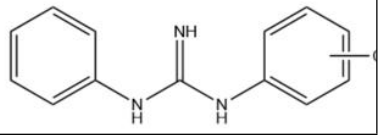

DPG-260	C13 H10 Cl N3 O	260.0586	260.0585	0.38	0.10	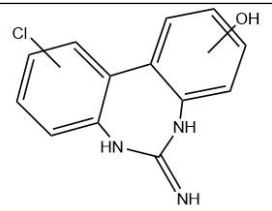

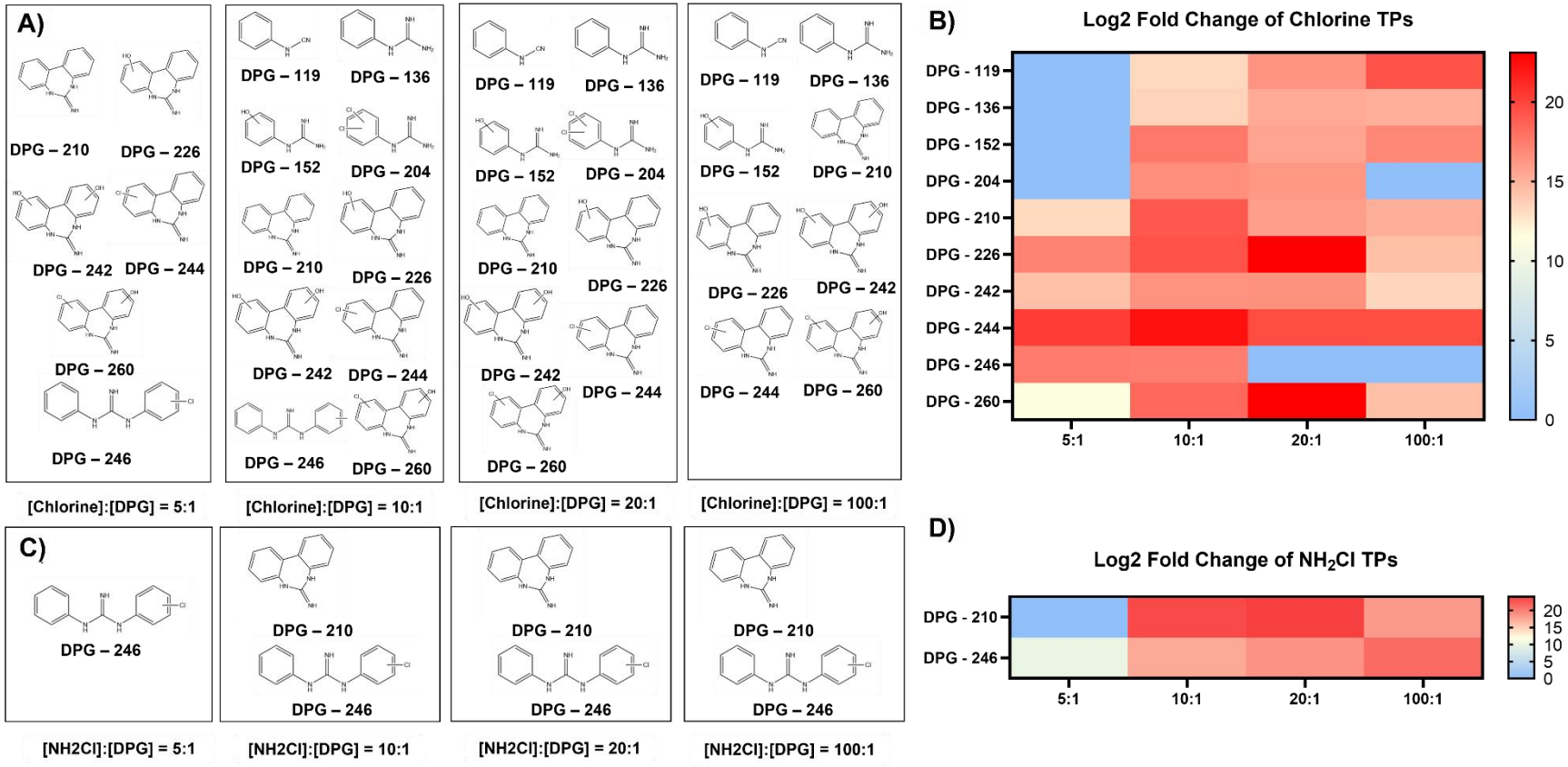

Figure 5.4 DPG transformation products from different ratio of oxidant to compound. A) Chlorine TPs. (B) Intensity of Chlorine TPs. C) NH_2Cl TPs. D) Intensity of NH_2Cl TPs.

6. CONCLUSION AND FUTURE WORK

6.1 Concluding Remarks

The increasing demand for safe drinking water remains a crucial topic worldwide. This study compared the degradation of DPG by UV, UV/chlorine and UV/chloramine processes. As a relatively stable compound, DPG was insensitive to the UV alone with unchanged concentration even exposed to high UV fluence, as shown in this study. However, DPG could be easily degraded by the chlorine alone at pH 7, while UV would accelerate the degradation speed by around 10%. UV/NH_2Cl, on the other hand, has little effects on the degradation of DPG at pH 7 with less than 10% decrease

This study also provides valuable insights into the reaction kinetics, cytotoxicity, mitochondrial function, and TPs associated with 1,3-diphenylguanidine (DPG) during monochloramination and chlorination processes. Monochloramination exhibits slower kinetics compared to chlorination, with pH 7 to pH 8 being the optimal condition. Additionally, the reactivity of monochloramine is significantly slower compared to chlorination of DPG, with the maximum efficiency observed at pH 7 to pH 8. K_{app} values for the reaction of NH2Cl increase in the order of phenol < resorcinol ≈ DPG ≈ methylamine < glycine < glycylglycine. The cytotoxicity tests conducted on HepG2 and THP-1 cells indicate that disinfection products have higher toxicity than the original compound, particularly at oxidant-to-DPG molar ratios of 10-20 with lowest EC_{50} achieved at 46.26 (chlorine 50 μM dose samples, HepG2 cell). Moreover, the MST and GRT experiments revealed that certain disinfection byproducts can induce mitochondrial dysfunction and enhance glycolytic function in cells, further highlighting the potential health implications. A LC-QTOF method was developed for the identification of TPs. The LC parameters (column, mobile phase, mobile phase, mobile phase modifiers, mobile phase gradients, flow rate, injection volume, needle wash method, and void time) and QTOF and MS parameters (source and compounds). Through TP analysis, a total of ten TPs were identified, with chlorination

resulting in more TPs compared to monochloramination. Notably, higher oxidant molar ratios during chlorination tend to break down the diphenylguandine's aromatic ring through intramolecular cyclization and hydroxylation processes and generate more monoguanidine TPs and hydroxylated DPG. The chlorine molar ratio 10 group with maximum TPs number and some highest TP intensity exhibits the maximum cytotoxicity in HepG2 cells and THP-1 cells, followed by the chlorine molar ratio 20 group with 9 identified TPs. This work also found that DPG-119 might contribute to the genotoxic response in chlorine molar ratio 20 and chlorine molar ratio 100 with its higher fold change in these two groups. These findings underscore the importance of careful handling and monitoring of DPG and disinfection processes to mitigate the associated risks to human health and the environment. Future studies should focus on the detailed characterization and toxicity evaluation of the identified TPs, providing further insights into their potential impact. Overall, this work contributes to the current understanding of DPG's behavior during disinfection procedures and highlights the significance of adopting appropriate safety measures in relevant industries and water treatment systems to mitigate potential risks to human health and the ecosystem.

6.2 Proposed future work

Future work includes:

(1) This work mostly compares chlorine and NH_2Cl effects on DPG Investigation of other oxidant effects on DPG to compare their degrading effects is needed. Besides, analysis of the radicals and ozone generation in the UV experiments is needed to figure out the reaction kinetics.

(2) NTA has been done in this work to identify the TPs of DPG after chlorination and monochloramination. Target analysis of TPs to verity their identity is required.

(3) This work only focused on DPG, one of the most leachable TWPs. A summarize of the TWPs characteristics regarding and TPs and their toxixicity is needed for future information of WTPs.

7. REFERENCES

Ali, S., & Coombes, R. C. (2000). Estrogen Receptor Alpha in Human Breast Cancer: Occurrence and Significance. *Journal of Mammary Gland Biology and Neoplasia*, *5*(3), 271–281. https://doi.org/10.1023/A:1009594727358

Allard, S., Cadee, K., Tung, R., & Croué, J.-P. (2018). Impact of brominated amines on monochloramine stability during in-line and pre-formed chloramination assessed by kinetic modelling. *Science of The Total Environment*, *618*, 1431–1439. https://doi.org/10.1016/j.scitotenv.2017.09.281

An, L., Liu, Q., Deng, Y., Wu, W., Gao, Y., & Ling, W. (2020). Sources of Microplastic in the Environment. In D. He & Y. Luo (Eds.), *Microplastics in Terrestrial Environments: Emerging Contaminants and Major Challenges* (pp. 143–159). Springer International Publishing. https://doi.org/10.1007/698_2020_449

Baensch-Baltruschat, B., Kocher, B., Stock, F., & Reifferscheid, G. (2020). Tyre and road wear particles (TRWP)—A review of generation, properties, emissions, human health risk, ecotoxicity, and fate in the environment. *Science of The Total Environment*, *733*, 137823. https://doi.org/10.1016/j.scitotenv.2020.137823

Baumann, W., & Ismeier, M. (1998). *Kautschuk und Gummi*. Springer. https://doi.org/10.1007/978-3-642-58916-4

Beita-Sandí, W., Selbes, M., Ersan, M. S., & Karanfil, T. (2019). Release of Nitrosamines and Nitrosamine Precursors from Scrap Tires. *Environmental Science & Technology Letters*, *6*(4), 251–256. https://doi.org/10.1021/acs.estlett.9b00172

Benitez, F. J., Acero, J. L., Real, F. J., Roldan, G., & Casas, F. (2011). Bromination of selected pharmaceuticals in water matrices. *Chemosphere*, *85*(9), 1430–1437. https://doi.org/10.1016/j.chemosphere.2011.08.022

Bolton, J. R., Beck, S. E., & Linden, K. G. (n.d.). *Protocol for the Determination of Fluence (UV Dose) Using A Low-Pressure or Low-Pressure High-Output UV Lamp in Bench-Scale Collimated Beam Ultraviolet Experiments*. 6.

Bougeard, C. M. M., Goslan, E. H., Jefferson, B., & Parsons, S. A. (2010). Comparison of the disinfection by-product formation potential of treated waters exposed to chlorine and monochloramine. *Water Research*, *44*(3), 729–740. https://doi.org/10.1016/j.watres.2009.10.008

Bricker, D. K., Taylor, E. B., Schell, J. C., Orsak, T., Boutron, A., Chen, Y.-C., Cox, J. E., Cardon, C. M., Van Vranken, J. G., Dephoure, N., Redin, C., Boudina, S., Gygi, S. P., Brivet, M., Thummel, C. S., & Rutter, J. (2012). A Mitochondrial Pyruvate Carrier Required for Pyruvate Uptake in Yeast, Drosophila, and Humans. *Science (New York, N.Y.)*, *337*(6090), 96–100. https://doi.org/10.1126/science.1218099

Bulman, D. M., Mezyk, S. P., & Remucal, C. K. (2019). The Impact of pH and Irradiation Wavelength on the Production of Reactive Oxidants during Chlorine

Photolysis. *Environmental Science & Technology*, *53*(8), 4450–4459. https://doi.org/10.1021/acs.est.8b07225

Burgoyne, R. D., & Morgan, A. (2003). Secretory Granule Exocytosis. *Physiological Reviews*, *83*(2), 581–632. https://doi.org/10.1152/physrev.00031.2002

Chibwe, L., Parrott, J. L., Shires, K., Khan, H., Clarence, S., Lavalle, C., Sullivan, C., O'Brien, A. M., De Silva, A. O., Muir, D. C. G., & Rochman, C. M. (2022). A Deep Dive into the Complex Chemical Mixture and Toxicity of Tire Wear Particle Leachate in Fathead Minnow. *Environmental Toxicology and Chemistry*, *41*(5), 1144–1153. https://doi.org/10.1002/etc.5140

Cimetiere, N., Dossier-Berne, F., & De Laat, J. (2009). Monochloramination of Resorcinol: Mechanism and Kinetic Modeling. *Environmental Science & Technology*, *43*(24), 9380–9385. https://doi.org/10.1021/es901425n

Dimeloe, S., Burgener, A.-V., Grählert, J., & Hess, C. (2017). T-cell metabolism governing activation, proliferation and differentiation; a modular view. *Immunology*, *150*(1), 35–44. https://doi.org/10.1111/imm.12655

Divakaruni, A., Paradyse, A., Ferrick, D., Murphy, A., & Jastroch, M. (2014). Analysis and Interpretation of Microplate-Based Oxygen Consumption and pH Data. *Methods in Enzymology*, *547*, 309–354. https://doi.org/10.1016/B978-0-12-801415-8.00016-3

Divakaruni, A. S., Wiley, S. E., Rogers, G. W., Andreyev, A. Y., Petrosyan, S., Loviscach, M., Wall, E. A., Yadava, N., Heuck, A. P., Ferrick, D. A., Henry, R. R., McDonald, W. G., Colca, J. R., Simon, M. I., Ciaraldi, T. P., & Murphy, A. N. (2013). Thiazolidinediones are acute, specific inhibitors of the mitochondrial pyruvate carrier. *Proceedings of the National Academy of Sciences of the United States of America*, *110*(14), 5422–5427.

Du, B., Tian, Z., Peter, K. T., Kolodziej, E. P., & Wong, C. S. (2020). Developing Unique Nontarget High-Resolution Mass Spectrometry Signatures to Track Contaminant Sources in Urban Waters. *Environmental Science & Technology Letters*, *7*(12), 923–930. https://doi.org/10.1021/acs.estlett.0c00749

Duirk, S. E., Gombert, B., Croué, J.-P., & Valentine, R. L. (2005). Modeling monochloramine loss in the presence of natural organic matter. *Water Research*, *39*(14), 3418–3431. https://doi.org/10.1016/j.watres.2005.06.003

Gallampois, C. M. J., Schymanski, E. L., Krauss, M., Ulrich, N., Bataineh, M., & Brack, W. (2015). Multicriteria Approach To Select Polyaromatic River Mutagen Candidates. *Environmental Science & Technology*, *49*(5), 2959–2968. https://doi.org/10.1021/es503640k

Gerets, H. H. J., Tilmant, K., Gerin, B., Chanteux, H., Depelchin, B. O., Dhalluin, S., & Atienzar, F. A. (2012). Characterization of primary human hepatocytes, HepG2 cells, and HepaRG cells at the mRNA level and CYP activity in response to inducers and

their predictivity for the detection of human hepatotoxins. *Cell Biology and Toxicology*, *28*(2), 69–87. https://doi.org/10.1007/s10565-011-9208-4

Ghanadi, M., Kah, M., Kookana, R. S., & Padhye, L. P. (2023). Formation of disinfection by-products from microplastics, tire wear particles, and other polymer-based materials. *Water Research*, *230*, 119528. https://doi.org/10.1016/j.watres.2022.119528

Gledhill, M., Beck, A. J., Stamer, B., Schlosser, C., & Achterberg, E. P. (2019). Quantification of munition compounds in the marine environment by solid phase extraction – ultra high performance liquid chromatography with detection by electrospray ionisation – mass spectrometry. *Talanta*, *200*, 366–372. https://doi.org/10.1016/j.talanta.2019.03.050

Goeury, K., Vo Duy, S., Munoz, G., Prévost, M., & Sauvé, S. (2019). Analysis of Environmental Protection Agency priority endocrine disruptor hormones and bisphenol A in tap, surface and wastewater by online concentration liquid chromatography tandem mass spectrometry. *Journal of Chromatography A*, *1591*, 87–98. https://doi.org/10.1016/j.chroma.2019.01.016

Gu, X., Ma, Y., Liu, Y., & Wan, Q. (2021). Measurement of mitochondrial respiration in adherent cells by Seahorse XF96 Cell Mito Stress Test. *STAR Protocols*, *2*(1), 100245. https://doi.org/10.1016/j.xpro.2020.100245

Guay, C., Rodriguez, M., & Sérodes, J. (2005). Using ozonation and chloramination to reduce the formation of trihalomethanes and haloacetic acids in drinking water. *Desalination*, *176*(1), 229–240. https://doi.org/10.1016/j.desal.2004.10.015

Guo, K., Wu, Z., Shang, C., Yao, B., Hou, S., Yang, X., Song, W., & Fang, J. (2017). Radical Chemistry and Structural Relationships of PPCP Degradation by UV/Chlorine Treatment in Simulated Drinking Water. *Environmental Science & Technology*, *51*(18), 10431–10439. https://doi.org/10.1021/acs.est.7b02059

Hafner, A., Bulyk, M. L., Jambhekar, A., & Lahav, G. (2019). The multiple mechanisms that regulate p53 activity and cell fate. *Nature Reviews Molecular Cell Biology*, *20*(4), Article 4. https://doi.org/10.1038/s41580-019-0110-x

Heeb, M. B., Kristiana, I., Trogolo, D., Arey, J. S., & von Gunten, U. (2017). Formation and reactivity of inorganic and organic chloramines and bromamines during oxidative water treatment. *Water Research*, *110*, 91–101. https://doi.org/10.1016/j.watres.2016.11.065

Hu, C., Xiong, C., Lin, Y.-L., Zhu, Y., Wang, Q., Xu, L., & Huang, D. (2022). Degradation of 2-phenylbenzimidazole 5-sulfonic acid by UV/chlorine advanced oxidation technology: Kinetic model, degradation byproducts and reaction pathways. *Journal of Hazardous Materials*, *431*, 128574. https://doi.org/10.1016/j.jhazmat.2022.128574

Hu, W., Lauritsen, F. R., & Allard, S. (2021). Identification and quantification of chloramines, bromamines and bromochloramine by Membrane Introduction Mass Spectrometry (MIMS). *Science of The Total Environment*, *751*, 142303. https://doi.org/10.1016/j.scitotenv.2020.142303

Hua, G., & Reckhow, D. A. (2007). Comparison of disinfection byproduct formation from chlorine and alternative disinfectants. *Water Research*, *41*(8), 1667–1678. https://doi.org/10.1016/j.watres.2007.01.032

Isaac, R. A., & Morris, J. Carrell. (1985). Transfer of active chlorine from chloramine to nitrogenous organic compounds. 2. Mechanism. *Environmental Science & Technology*, *19*(9), 810–814. https://doi.org/10.1021/es00139a007

Ishaq, M. S., Afsheen, Z., Khan, A., Khan, A., Ishaq, M. S., Afsheen, Z., Khan, A., & Khan, A. (2018). Disinfection Methods. In *Photocatalysts—Applications and Attributes*. IntechOpen. https://doi.org/10.5772/intechopen.80999

Jia, S., Marques Dos Santos, M., Li, C., Fang, M., Sureshkumar, M., & Snyder, S. A. (2023). Analogy or fallacy, unsafe chemical alternatives: Mechanistic insights into energy metabolism dysfunction induced by Bisphenol analogs in HepG2 cells. *Environment International*, *175*, 107942. https://doi.org/10.1016/j.envint.2023.107942

Jin, J., van Swaaij, A. P. J., Noordermeer, J. W. M., Blume, A., & Dierkes, W. K. (2021). On the various roles of 1,3-DIPHENYL Guanidine in silica/silane reinforced sbr/br blends. *Polymer Testing*, *93*, 106858. https://doi.org/10.1016/j.polymertesting.2020.106858

Johannessen, C., Helm, P., Lashuk, B., Yargeau, V., & Metcalfe, C. D. (2022). The Tire Wear Compounds 6PPD-Quinone and 1,3-Diphenylguanidine in an Urban Watershed. *Archives of Environmental Contamination and Toxicology*, *82*(2), 171–179. https://doi.org/10.1007/s00244-021-00878-4

Kloepfer, A., Jekel, M., & Reemtsma, T. (2004). Determination of benzothiazoles from complex aqueous samples by liquid chromatography–mass spectrometry following solid-phase extraction. *Journal of Chromatography A*, *1058*(1), 81–88. https://doi.org/10.1016/j.chroma.2004.08.081

Kole, P. J., Löhr, A. J., Van Belleghem, F. G. A. J., & Ragas, A. M. J. (2017). Wear and Tear of Tyres: A Stealthy Source of Microplastics in the Environment. *International Journal of Environmental Research and Public Health*, *14*(10), Article 10. https://doi.org/10.3390/ijerph14101265

Kolomijeca, A., Parrott, J., Khan, H., Shires, K., Clarence, S., Sullivan, C., Chibwe, L., Sinton, D., & Rochman, C. M. (2020). Increased Temperature and Turbulence Alter the Effects of Leachates from Tire Particles on Fathead Minnow (Pimephales promelas). *Environmental Science & Technology*, *54*(3), 1750–1759. https://doi.org/10.1021/acs.est.9b05994

Lankoff, A., Sandberg, W. J., Wegierek-Ciuk, A., Lisowska, H., Refsnes, M., Sartowska, B., Schwarze, P. E., Meczynska-Wielgosz, S., Wojewodzka, M., & Kruszewski, M. (2012). The effect of agglomeration state of silver and titanium dioxide nanoparticles on cellular response of HepG2, A549 and THP-1 cells. *Toxicology Letters*, *208*(3), 197–213. https://doi.org/10.1016/j.toxlet.2011.11.006

Leclercq, G. (2018). Natural Anti-Estrogen Receptor Alpha Antibodies Able to Induce Estrogenic Responses in Breast Cancer Cells: Hypotheses Concerning Their Mechanisms of Action and Emergence. *International Journal of Molecular Sciences*, *19*(2), Article 2. https://doi.org/10.3390/ijms19020411

Li, Z.-M., & Kannan, K. (2023). Determination of 1,3-Diphenylguanidine, 1,3-Di- *o* -tolylguanidine, and 1,2,3-Triphenylguanidine in Human Urine Using Liquid Chromatography-Tandem Mass Spectrometry. *Environmental Science & Technology*, *57*(24), 8883–8889. https://doi.org/10.1021/acs.est.3c00412

Magnusson, K., Eliasson, K., Fråne, A., Haikonen, K., Hultén, J., Olshammar, M., Stadmark, J., & Voisin, A. (n.d.). *Swedish sources and pathways for microplastics to the marine environment*.

Marei, H. E., Althani, A., Afifi, N., Hasan, A., Caceci, T., Pozzoli, G., Morrione, A., Giordano, A., & Cenciarelli, C. (2021). P53 signaling in cancer progression and therapy. *Cancer Cell International*, *21*(1), 703. https://doi.org/10.1186/s12935-021-02396-8

Marques Dos Santos, M., Cheriaux, C., Jia, S., Thomas, M., Gallard, H., Croué, J.-P., Carato, P., & Snyder, S. A. (2022). Genotoxic effects of chlorinated disinfection by-products of 1,3-diphenylguanidine (DPG): Cell-based in-vitro testing and formation potential during water disinfection. *Journal of Hazardous Materials*, *436*, 129114. https://doi.org/10.1016/j.jhazmat.2022.129114

Mohamed, B. M., Verma, N. K., Prina-Mello, A., Williams, Y., Davies, A. M., Bakos, G., Tormey, L., Edwards, C., Hanrahan, J., Salvati, A., Lynch, I., Dawson, K., Kelleher, D., & Volkov, Y. (2011). Activation of stress-related signalling pathway in human cells upon SiO2 nanoparticles exposure as an early indicator of cytotoxicity. *Journal of Nanobiotechnology*, *9*(1), 29. https://doi.org/10.1186/1477-3155-9-29

Müller, K., Hübner, D., Huppertsberg, S., Knepper, T. P., & Zahn, D. (2022). Probing the chemical complexity of tires: Identification of potential tire-borne water contaminants with high-resolution mass spectrometry. *Science of The Total Environment*, *802*, 149799. https://doi.org/10.1016/j.scitotenv.2021.149799

Muller, P. A. J., & Vousden, K. H. (2013). P53 mutations in cancer. *Nature Cell Biology*, *15*(1), Article 1. https://doi.org/10.1038/ncb2641

Ochocki, J. D., & Simon, M. C. (2013). Nutrient-sensing pathways and metabolic regulation in stem cells. *Journal of Cell Biology*, *203*(1), 23–33. https://doi.org/10.1083/jcb.201303110

Peter, K. T., Tian, Z., Wu, C., Lin, P., White, S., Du, B., McIntyre, J. K., Scholz, N. L., & Kolodziej, E. P. (2018). Using High-Resolution Mass Spectrometry to Identify Organic Contaminants Linked to Urban Stormwater Mortality Syndrome in Coho Salmon. *Environmental Science & Technology*, *52*(18), 10317–10327. https://doi.org/10.1021/acs.est.8b03287

Petrie, B., Youdan, J., Barden, R., & Kasprzyk-Hordern, B. (2016). Multi-residue analysis of 90 emerging contaminants in liquid and solid environmental matrices by ultra-high-performance liquid chromatography tandem mass spectrometry. *Journal of Chromatography A*, *1431*, 64–78. https://doi.org/10.1016/j.chroma.2015.12.036

Phillips, A. L., Williams, A. J., Sobus, J. R., Ulrich, E. M., Gundersen, J., Langlois-Miller, C., & Newton, S. R. (2022). A Framework for Utilizing High-Resolution Mass Spectrometry and Nontargeted Analysis in Rapid Response and Emergency Situations. *Environmental Toxicology and Chemistry*, *41*(5), 1117–1130. https://doi.org/10.1002/etc.5196

Quintana, J. B., Rodil, R., & Rodríguez, I. (2014). Transformation Products of Emerging Contaminants upon Reaction with Conventional Water Disinfection Oxidants. In *Transformation Products of Emerging Contaminants in the Environment* (pp. 123–160). John Wiley & Sons, Ltd. https://doi.org/10.1002/9781118339558.ch04

Redondo-Hasselerharm, P. E., de Ruijter, V. N., Mintenig, S. M., Verschoor, A., & Koelmans, A. A. (2018). Ingestion and Chronic Effects of Car Tire Tread Particles on Freshwater Benthic Macroinvertebrates. *Environmental Science & Technology*, *52*(23), 13986–13994. https://doi.org/10.1021/acs.est.8b05035

Santen, R., Cavalieri, E., Rogan, E., Russo, J., Guttenplan, J., Ingle, J., & Yue, W. (2009). Estrogen Mediation of Breast Tumor Formation Involves Estrogen Receptor-Dependent, as Well as Independent, Genotoxic Effects. *Annals of the New York Academy of Sciences*, *1155*(1), 132–140. https://doi.org/10.1111/j.1749-6632.2008.03685.x

Schulze, S., Zahn, D., Montes, R., Rodil, R., Quintana, J. B., Knepper, T. P., Reemtsma, T., & Berger, U. (2019). Occurrence of emerging persistent and mobile organic contaminants in European water samples. *Water Research*, *153*, 80–90. https://doi.org/10.1016/j.watres.2019.01.008

Seidel, C. J., McGuire, M. J., Summers, R. S., & Via, S. (2005). Have utilities switched to chloramines? *Journal AWWA*, *97*(10), 87–97. https://doi.org/10.1002/j.1551-8833.2005.tb07497.x

Seiwert, B., Klöckner, P., Wagner, S., & Reemtsma, T. (2020). Source-related smart suspect screening in the aqueous environment: Search for tire-derived persistent and mobile trace organic contaminants in surface waters. *Analytical and Bioanalytical Chemistry*, *412*(20), 4909–4919. https://doi.org/10.1007/s00216-020-02653-1

Sieira, B. J., Montes, R., Touffet, A., Rodil, R., Cela, R., Gallard, H., & Quintana, J. B. (2020). Chlorination and bromination of 1,3-diphenylguanidine and 1,3-di-o-

tolylguanidine: Kinetics, transformation products and toxicity assessment. *Journal of Hazardous Materials*, *385*, 121590. https://doi.org/10.1016/j.jhazmat.2019.121590

Smith, R. A. J., Hartley, R. C., Cochemé, H. M., & Murphy, M. P. (2012). Mitochondrial pharmacology. *Trends in Pharmacological Sciences*, *33*(6), 341–352. https://doi.org/10.1016/j.tips.2012.03.010

Snyder, M. P., & Margerum, D. W. (1982). Kinetics of chlorine transfer from chloramine to amines, amino acids, and peptides. *Inorganic Chemistry*, *21*(7), 2545–2550. https://doi.org/10.1021/ic00137a005

Snyder, S. A. (2014). Emerging chemical contaminants: Looking for greater harmony. *Journal (American Water Works Association)*, *106*(8), 38–52.

Tang, S., Sun, X., Qiao, X., Cui, W., Yu, F., Zeng, X., Covaci, A., & Chen, D. (2022). Prenatal Exposure to Emerging Plasticizers and Synthetic Antioxidants and Their Potency to Cross Human Placenta. *Environmental Science & Technology*, *56*(12), 8507–8517. https://doi.org/10.1021/acs.est.2c01141

Unice, K. M., Bare, J. L., Kreider, M. L., & Panko, J. M. (2015). Experimental methodology for assessing the environmental fate of organic chemicals in polymer matrices using column leaching studies and OECD 308 water/sediment systems: Application to tire and road wear particles. *Science of The Total Environment*, *533*, 476–487. https://doi.org/10.1016/j.scitotenv.2015.06.053

Vikesland, P. J., Ozekin, K., & Valentine, R. L. (1998). Effect of Natural Organic Matter on Monochloramine Decomposition: Pathway Elucidation through the Use of Mass and Redox Balances. *Environmental Science & Technology*, *32*(10), 1409–1416. https://doi.org/10.1021/es970589a

Wagner, S., Hüffer, T., Klöckner, P., Wehrhahn, M., Hofmann, T., & Reemtsma, T. (2018). S. *Water Research*, *139*, 83–100. https://doi.org/10.1016/j.watres.2018.03.051

Wik, A., & Dave, G. (2009). Occurrence and effects of tire wear particles in the environment – A critical review and an initial risk assessment. *Environmental Pollution*, *157*(1), 1–11. https://doi.org/10.1016/j.envpol.2008.09.028

Xu, C., Zhang, B., Gu, C., Shen, C., Yin, S., Aamir, M., & Li, F. (2020). Are we underestimating the sources of microplastic pollution in terrestrial environment? *Journal of Hazardous Materials*, *400*, 123228. https://doi.org/10.1016/j.jhazmat.2020.123228

Yen, J.-H., Weng, C.-Y., Li, S., Lo, Y.-H., Pan, M.-H., Fu, S.-H., Ho, C.-T., & Wu, M.-J. (2011). Citrus flavonoid 5-demethylnobiletin suppresses scavenger receptor expression in THP-1 cells and alters lipid homeostasis in HepG2 liver cells. *Molecular Nutrition & Food Research*, *55*(5), 733–748. https://doi.org/10.1002/mnfr.201000226

Zahn, D., Mucha, P., Zilles, V., Touffet, A., Gallard, H., Knepper, T. P., & Frömel, T. (2019). Identification of potentially mobile and persistent transformation products of

REACH-registered chemicals and their occurrence in surface waters. *Water Research*, *150*, 86–96. https://doi.org/10.1016/j.watres.2018.11.042

Zhang, A., Jia, A., Park, M., Li, Y., & Snyder, S. A. (2019). Genotoxicity assay and potential byproduct identification during different UV-based water treatment processes. *Chemosphere*, *217*, 176–182. https://doi.org/10.1016/j.chemosphere.2018.11.031

Zhang, Z., Zhou, Y., Han, L., Guo, X., Wu, Z., Fang, J., Hou, B., Cai, Y., Jiang, J., & Yang, Z. (2021). Impacts of COVID-19 pandemic on the aquatic environment associated with disinfection byproducts and pharmaceuticals. *Science of The Total Environment*, 151409. https://doi.org/10.1016/j.scitotenv.2021.151409

Zhao, J., Peng, J., Yin, R., Fan, M., Yang, X., & Shang, C. (2022). Multi-angle comparison of UV/chlorine, UV/monochloramine, and UV/chlorine dioxide processes for water treatment and reuse. *Water Research*, 118414. https://doi.org/10.1016/j.watres.2022.118414

Zuo, Y.-T., Hu, Y., Lu, W.-W., Cao, J.-J., Wang, F., Han, X., Lu, W.-Q., & Liu, A.-L. (2017). Toxicity of 2, 6-dichloro-1, 4-benzoquinone and five regulated drinking water disinfection by-products for the Caenorhabditis elegans nematode. *Journal of Hazardous Materials*, *321*, 456–463.

8. APPENDIX A

Colorimetric Reaction of DPD

Object	Chloramine (Mono)	Chlorine, Free	Chlorine, Total
Instrument	**HACH DR900 (Orientation mark toward user)**		
Method	Indophenol Method	USEPA DPD Method	
Range	0.02 – 2.00 mg/L Cl_2 (LR)	0.02 – 2.00 mg/L Cl_2	0.02 – 2.00 mg/L Cl_2
Program	Monochloramine LR	80 Chlorine F&T PP	80 Chlorine F&T PP
Blank	10 mL sample in sample cell		
Powder	Monochlor F	Free chlorine	
Mixture	Shake (Up and Down) 20s	Swirl 20s	Swirl 20s
Color	Yellow->Green	Pink	Pink
Reaction time	5 min (18–20 ºC) 2.5 min (23 ºC) 2min (above 25 ºC)	Within 60s	3 min
Note	Test results are strongly influenced by temperature. If T<10° C, measure again after 5-10 min.		

9. APPENDIX B

Method of SPE

1) Condition cartridge with 5.0 mL of Solvent 3 into solvent waste
2) Condition cartridge with 5.0 mL methanol (MeOH) into solvent waste
3) Condition cartridge with 5.0 mL of water into aqueous waste
4) Load sample onto cartridge
5) Rinse cartridge with 5.0 mL of water into aqueous waste
6) Dry cartridge with gas for 45.0 minutes
7) Wash Syringe with 5.0 mL of MeOH
8) Collect 5.0mL fraction into sample tube using methanol
9) Wash syringe with 5.0 mL of 10% methanol in MTBE (methyl tert-butyl ether)
10) Collect 5.0 mL fraction into sample tube using 10% MeOH in MTBE

10. APPENDIX C

LC/MS Method Condition

LC conditions				
Guard-column	Poroshell 120 EC-C18, 1.9 μm (2.1 mm x 5 mm)			
Column	Poroshell 120 EC-C18, 1.9 μm (2.1 mm x 100 mm)			
Column Temperature	40 °C			
Injection Volume	20 μL			
Binary Pump Flow	0.4 mL/min			
Solvent A	Water + 0.1% Formic Acid			
Solvent B	Acetonitrile + 0.1% Formic Acid			
LC Gradient				
Time (min)	**A (%)**	**B (%)**		
0	95	5		
1	95	5		
3	0	100		
4	0	100		
Post Analysis Time	1.5 minutes			
MS conditions				
Gas Temp (°C)	150			
Gas Flow (l/min)	15			
Nebulizer (psi)	40			
Sheath Gas Heater	400			
Sheath Gas Flow	12			
Capillary (V)	3500			
VCharging	1500			
Pos High Pressure RF (V)	70			
Pos Low Pressure RF (V)	40			
Fragmentor (V)	166			
Collision Cell Accelerator (V)	5			
MS Transitions				
Compound	**Precursor Ion (m/z)**	**Product Ion (m/z)**	**Collision Energy (V)**	**Retention Time (min)**
DPG	212.12	119.1	24	2.2
	(212.12)	(77.1)	48	

11. APPENDIX D

LC/QTOF-MS Method Condition

LC conditions		
Guard-column	Poroshell 120 EC-C18, 1.9 μm (2.1 mm x 5 mm)	
Column	Poroshell 120 EC-C18, 1.9 μm (2.1 mm x 100 mm)	
Column Temperature	30 °C	
Injection Volume	10.00 μL	
Binary Pump Flow	0.4 mL/min	
Solvent A	Water + 0.1% Formic Acid	
Solvent B	Acetonitrile + 0.1% Formic Acid	
LC Gradient		
Time (min)	**A (%)**	**B (%)**
0	95	5
4	95	5
8	10	90
8.1	0	100
10	0	100
10.1	95	5
20	95	5
MS Q-TOF conditions		
Polarity	Positive	
Gas Temp (°C)	200	
Gas Flow (l/min)	14	
Nebulizer (psi)	35	
Sheath Gas Heater	350	
Sheath Gas Flow	11	
Capillary (V)	3500	
VCharging	1000	
Pos High Pressure RF (V)	70	
Pos Low Pressure RF (V)	40	
Fragmentor (V)	175	
Collision Cell Accelerator (V)	5	
MS/MS conditions		
MS Min Range (m/z)	100	
MS Max Range (m/z)	1700	
MS/MS Min Range (m/z)	50	
MS/MS Max Range (m/z)	1700	
Collision Energies	20.00, 30.00	
Gas Temp (°C)	200	
Gas Flow (l/min)	14	
Nebulizer (psi)	35	

Sheath Gas Heater	350
Sheath Gas Flow	11

12. APPENDIX E

MS/MS spectrum ot DPG TPs

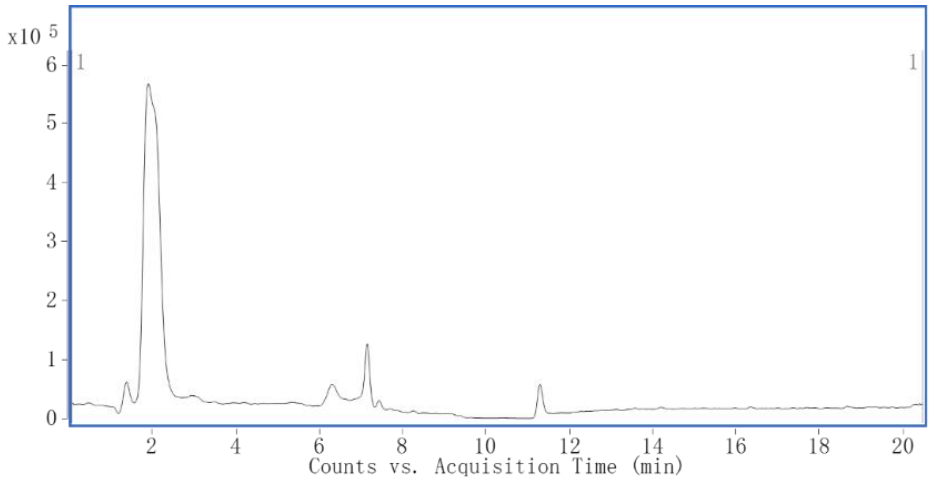

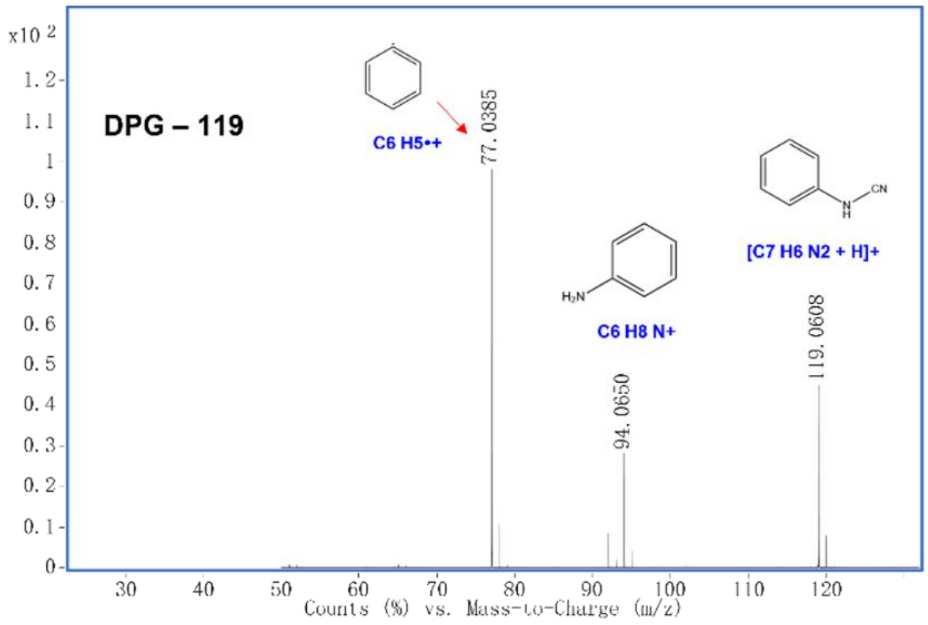

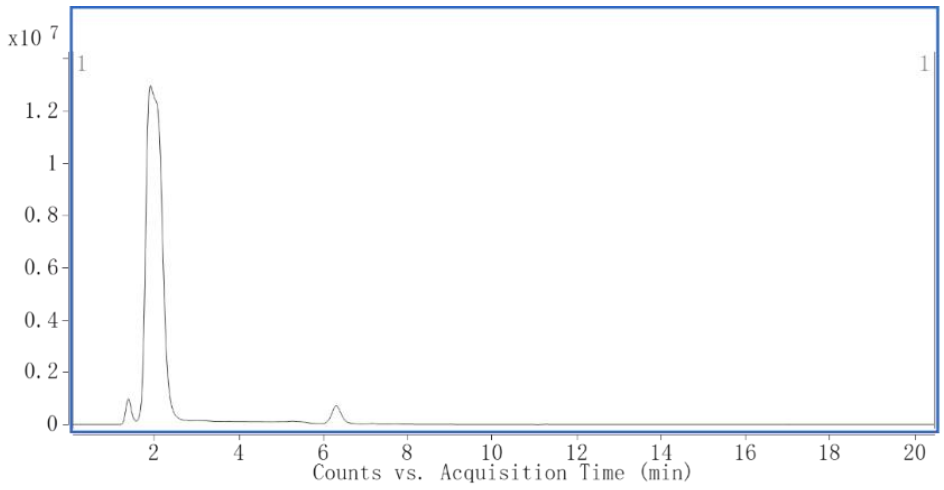
x10 7
1
1
1.2
1
0.8
0.6
0.4
0.2
0
2
4
6
8
10
12
14
16
18
20
Counts vs. Acquisition Time (min)

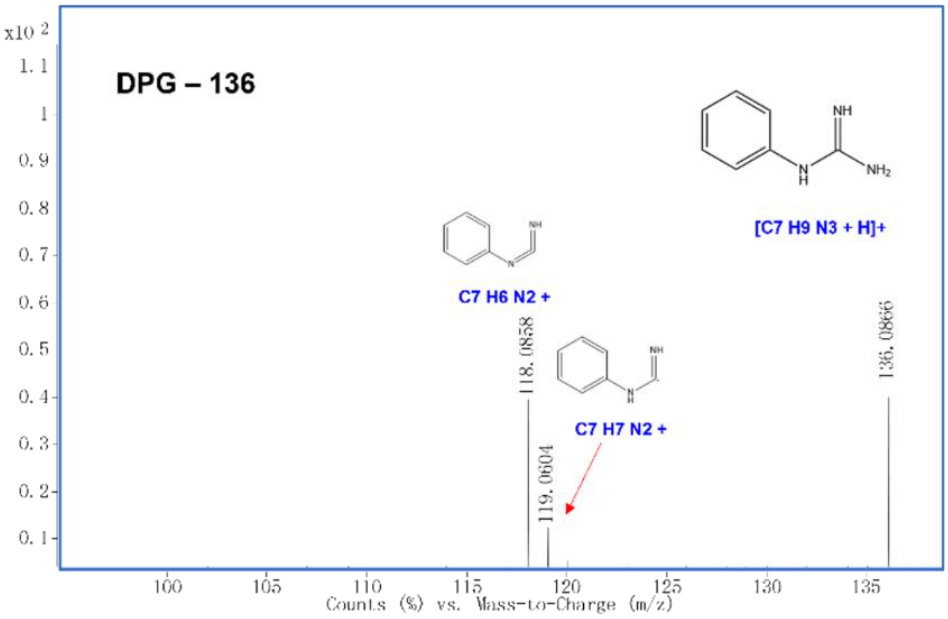
x10 2
1.1
1
0.9
0.8
0.7
0.6
0.5
0.4
0.3
0.2
0.1
DPG – 136
NH
N
H
NH2
[C7 H9 N3 + H]+
NH
N
C7 H6 N2 +
118.0858
NH
N
C7 H7 N2 +
119.0604
136.0866
100
105
110
115
120
125
130
135
Counts (%) vs. Mass-to-Charge (m/z)

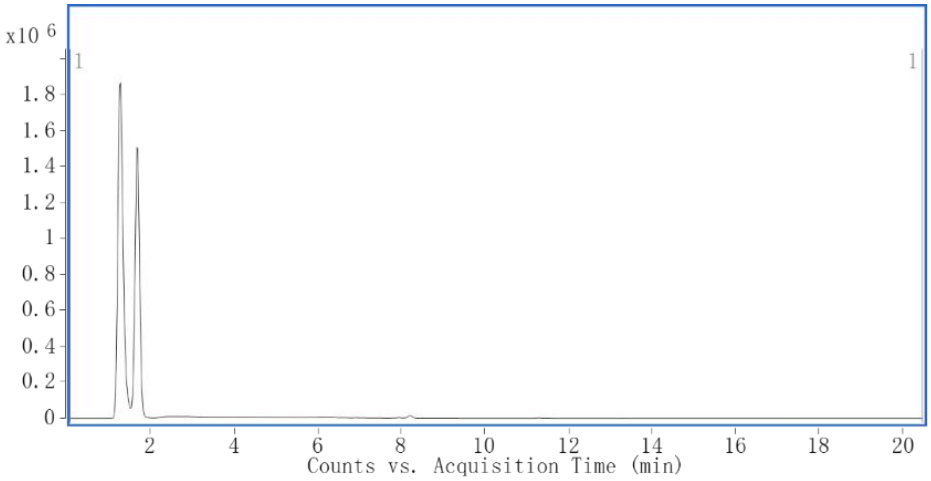
x10 6
1
1
1.8
1.6
1.4
1.2
1
0.8
0.6
0.4
0.2
0
2
4
6
8
10
12
14
16
18
20
Counts vs. Acquisition Time (min)

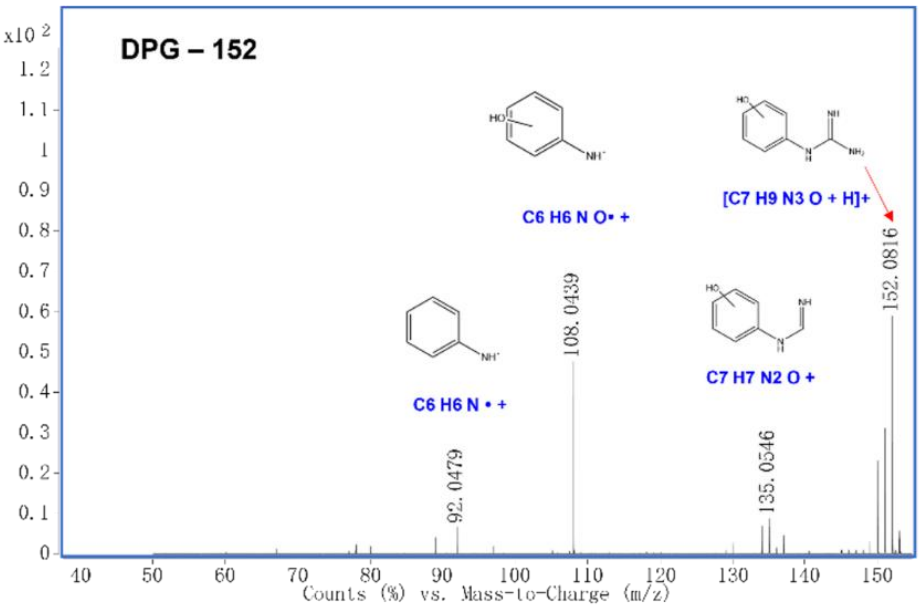
DPG – 152
x10 2
1.2
1.1
1
0.9
0.8
0.7
0.6
0.5
0.4
0.3
0.2
0.1
0
C6 H6 N O• +
[C7 H9 N3 O + H]+
C6 H6 N • +
C7 H7 N2 O +
92.0479
108.0439
135.0546
152.0816
40
50
60
70
80
90
100
110
120
130
140
150
Counts (%) vs. Mass-to-Charge (m/z)

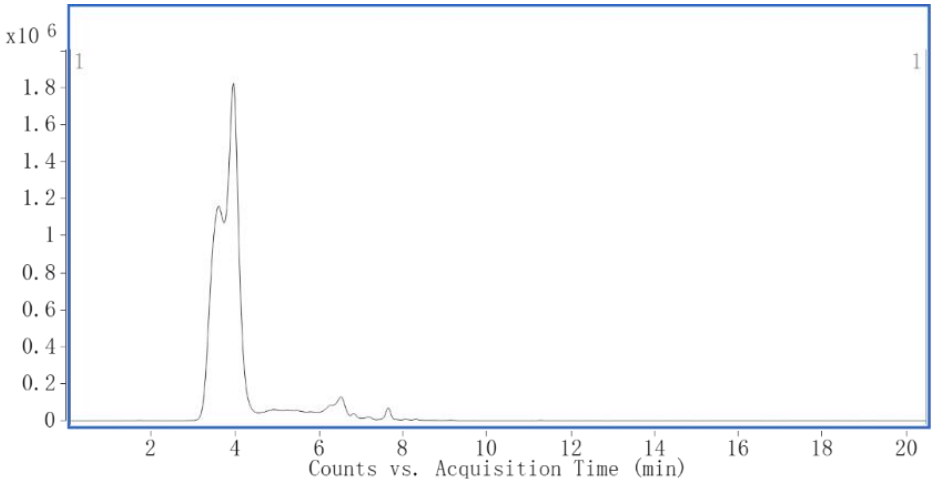
x10 6
1
1
1.8
1.6
1.4
1.2
1
0.8
0.6
0.4
0.2
0
2
4
6
8
10
12
14
16
18
20
Counts vs. Acquisition Time (min)

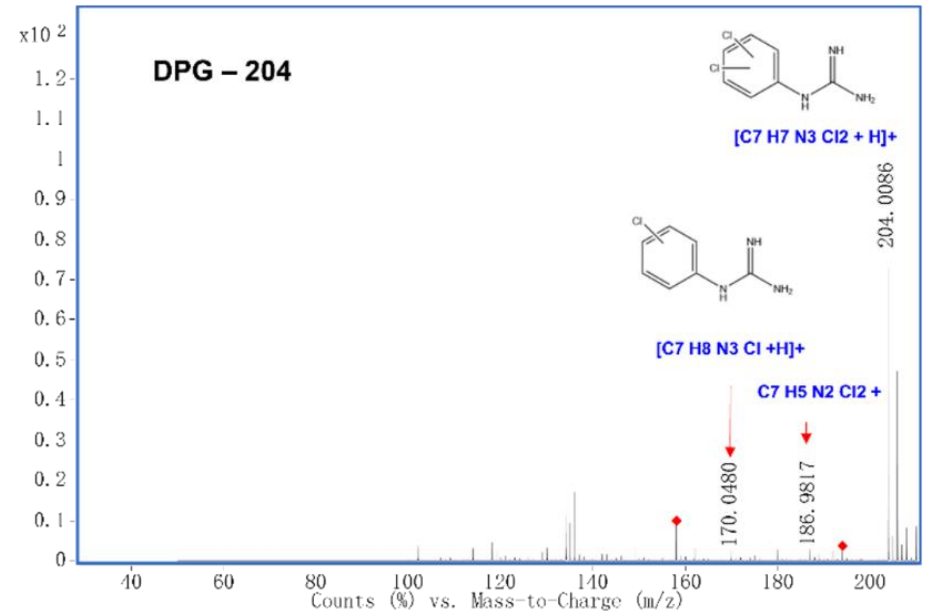
x10 2
DPG – 204
[C7 H7 N3 Cl2 + H]+
204.0086
[C7 H8 N3 Cl +H]+
C7 H5 N2 Cl2 +
170.0480
186.9817
1.2
1.1
1
0.9
0.8
0.7
0.6
0.5
0.4
0.3
0.2
0.1
0
40
60
80
100
120
140
160
180
200
Counts (%) vs. Mass-to-Charge (m/z)

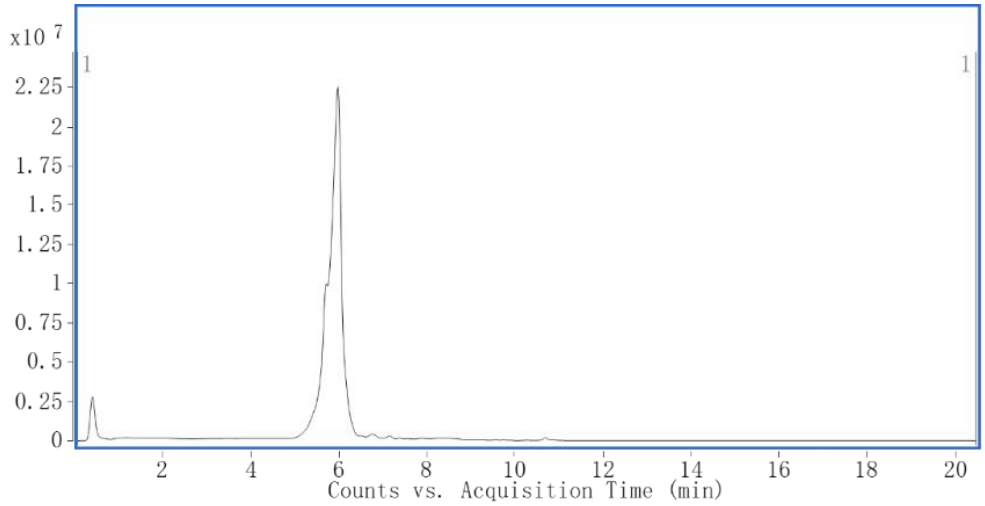
x10 7
2.25
2
1.75
1.5
1.25
1
0.75
0.5
0.25
0
2
4
6
8
10
12
14
16
18
20
Counts vs. Acquisition Time (min)

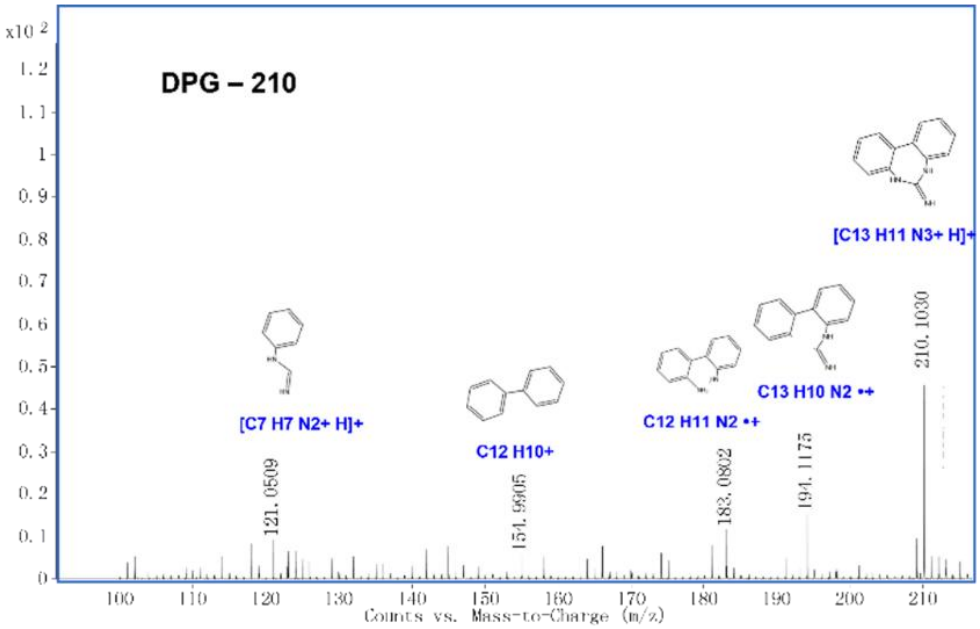
x10 2
DPG – 210
[C13 H11 N3+ H]+
[C7 H7 N2+ H]+
C12 H10+
C12 H11 N2 •+
C13 H10 N2 •+
121.0509
154.0965
183.0802
194.1175
210.1030
100
110
120
130
140
150
160
170
180
190
200
210
Counts vs. Mass-to-Charge (m/z)

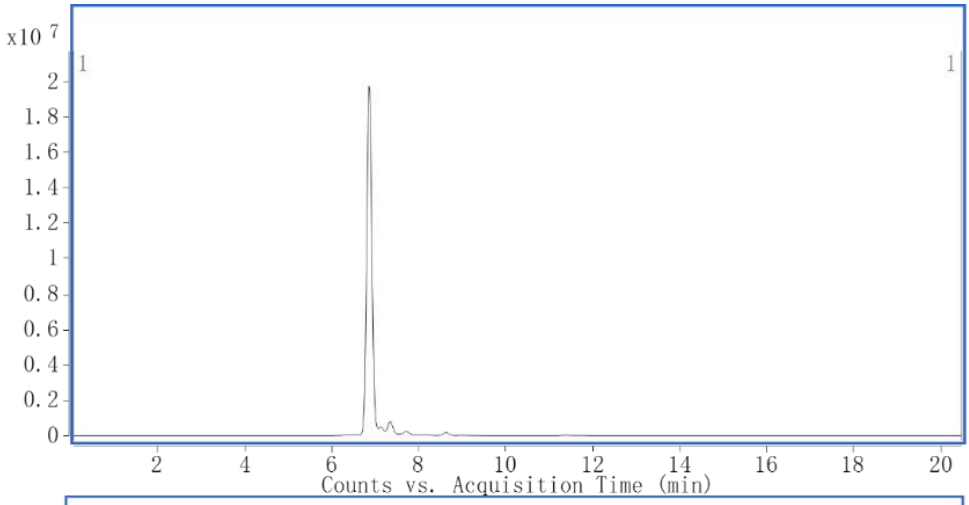
x10 7
1
1
2
1.8
1.6
1.4
1.2
1
0.8
0.6
0.4
0.2
0
2
4
6
8
10
12
14
16
18
20
Counts vs. Acquisition Time (min)

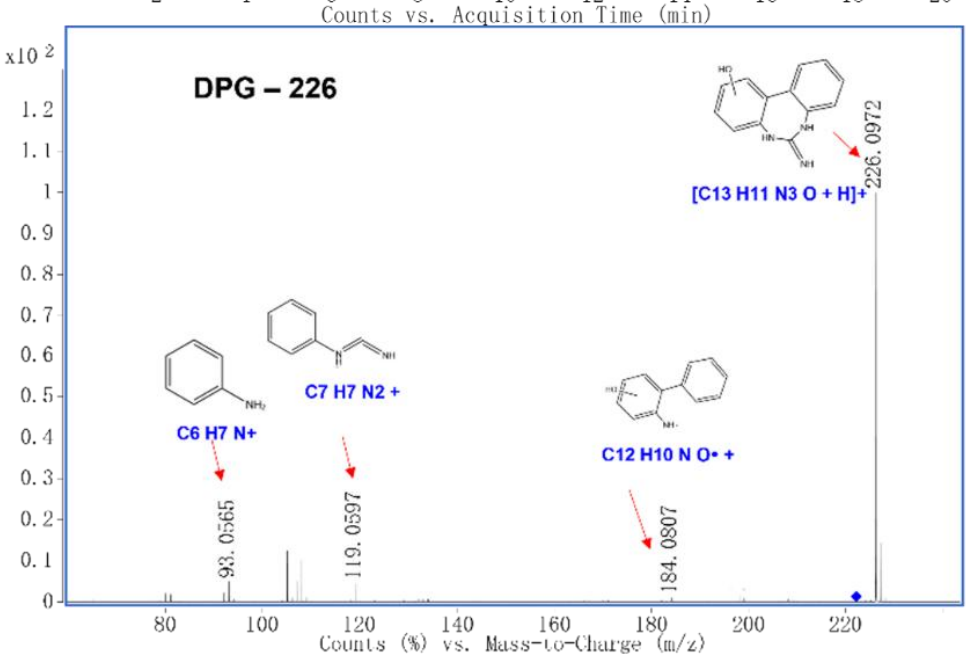
x10 2
DPG – 226
[C13 H11 N3 O + H]+
226.0972
C7 H7 N2 +
C6 H7 N+
C12 H10 N O• +
93.0565
119.0597
184.0807
1.2
1.1
1
0.9
0.8
0.7
0.6
0.5
0.4
0.3
0.2
0.1
0
80
100
120
140
160
180
200
220
Counts (%) vs. Mass-to-Charge (m/z)

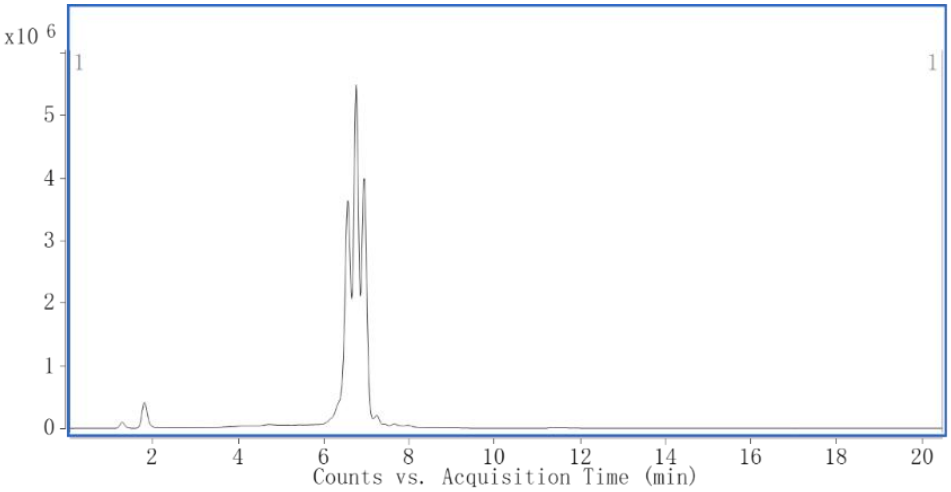
x10 6
1
1
5
4
3
2
1
0
2
4
6
8
10
12
14
16
18
20
Counts vs. Acquisition Time (min)

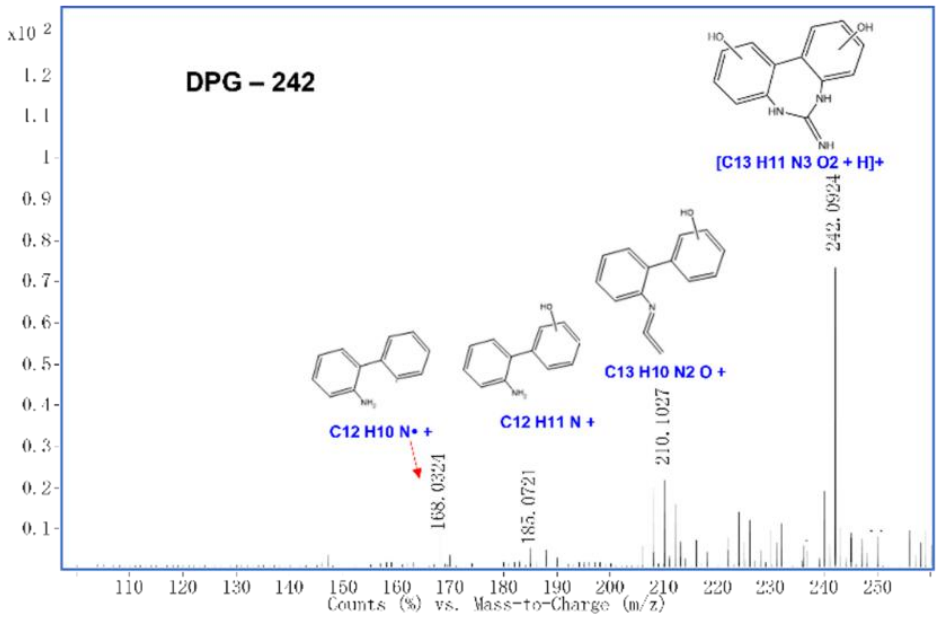
x10 2
DPG – 242
1.2
1.1
1
0.9
0.8
0.7
0.6
0.5
0.4
0.3
0.2
0.1
[C13 H11 N3 O2 + H]+
242.0924
C13 H10 N2 O +
210.1027
C12 H11 N +
185.0721
C12 H10 N• +
168.0324
110
120
130
140
150
160
170
180
190
200
210
220
230
240
250
Counts (%) vs. Mass-to-Charge (m/z)

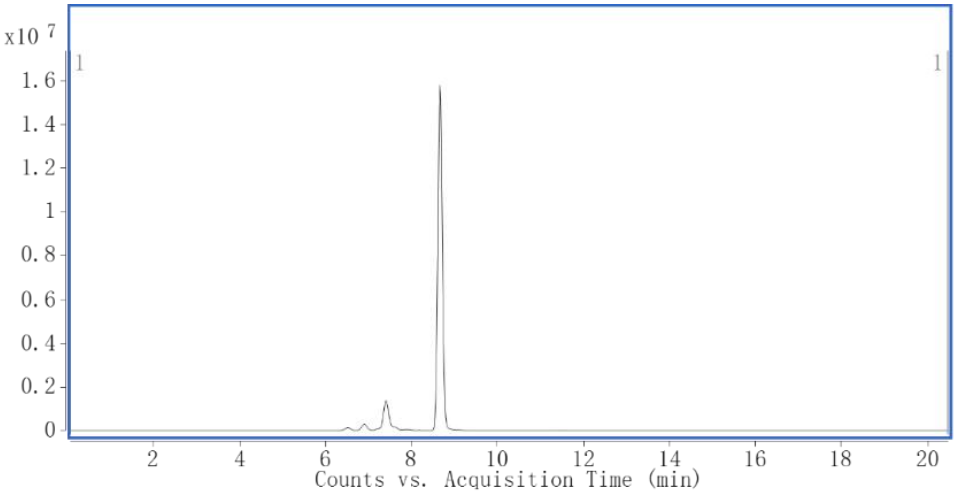
x10 7
1.6
1.4
1.2
1
0.8
0.6
0.4
0.2
0
2
4
6
8
10
12
14
16
18
20
Counts vs. Acquisition Time (min)

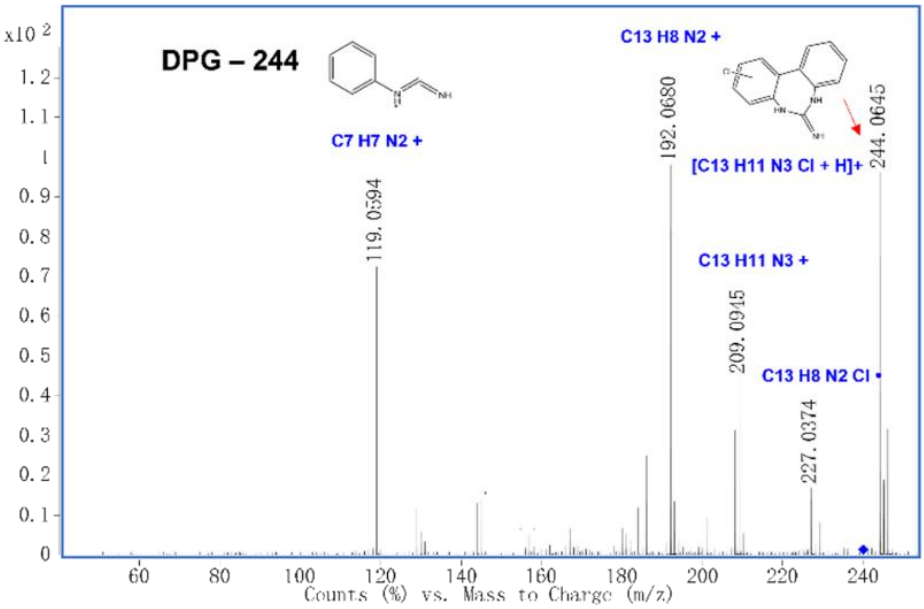
DPG – 244
C7 H7 N2 +
C13 H8 N2 +
[C13 H11 N3 Cl + H]+
C13 H11 N3 +
C13 H8 N2 Cl •
119.0594
192.0680
209.0945
227.0374
244.0645
x10 2
1.2
1.1
1
0.9
0.8
0.7
0.6
0.5
0.4
0.3
0.2
0.1
0
60
80
100
120
140
160
180
200
220
240
Counts (%) vs. Mass to Charge (m/z)

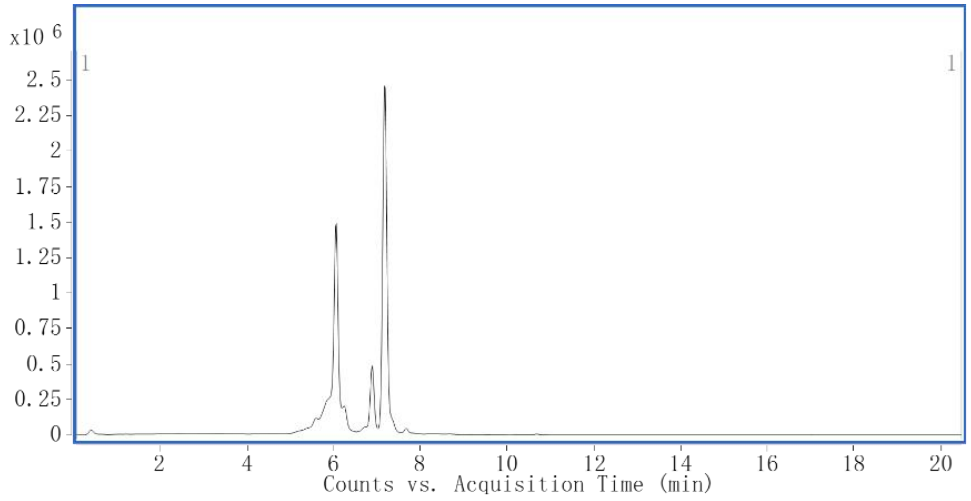
x10 6
2.5
2.25
2
1.75
1.5
1.25
1
0.75
0.5
0.25
0
2
4
6
8
10
12
14
16
18
20
Counts vs. Acquisition Time (min)

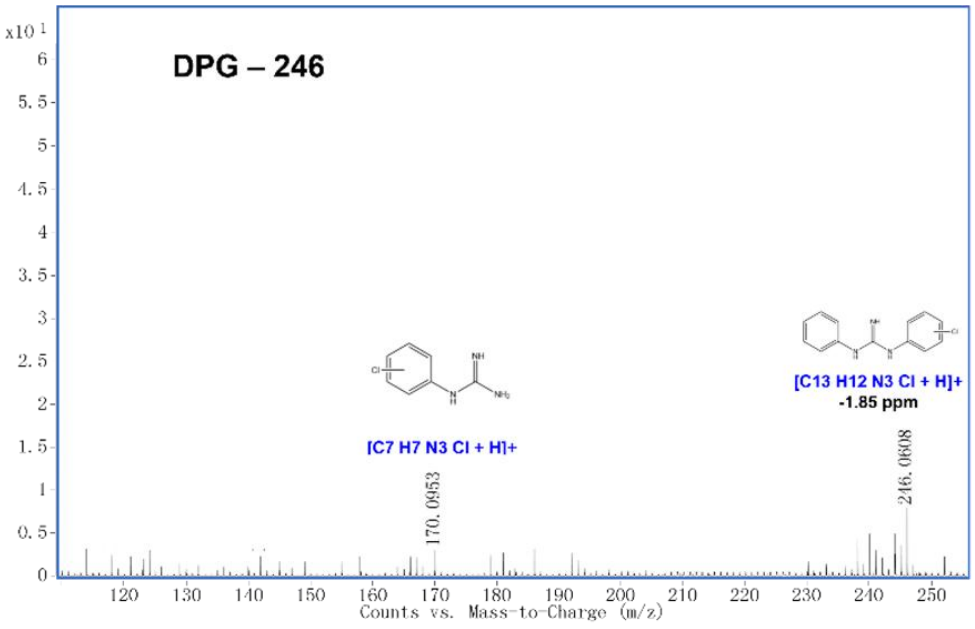
DPG – 246
x10 1
6
5.5
5
4.5
4
3.5
3
2.5
2
1.5
1
0.5
0
[C7 H7 N3 Cl + H]+
170.0953
[C13 H12 N3 Cl + H]+
-1.85 ppm
246.0608
120
130
140
150
160
170
180
190
200
210
220
230
240
250
Counts vs. Mass-to-Charge (m/z)

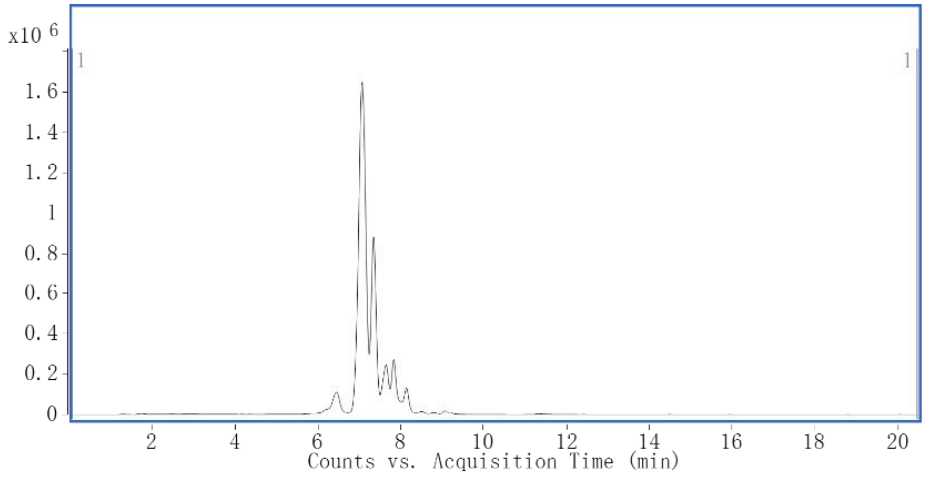
x10 6
1.6
1.4
1.2
1
0.8
0.6
0.4
0.2
0
2
4
6
8
10
12
14
16
18
20
Counts vs. Acquisition Time (min)

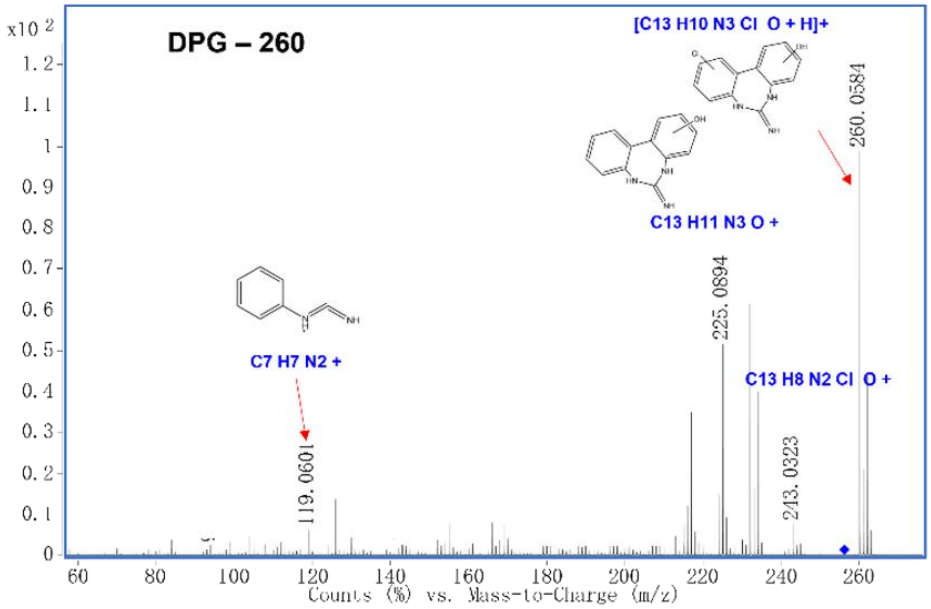
DPG – 260
x10 2
1.2
1.1
1
0.9
0.8
0.7
0.6
0.5
0.4
0.3
0.2
0.1
0
[C13 H10 N3 Cl O + H]+
C13 H11 N3 O +
C7 H7 N2 +
C13 H8 N2 Cl O +
260.0584
225.0894
243.0323
119.0601
60
80
100
120
140
160
180
200
220
240
260
Counts (%) vs. Mass-to-Charge (m/z)